

8 Bottom-hadron decays and mixings

Authors: Y. Aoki, M. Della Morte, E. Lunghi, S. Meinel, C. Monahan, A. Vaquero

Exclusive (semi)leptonic decays and mixing processes of $B_{(s)}$ mesons play a crucial role in flavour physics. In particular, they contain important information for the investigation of the b – d unitarity triangle in the Cabibbo-Kobayashi-Maskawa (CKM) matrix, and provide ideal probes of physics beyond the Standard Model. The charged-current decay channels $B^+ \rightarrow l^+ \nu_l$ and $B^0 \rightarrow \pi^- l^+ \nu_l$, where l^+ is a charged lepton with ν_l being the corresponding neutrino, are essential in extracting the CKM matrix element $|V_{ub}|$. Similarly, the B to $D^{(*)}$ semileptonic transitions can be used to determine $|V_{cb}|$. Flavour-changing neutral-current (FCNC) processes, such as $B \rightarrow K^{(*)} \ell^+ \ell^-$ and $B_{d(s)} \rightarrow \ell^+ \ell^-$, occur only beyond the tree level in weak interactions and are suppressed in the Standard Model. Therefore, these processes could be sensitive to new physics, since heavy particles can contribute to the loop diagrams. FCNC processes are also suitable channels for the extraction of the CKM matrix elements involving the top quark, which appears in loop contributions. The decays $B \rightarrow D^{(*)} \ell \nu$ and $B \rightarrow K^{(*)} \ell \ell$ can also be used to test lepton flavour universality by comparing results for $\ell = e, \mu$ and τ . In particular, anomalies have been seen in the ratios $R(D^{(*)}) = \mathcal{B}(B \rightarrow D^{(*)} \tau \nu) / \mathcal{B}(B \rightarrow D^{(*)} \ell \nu)_{\ell=e,\mu}$ and $R(K^{(*)}) = \mathcal{B}(B \rightarrow K^{(*)} \mu \mu) / \mathcal{B}(B \rightarrow K^{(*)} e e)$, although the latter are no longer statistically significant. In addition, the neutral $B_{d(s)}$ -meson mixings are FCNC processes and are dominated by the 1-loop “box” diagrams containing the top quark and the W bosons. Thus, using the experimentally measured neutral $B_{d(s)}^0$ -meson oscillation frequencies, $\Delta M_{d(s)}$, and the theoretical calculations for the relevant hadronic mixing matrix elements, one can obtain $|V_{td}|$ and $|V_{ts}|$ in the Standard Model.

At the Large Hadron Collider, decays of b quarks can also be probed with Λ_b and other bottom baryons, which can provide complementary constraints on physics beyond the Standard Model. The most important processes are the charged-current decays $\Lambda_b \rightarrow p \ell \bar{\nu}$ and $\Lambda_b \rightarrow \Lambda_c \ell \bar{\nu}$, and the neutral-current decay $\Lambda_b \rightarrow \Lambda \ell^+ \ell^-$.

Accommodating the light quarks and the b quark simultaneously in lattice-QCD computations is a challenging endeavour. To incorporate the pion and the b hadrons with their physical masses, the simulations have to be performed using a lattice that is large enough in physical units to accommodate light pions without significant finite-volume effects, but, at the same time, fine enough to keep the heavy quark discretization errors under control. This usually results in a lattice size $\hat{L} = L/a \sim \mathcal{O}(10^2)$, where a is the lattice spacing and L is the physical (dimensionful) box size. The most ambitious calculations are now using such volumes; however, many ensembles are smaller. Therefore, in addition to employing chiral perturbation theory for the extrapolations in the light-quark mass, current lattice calculations for quantities involving b hadrons often make use of effective theories that allow one to expand in inverse powers of m_b . In this regard, two general approaches are widely adopted. On the one hand, effective field theories such as Heavy-Quark Effective Theory (HQET) and Nonrelativistic QCD (NRQCD) can be directly implemented in numerical computations. On the other hand, a relativistic quark action can be improved *à la* Symanzik to suppress cutoff errors, and then re-interpreted in a manner that is suitable for heavy-quark physics calculations. This latter strategy is often referred to as the method of the Relativistic Heavy-Quark Action (RHQA). The utilization of such effective theories inevitably introduces systematic uncertainties that are not present in light-quark calculations. These uncertainties can arise from the truncation of the expansion in constructing the effective theories (as in HQET and

NRQCD), or from more intricate cutoff effects (as in NRQCD and RHQA). They can also be introduced through more complicated renormalization procedures, which often lead to significant systematic effects in matching the lattice operators to their continuum counterparts. For instance, due to the use of different actions for the heavy and the light quarks, it is more difficult to construct absolutely normalized bottom-light currents.

Complementary to the above “effective theory approaches”, another popular method is to simulate the heavy and the light quarks using the same (typically Symanzik-improved) lattice action at several values of the heavy-quark mass m_h with $am_h < 1$ and $m_h < m_b$. This enables one to employ HQET-inspired relations to extrapolate the computed quantities to the physical b mass. When combined with results obtained in the static heavy-quark limit, this approach can be rendered into an interpolation, instead of extrapolation, in m_h . The discretization errors are the main source of the systematic effects in this method, and very small lattice spacings are needed to keep such errors under control.

In recent years, it has also been possible to perform lattice simulations at very fine lattice spacings and treat heavy quarks as fully relativistic fermions without resorting to effective field theories. Such simulations are, of course, very demanding in computing resources.

Because of the challenge described above, efforts to obtain reliable, accurate lattice-QCD results for the physics of the b quark have been enormous. These efforts include significant theoretical progress in formulating QCD with heavy quarks on the lattice. This aspect is briefly reviewed in Appendix A.1.3 of FLAG 19 [1].

In this section, we summarize the results of the B -meson leptonic decay constants, the neutral B -mixing parameters, and the semileptonic form factors of B mesons and Λ_b baryons, from lattice QCD. To focus on the calculations that have strong phenomenological impact, we limit the review to results based on modern simulations containing dynamical fermions with reasonably light pion masses (below approximately 500 MeV).

For heavy-meson decay constants and mixing parameters, estimates of the quantity $\delta(a_{\min})$ described in Sec. 2.1.2 are provided, where possible, for all computations entering the final FLAG averages or ranges. For heavy-hadron semileptonic-decay form factors, implementing this data-driven continuum-limit criterion was found to be not feasible. The problem is that these quantities are functions of the momentum transfer in addition to the other lattice parameters, and many calculations are based on global fits whose reconstruction was not possible.

Following our review of $B_{(s)}$ -meson leptonic decay constants, the neutral B -meson mixing parameters, and semileptonic form factors, we then interpret our results within the context of the Standard Model. We combine our best-determined values of the hadronic matrix elements with the most recent experimentally-measured branching fractions to obtain $|V_{ub}|$ and $|V_{cb}|$, and compare these results to those obtained from inclusive semileptonic B decays.

8.1 Leptonic decay constants f_B and f_{B_s}

The B - and B_s -meson decay constants are crucial inputs for extracting information from leptonic B decays. Charged B mesons can decay to a lepton-neutrino final state through the charged-current weak interaction. On the other hand, neutral $B_{d(s)}$ mesons can decay to a charged-lepton pair via a FCNC process.

In the Standard Model, the decay rate for $B_{(s)}^+ \rightarrow \ell^+ \nu_\ell$ is described by a formula identical to Eq. (124), with $D_{(s)}$ replaced by $B_{(s)}$, $f_{D_{(s)}}$ replaced by $f_{B_{(s)}}$, and the relevant CKM matrix

element V_{cq} replaced by V_{bq} ,

$$\Gamma(B_{(s)} \rightarrow \ell \nu_\ell) = \frac{m_{B_{(s)}}}{8\pi} G_F^2 f_{B_{(s)}}^2 |V_{bq}|^2 m_\ell^2 \left(1 - \frac{m_\ell^2}{m_{B_{(s)}}^2}\right)^2. \quad (155)$$

The only two-body charged-current B -meson decay that has been observed so far is $B^+ \rightarrow \tau^+ \nu_\tau$, which has been measured by the Belle and Babar collaborations [2, 3]. Both collaborations have reported results with errors around 20%. These measurements can be used to extract $|V_{ub}|$ when combined with lattice-QCD predictions of the corresponding decay constant, but the experimental uncertainties currently preclude a precise determination.

Neutral $B_{d(s)}$ -meson decays to a charged-lepton pair $B_{d(s)} \rightarrow \ell^+ \ell^-$ is a FCNC process, and can only occur at 1-loop in the Standard Model. Hence these processes are expected to be rare, and are sensitive to physics beyond the Standard Model. The corresponding expression for the branching fraction has the form

$$B(B_q \rightarrow \ell^+ \ell^-) = \tau_{B_q} \frac{G_F^2}{\pi} Y \left(\frac{\alpha_s}{4\pi \sin^2 \Theta_W} \right)^2 m_{B_q} f_{B_q}^2 |V_{tb}^* V_{tq}|^2 m_\ell^2 \sqrt{1 - 4 \frac{m_\ell^2}{m_{B_q}^2}}, \quad (156)$$

where the light quark $q = s$ or d , τ_{B_q} is the mean meson lifetime, and the function Y includes NLO QCD and electro-weak corrections that depend on the strong coupling α_s and the weak mixing angle Θ_W [4, 5]. Evidence for the $B_s \rightarrow \mu^+ \mu^-$ decay was first observed by the LHCb [6] and CMS collaborations, and a combined analysis was presented in 2014 in Ref. [7]. In 2020, the ATLAS [8], CMS [9] and LHCb [10] collaborations reported their measurements from a preliminary combined analysis as [11]

$$\begin{aligned} B(B \rightarrow \mu^+ \mu^-) &< 1.9 \times 10^{-10} \text{ at 95\% CL,} \\ B(B_s \rightarrow \mu^+ \mu^-) &= (2.69_{-0.35}^{+0.37}) \times 10^{-9}, \end{aligned} \quad (157)$$

which are compatible with the Standard Model predictions within approximately 2 standard deviations [12]. More recently, updated observations have been reported by the LHCb collaboration [13] and the CMS collaboration [14], but these results do not improve on the precision of the combined analysis.¹ We note that the errors of these results are currently too large to enable a precise determination of $|V_{td}|$ and $|V_{ts}|$.

The related radiative leptonic decay, $B_s \rightarrow \mu^+ \mu^- \gamma$, is another FCNC process that is sensitive to new physics and is expected to occur at a comparable rate to $B_s \rightarrow \mu^+ \mu^-$. Recent searches for this decay by the LHCb collaboration found an upper limit of [13, 17]

$$B(B_s \rightarrow \mu^+ \mu^- \gamma) < 2.0 \times 10^{-9} \text{ at 95\% CL,} \quad (158)$$

in the kinematic region $m_{\mu\mu} > 4.9$ GeV. The dominant hadronic contributions are parameterized by local form factors and by nonlocal resonance contributions, which have been estimated using light-cone sum rules [18], QCD-inspired models [19, 20], and from models of the transition form factors based on lattice calculations of the D_s meson, assuming vector-meson dominance [21]. The first lattice calculation of the local form factors were reported in [22]. The form factors provide a reasonable estimate of the decay rate for large di-muon invariant

¹The PDG quotes the branching fraction $B(B^0 \rightarrow \mu^+ \mu^-) < 1.5 \times 10^{-10}$ at 90% CL [15]. Ref. [16] obtains $B(B^0 \rightarrow \mu^+ \mu^-) = (0.56 \pm 70) \times 10^{-10}$ using a correlated global analysis.

mass, $q^2 > (4.15 \text{ GeV})^2$, where long-distance contributions are expected to be subdominant. Improved determinations of the branching fraction at lower di-muon invariant masses requires a systematic and quantitative treatment of the resonance region.

The rare leptonic $B^+ \rightarrow \ell^+ \nu_\ell \gamma$ decay is proportional to $|V_{ub}|^2$ and has been constrained by the CLEO [23], BaBar [24], and Belle Collaborations [25, 26]. The most stringent constraint, in the region $E_\gamma > 1 \text{ GeV}$, is [26]

$$B(B^+ \rightarrow \ell^+ \nu_\ell \gamma) < 3.0 \times 10^{-6} \text{ at } 90\% \text{ CL.} \quad (159)$$

This branching fraction can be expressed in terms of form factors that are yet to be directly determined on the lattice but have been modelled using QCD sum rules and dispersive approaches combined with an expansion in Λ_{QCD}/m_B and $\Lambda_{\text{QCD}}/E_\gamma$ [27]. At leading order in this expansion, the branching fraction depends only on the light-cone distribution amplitude of the B meson. At present, this channel is primarily viewed as providing experimental constraints on the light-cone distribution amplitude. Direct calculations of this distribution amplitude from lattice QCD are now feasible with recent theoretical developments [28, 29] and, in combination with experimental data, would provide a novel method for the determination of $|V_{ub}|^2$.

The decay constants f_{B_q} (with $q = u, d, s$) parameterize the matrix elements of the corresponding axial-vector currents $A_{bq}^\mu = \bar{b} \gamma^\mu \gamma^5 q$ analogously to the definition of f_{D_q} in Sec. 7.1:

$$\langle 0 | A^\mu | B_q(p) \rangle = i p_{B_q}^\mu f_{B_q}. \quad (160)$$

For heavy-light mesons, it is convenient to define and analyse the quantity

$$\Phi_{B_q} \equiv f_{B_q} \sqrt{m_{B_q}}, \quad (161)$$

which approaches a constant (up to logarithmic corrections) in the $m_{B_q} \rightarrow \infty$ limit, because of heavy-quark symmetry. In the following discussion, we denote lattice data for Φ , and the corresponding decay constant f , obtained at a heavy-quark mass m_h and light valence-quark mass m_ℓ as $\Phi_{h\ell}$ and $f_{h\ell}$, to differentiate them from the corresponding quantities at the physical b and light-quark masses.

The SU(3)-breaking ratio f_{B_s}/f_B is of phenomenological interest, because many systematic effects can be partially reduced in lattice-QCD calculations of this ratio. The discretization errors, heavy-quark-mass tuning effects, and renormalization/matching errors may all be partially reduced.

This SU(3)-breaking ratio is, however, still sensitive to the chiral extrapolation. Provided the chiral extrapolation is under control, one can then adopt f_{B_s}/f_B as an input in extracting phenomenologically-interesting quantities. In addition, it often happens to be easier to obtain lattice results for f_{B_s} with smaller errors than direct calculations of f_B . Therefore, one can combine the B_s -meson decay constant with the SU(3)-breaking ratio to calculate f_B . Such a strategy can lead to better precision in the computation of the B -meson decay constant, and has been adopted by the ETM [30, 31] and the HPQCD collaborations [32]. An alternative strategy to the direct calculation of f_{B_s} , used in Ref. [33], is to obtain the B_s -meson decay constant by combining the D_s -meson decay constant with the ratio f_{B_s}/f_{D_s} .

It is clear that the decay constants for charged and neutral B mesons play different roles in flavour-physics phenomenology. Knowledge of the B^+ -meson decay constant f_{B^+} is essential for extracting $|V_{ub}|$ from leptonic B^+ decays. The neutral B -meson decay constants f_{B^0} and

f_{B_s} are inputs to searches for new physics in rare leptonic B^0 decays. In view of this, it is desirable to include isospin-breaking effects in lattice computations for these quantities and to provide lattice results for both f_{B^+} and f_{B^0} . With the high precision of recent lattice calculations, isospin splittings for B -meson decay constants can be significant, and will play an important role in the foreseeable future.

A few collaborations have reported f_{B^+} and f_{B^0} separately by taking into account strong isospin effects in the valence sector, and estimated the corrections from electromagnetism [34–37]. The $N_f = 2 + 1 + 1$ strong isospin-breaking effect was computed in HPQCD 13 [36] (see Tab. 33 in this subsection). However, since only unitary points (with equal sea- and valence-quark masses) were considered in HPQCD 13 [36], this procedure only correctly accounts for the effect from the valence-quark masses, while introducing a spurious sea-quark contribution. The decay constants f_{B^+} and f_{B^0} are also separately reported in FNAL/MILC 17 [34] by taking into account the strong-isospin effect. The FNAL/MILC results were obtained by keeping the averaged light sea-quark mass fixed when varying the quark masses in their analysis procedure. Their finding indicates that the strong isospin-breaking effects, $f_{B^+} - f_B \sim 0.5$ MeV, could be smaller than those suggested by previous computations. One would have to take into account QED effects in the B -meson leptonic decay rates to properly use these results for extracting phenomenologically relevant information.² Currently, errors on the experimental measurements of these decay rates are still very large. In this review, we will therefore concentrate on the isospin-averaged result f_B and the B_s -meson decay constant, as well as the SU(3)-breaking ratio f_{B_s}/f_B .

The status of lattice-QCD computations for B -meson decay constants and the SU(3)-breaking ratio, using gauge-field ensembles with light dynamical fermions, is summarized in Tabs. 33 and 34. Figs. 21 and 22 contain the graphical presentation of the collected results and our averages. Most results in these tables and plots have been reviewed in detail in FLAG 19 [1] and in FLAG 21 [39]. Here, we describe the new results that have appeared since January 2021.

We also review the continuum-limit quantity, $\delta(a_{\min})$, described in Sec. 2. We estimate, where possible, $\delta(a_{\min})$ for results entering the FLAG averages of f_B , f_{B_s} , and f_{B_s}/f_B , but we do not use $\delta(a_{\min})$ for averaging. We include estimates of $\delta(a_{\min})$ for those calculations that explicitly provide the relevant data in the manuscript.

As lattice calculations of leptonic decays have become statistically more precise, results are often dominated by systematic uncertainties. The continuum extrapolation is frequently the largest source of systematic uncertainty for lattice calculations of heavy quarks, for which the heavy-quark discretization can introduce effects of the $\mathcal{O}(am)^n$, and a more quantitative measure of discretization effects is a useful guide to the quality of the continuum extrapolation. For the lattice calculations of leptonic decay constants of bottom hadrons that appear in this review, the continuum-limit quantity should be interpreted with caution, because many final results are quoted from combined chiral-continuum extrapolations and, typically, more recent computations do not quote numerical values for the leptonic decay constants at the finest lattice spacings. Moreover, the finest ensembles may not be at, or close to, the physical pion mass. Thus, we generally quote our estimations of $\delta(a_{\min})$ to one significant figure because the natural size of the uncertainty on $\delta(a_{\min})$ is $\mathcal{O}(1)$.

There have been no new $N_f = 2$ calculations of f_B , f_{B_s} , or f_{B_s}/f_B . Therefore, our averages for these quantities stay the same as those in FLAG 21 [39]. Our estimates for the

²See Ref. [38] for a strategy that has been proposed to account for QED effects.

Collaboration	Ref.	N_f	publication status	continuum extrapolation	chiral extrapolation	finite volume	renormalization/matching	heavy-quark treatment	f_{B^+}	f_{B^0}	f_B	f_{B_s}
Frezzotti 24	[22]	2+1+1	P	★	★	★	★	✓	—	—	—	224.5(5.0)
FNAL/MILC 17	[34]	2+1+1	A	★	★	★	★	✓	189.4(1.4)	190.5(1.3)	189.9(1.4)	230.7(1.2)
HPQCD 17A	[40]	2+1+1	A	○	★	★	○	✓	—	—	196(6)	236(7)
ETM 16B	[31]	2+1+1	A	★	○	○	○	✓	—	—	193(6)	229(5)
ETM 13E	[41]	2+1+1	C	★	○	○	○	✓	—	—	196(9)	235(9)
HPQCD 13	[36]	2+1+1	A	○	★	★	○	✓	184(4)	188(4)	186(4)	224(5)
RBC/UKQCD 14	[37]	2+1	A	○	○	○	○	✓	195.6(14.9)	199.5(12.6)	—	235.4(12.2)
RBC/UKQCD 14A	[42]	2+1	A	○	○	○	○	✓	—	—	219(31)	264(37)
RBC/UKQCD 13A	[43]	2+1	C	○	○	○	○	✓	—	—	191(6) _{stat}	233(5) _{stat}
HPQCD 12	[32]	2+1	A	○	○	○	○	✓	—	—	191(9)	228(10)
HPQCD 12	[32]	2+1	A	○	○	○	○	✓	—	—	189(4) [△]	—
HPQCD 11A	[44]	2+1	A	★	○	★	★	✓	—	—	—	225(4) [▽]
FNAL/MILC 11	[35]	2+1	A	○	○	★	○	✓	197(9)	—	—	242(10)
HPQCD 09	[45]	2+1	A	○	○	○	○	✓	—	—	190(13) [•]	231(15) [•]
Balasubramanian 19 [†]	[33]	2	A	★	★	★	○	✓	—	—	—	215(10)(2)(⁺² ₋₅)
ALPHA 14	[46]	2	A	★	★	★	★	✓	—	—	186(13)	224(14)
ALPHA 13	[47]	2	C	★	★	★	★	✓	—	—	187(12)(2)	224(13)
ETM 13B, 13C [‡]	[30, 48]	2	A	★	○	★	○	✓	—	—	189(8)	228(8)
ALPHA 12A	[49]	2	C	★	★	★	★	✓	—	—	193(9)(4)	219(12)
ETM 12B	[50]	2	C	★	○	★	○	✓	—	—	197(10)	234(6)
ALPHA 11	[51]	2	C	★	○	★	★	✓	—	—	174(11)(2)	—
ETM 11A	[52]	2	A	★	○	★	○	✓	—	—	195(12)	232(10)
ETM 09D	[53]	2	A	★	○	○	○	✓	—	—	194(16)	235(12)

[◇]Statistical errors only.

[△]Obtained by combining f_{B_s} from HPQCD 11A with f_{B_s}/f_B calculated in this work.

[▽]This result uses one ensemble per lattice spacing with light to strange sea-quark mass ratio $m_\ell/m_s \approx 0.2$.

[•]This result uses an old determination of $r_1 = 0.321(5)$ fm from Ref. [54] that has since been superseded.

[†]Obtained by combining f_{D_s} , updated in this work, with f_{B_s}/f_{D_s} , calculated in this work.

[‡]Update of ETM 11A and 12B.

Table 33: Decay constants of the B , B^+ , B^0 and B_s mesons (in MeV). Here f_B stands for the mean value of f_{B^+} and f_{B^0} , extrapolated (or interpolated) in the mass of the light valence-quark to the physical value of m_{ud} .

continuum-limit quantity $\delta(a_{\min})$ are $\delta(a_{\min}) = 0.01$ for f_{B_s} in Ref. [30]. Data do not permit estimates of the continuum-limit quantity for f_B and f_{B_s}/f_B from Ref. [30], but discretization

Collaboration	Ref.	N_f		publication status	continuum extrapolation	chiral extrapolation	finite volume	renormalization/matching	heavy-quark treatment	f_{B_s}/f_{B^+}	f_{B_s}/f_{B^0}	f_{B_s}/f_B
FNAL/MILC 17	[34]	2+1+1	A	★	★	★	★	✓		1.2180(49)	1.2109(41)	—
HPQCD 17A	[40]	2+1+1	A	○	★	★	○	✓		—	—	1.207(7)
ETM 16B	[31]	2+1+1	A	★	○	○	○	✓		—	—	1.184(25)
ETM 13E	[41]	2+1+1	C	★	○	○	○	✓		—	—	1.201(25)
HPQCD 13	[36]	2+1+1	A	○	★	★	○	✓		1.217(8)	1.194(7)	1.205(7)
QCDSF/UKQCD/CSSM 22	[55]	2+1	C	★	★	○	○	✓		—	—	1.159(15)($^{+76}_{-71}$)
RBC/UKQCD 18A	[56]	2+1	P	★	★	★	★	✓		—	—	1.1949(60)($^{+95}_{-175}$)
RBC/UKQCD 14	[37]	2+1	A	○	○	○	○	✓		1.223(71)	1.197(50)	—
RBC/UKQCD 14A	[42]	2+1	A	○	○	○	○	✓		—	—	1.193(48)
RBC/UKQCD 13A	[43]	2+1	C	○	○	○	○	✓		—	—	1.20(2) $^{\diamond}_{\text{stat}}$
HPQCD 12	[32]	2+1	A	○	○	○	○	✓		—	—	1.188(18)
FNAL/MILC 11	[35]	2+1	A	○	○	★	○	✓		1.229(26)	—	—
RBC/UKQCD 10C	[57]	2+1	A	■	■	■	○	✓		—	—	1.15(12)
HPQCD 09	[45]	2+1	A	○	○	○	○	✓		—	—	1.226(26)
ALPHA 14	[46]	2	A	★	★	★	★	✓		—	—	1.203(65)
ALPHA 13	[47]	2	C	★	★	★	★	✓		—	—	1.195(61)(20)
ETM 13B, 13C †	[30, 48]	2	A	★	○	★	○	✓		—	—	1.206(24)
ALPHA 12A	[49]	2	C	★	★	★	★	✓		—	—	1.13(6)
ETM 12B	[50]	2	C	★	○	★	○	✓		—	—	1.19(5)
ETM 11A	[52]	2	A	○	○	★	○	✓		—	—	1.19(5)

$^{\diamond}$ Statistical errors only.

† Update of ETM 11A and 12B.

Table 34: Ratios of decay constants of the B and B_s mesons (for details see Tab. 33).

effects are generally small. From Ref. [46] we obtain $\delta(a_{\min}) = 0.6$ for f_B , $\delta(a_{\min}) = 0.3$ for f_{B_s} , and $\delta(a_{\min}) = 0.3$ for f_{B_s}/f_B . Finally, $\delta(a_{\min}) = 2.6$ for f_{B_s} in [33].

Our averages of the $N_f = 2$ results are:

$$N_f = 2 : \quad f_B = 188(7) \text{ MeV} \quad \text{Refs. [30, 46],} \quad (162)$$

$$N_f = 2 : \quad f_{B_s} = 225.3(6.6) \text{ MeV} \quad \text{Refs. [30, 33, 46],} \quad (163)$$

$$N_f = 2 : \quad \frac{f_{B_s}}{f_B} = 1.206(0.023) \quad \text{Refs. [30, 46].} \quad (164)$$

Two new $N_f = 2 + 1$ calculations of f_{B_s}/f_B were presented in conference proceedings

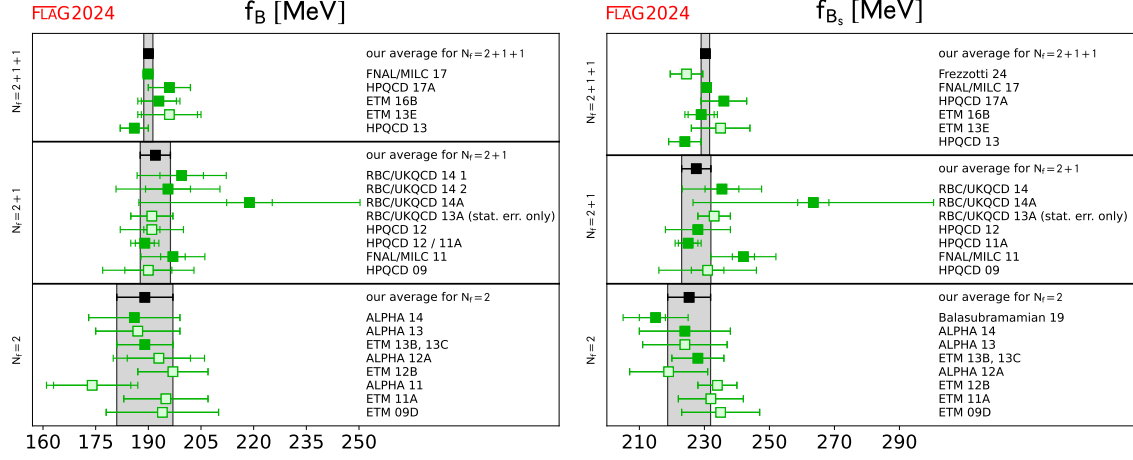


Figure 21: Decay constants of the B and B_s mesons. The values are taken from Tab. 33 (the f_B entry for FNAL/MILC 11 represents f_{B^+}). The significance of the colours is explained in Sec. 2. The black squares and grey bands indicate our averages in Eqs. (162), (165), (168), (163), (166) and (169).

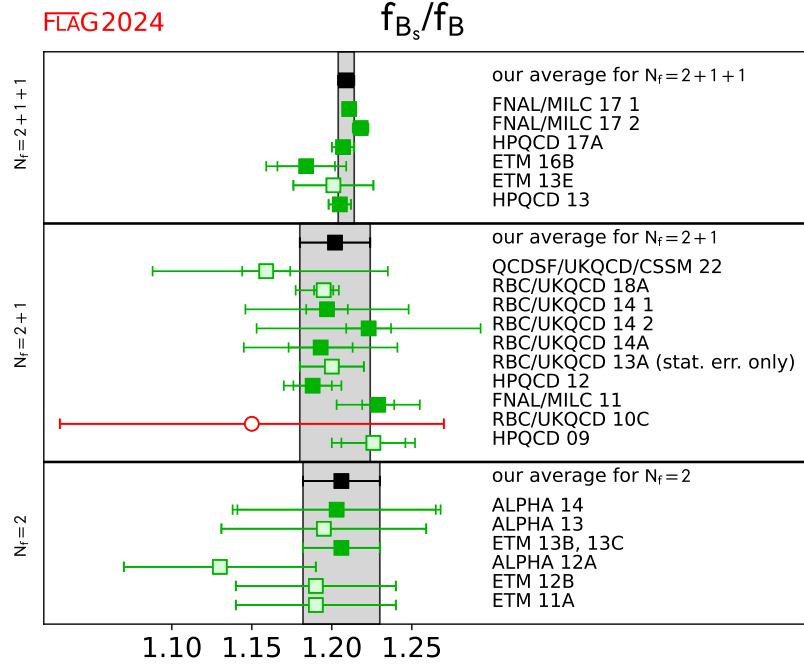


Figure 22: Ratio of the decay constants of the B and B_s mesons. The values are taken from Tab. 34. Results labelled as FNAL/MILC 17 1 and FNAL/MILC 17 2 correspond to those for f_{B_s}/f_{B^0} and f_{B_s}/f_{B^+} reported in FNAL/MILC 17. The significance of the colours is explained in Sec. 2. The black squares and grey bands indicate our averages in Eqs. (164), (167), and (170).

after the publication of FLAG 21 [39]. Only one of these calculations, Ref. [55], provides a

preliminary quantitative result. In Tab. 34, this result is labelled QCDSF/UKQCD/CSSM 22 [55]. The second work, Ref. [58], is described in the text below, but not listed in Tab. 34.

In QCDSF/UKQCD/CSSM 22 [55] the QCDSF/UKQCD/CSSM collaboration presented the ratio of decay constants, f_{B_s}/f_B , using $N_f = 2 + 1$ dynamical ensembles generated using nonperturbatively $\mathcal{O}(a)$ -improved clover-Wilson fermions. Four lattice spacings, of $a = 0.082, 0.074, 0.068$, and 0.059 fm, were used, with pion masses ranging from 155 to 468 MeV, and lattice sizes between 2.37 and 4.35 fm. The light-quark masses were tuned using the QCDSF procedure [59], for fixing the light- and strange-quark masses. Quark masses were chosen to keep the value of the SU(3) flavour-singlet mass, $\bar{m} = (2m_\ell + m_s)/3$, constant. Heavy quarks were simulated with a relativistic heavy-quark (RHQ) action, with bare-quark masses chosen to keep the SU(3) flavour-singlet mass, $X_B^2 = (2M_{B_\ell} + M_{B_s})/3$, constant. The bare parameters of the RHQ action were chosen to ensure that the masses and hyperfine splitting of the X_B and X_{B^*} mesons reproduce the properties of the physical, spin-averaged X_B and X_{B^*} [60].

The chiral extrapolation was performed using both linear and quadratic terms in $(M_\pi^2/M_X^2 - 1)$ and assuming that the SU(3) flavour breaking does not depend on the lattice spacing. The reported value for the ratio of decay constants assumes that the renormalization parameters for light- and strange-quark currents are approximately equal, but this is only true near the SU(3)-symmetric point. Effects of the order of 1-2% are expected near the physical point and calculations of the relevant parameters on near-physical ensembles are underway. Tests of $\mathcal{O}(a^2)$ discretization effects indicate little dependence and the final results are quoted from the subset of ensembles with $m_\pi L > 4$ and assuming no dependence on a^2 . Tests of heavy-quark mistuning effects indicate that the ratio of decay constants are minimally affected.

The RBC/UKQCD collaboration described ongoing efforts to calculate pseudoscalar and vector heavy-meson decay constants in Ref. [58], using $N_f = 2 + 1$ dynamical ensembles generated using Domain Wall Fermions (DWF). Four lattice spacings, of $a = 0.11, 0.083, 0.071$, and 0.063 fm were used, with pion masses ranging from 267 to 433 MeV, and lattice sizes between 2.0 and 3.4 fm. Light and strange quarks were simulated with the Shamir DWF discretization and charm quarks were simulated with Möbius DWF action. These discretizations correspond to two different choices for the DWF kernel. The Möbius DWF are loosely equivalent to Shamir DWF at twice the extension in the fifth dimensions [61]. Ref. [58] presents a preliminary analysis with a two-step procedure. The first step corrects for strange-quark-mass mistunings and the second applies NLO SU(2) heavy-meson chiral perturbation theory to carry out a chiral-continuum extrapolation using various fit Ansätze to enable a full systematic error analysis. This analysis is ongoing at time of publication.

The results of Refs. [55] and [58] have not been published and therefore neither calculation is included in our average. Thus, our averages remain the same as in FLAG 21 [39],

$$N_f = 2 + 1 : \quad f_B = 192.0(4.3) \text{ MeV} \quad \text{Refs. [32, 35, 37, 42, 44]}, \quad (165)$$

$$N_f = 2 + 1 : \quad f_{B_s} = 228.4(3.7) \text{ MeV} \quad \text{Refs. [32, 35, 37, 42, 44]}, \quad (166)$$

$$N_f = 2 + 1 : \quad \frac{f_{B_s}}{f_B} = 1.201(0.016) \quad \text{Refs. [32, 35, 37, 42, 56]}. \quad (167)$$

Our estimates for the continuum-limit quantity $\delta(a_{\min})$ for the results entering the FLAG averages for the $N_f = 2 + 1$ bottom-hadron leptonic decay constants, and their ratio, are: $\delta(a_{\min}) = 5.6$ and $\delta(a_{\min}) = 7.4$ for f_{B_s} and f_B , respectively, in Ref. [35]; $\delta(a_{\min}) = 1.5$ for f_B in Ref. [44]; $\delta(a_{\min}) = 0.01$ and $\delta(a_{\min}) = 0.6$ for f_{B_s} and f_B , respectively, in Ref. [32];

$\delta(a_{\min}) = 1.9$ and $\delta(a_{\min}) = 2.3$ for f_{B_s} and f_B , respectively, in Ref. [42]; and $\delta(a_{\min}) = 1.7$ for f_{B_s} in Ref. [37]. For f_{B_s}/f_B we obtain approximately $\delta(a_{\min}) = 0.4$ for [35], approximately 2 for [32] and [42], 3 for [37], and around 0.5 for [56].

No new $N_f = 2 + 1 + 1$ calculations of f_B and f_{B_s}/f_B have appeared since FLAG 21. There has been one new calculation of $f_{B(s)}$ in Ref. [22], labelled Frezzotti 24 in Tab. 33.

As part of the determination of the form factors for the radiative leptonic decay $B_s \rightarrow \mu^+ \mu^- \gamma$, the decay constant f_{B_s} was determined in Ref. [22]. This work used ensembles with $N_f = 2 + 1 + 1$ clover-Wilson twisted-mass fermions at maximal twist. Four lattice spacings, ranging from 0.057 to 0.091 fm, were included and pion masses spanned a range from 137 to 175 MeV. The heavy-strange meson was simulated using clover-Wilson twisted-mass fermions at a range of heavy-strange masses, extrapolated up to the physical B_s mass. Ref. [22] determined f_{H_s} from both two-point functions and the spatial part of the axial hadronic tensor to better constrain the continuum limit because these determinations differ only by discretization effects. The results from both methods were simultaneously extrapolated to the continuum limit at fixed values of the heavy-strange meson mass M_{H_s} , with six different fit variations for each of the five values of M_{H_s} . The results of each fit were combined using the Akaike Information Criterion [62] and the corresponding continuum decay constants were then extrapolated to the physical B_s mass. The extrapolation in the heavy-strange mass was carried out using a fit form guided by HQET, with modifications to account for the anomalous dimension of the axial current in HQET and the matching between QCD and HQET.

Ref. [22] has not been published at the time of publication of this review. Therefore, our averages for f_B , $f_{B(s)}$ and f_{B_s}/f_B remain the same as in FLAG 21 [39],

$$N_f = 2 + 1 + 1 : \quad f_B = 190.0(1.3) \text{ MeV} \quad \text{Refs. [31, 34, 36, 40]}, \quad (168)$$

$$N_f = 2 + 1 + 1 : \quad f_{B_s} = 230.3(1.3) \text{ MeV} \quad \text{Refs. [31, 34, 36, 40]}, \quad (169)$$

$$N_f = 2 + 1 + 1 : \quad \frac{f_{B_s}}{f_B} = 1.209(0.005) \quad \text{Refs. [31, 34, 36, 40]}. \quad (170)$$

The data reported in the calculations that appear in these averages do not permit estimates of $\delta(a_{\min})$.

The PDG presented averages for the $N_f = 2 + 1$ and $N_f = 2 + 1 + 1$ lattice-QCD determinations of the isospin-averaged f_B , f_{B_s} and f_{B_s}/f_B in 2024 [15]. The $N_f = 2 + 1$ and $N_f = 2 + 1 + 1$ lattice-computation results used in Ref. [15] are identical to those included in our current work, and the averages quoted in Ref. [15] are those determined in [1] and [39].

8.2 Neutral B -meson mixing matrix elements

Neutral B -meson mixing is induced in the Standard Model through 1-loop box diagrams to lowest order in the electroweak theory, similar to those for short-distance effects in neutral kaon mixing. The effective Hamiltonian is given by

$$\mathcal{H}_{\text{eff}}^{\Delta B=2, \text{SM}} = \frac{G_F^2 M_W^2}{16\pi^2} (\mathcal{F}_d^0 \mathcal{Q}_1^d + \mathcal{F}_s^0 \mathcal{Q}_1^s) + \text{h.c.}, \quad (171)$$

with

$$\mathcal{Q}_1^q = [\bar{b}\gamma^\mu(1 - \gamma_5)q] [\bar{b}\gamma_\mu(1 - \gamma_5)q], \quad (172)$$

where $q = d$ or s . The short-distance function \mathcal{F}_q^0 in Eq. (171) is much simpler compared to the kaon mixing case due to the hierarchy in the CKM matrix elements. Here, only one term

is relevant,

$$\mathcal{F}_q^0 = \lambda_{tq}^2 S_0(x_t) \quad (173)$$

where

$$\lambda_{tq} = V_{tq}^* V_{tb}, \quad (174)$$

and where $S_0(x_t)$ is an Inami-Lim function with $x_t = m_t^2/M_W^2$, which describes the basic electroweak loop contributions without QCD [4].

The transition amplitude for B_q^0 with $q = d$ or s can be written as

$$\begin{aligned} \langle \bar{B}_q^0 | \mathcal{H}_{\text{eff}}^{\Delta B=2} | B_q^0 \rangle &= \frac{G_F^2 M_W^2}{16\pi^2} [\lambda_{tq}^2 S_0(x_t) \eta_{2B}] \\ &\times \left(\frac{\bar{g}(\mu)^2}{4\pi} \right)^{-\gamma_0/(2\beta_0)} \exp \left\{ \int_0^{\bar{g}(\mu)} dg \left(\frac{\gamma(g)}{\beta(g)} + \frac{\gamma_0}{\beta_0 g} \right) \right\} \\ &\times \langle \bar{B}_q^0 | Q_R^q(\mu) | B_q^0 \rangle + \text{h.c.} , \end{aligned} \quad (175)$$

where $Q_R^q(\mu)$ is the renormalized four-fermion operator (usually in the NDR scheme of $\overline{\text{MS}}$). The running coupling \bar{g} , the β -function $\beta(g)$, and the anomalous dimension of the four-quark operator $\gamma(g)$ are defined in Eqs. (95) and (96). The product of μ -dependent terms on the second line of Eq. (175) is, of course, μ -independent (up to truncation errors arising from the use of perturbation theory). The explicit expression for the short-distance QCD correction factor η_{2B} (calculated to NLO) can be found in Ref. [63].

For historical reasons the B -meson-mixing matrix elements are often parameterized in terms of bag parameters defined as

$$B_{B_q}(\mu) = \frac{\langle \bar{B}_q^0 | Q_R^q(\mu) | B_q^0 \rangle}{\frac{8}{3} f_{B_q}^2 m_{B_q}^2} . \quad (176)$$

The renormalization-group-independent (RGI) B parameter \hat{B} is defined as in the case of the kaon, and expressed to 2-loop order as

$$\hat{B}_{B_q} = \left(\frac{\bar{g}(\mu)^2}{4\pi} \right)^{-\gamma_0/(2\beta_0)} \left\{ 1 + \frac{\bar{g}(\mu)^2}{(4\pi)^2} \left[\frac{\beta_1 \gamma_0 - \beta_0 \gamma_1}{2\beta_0^2} \right] \right\} B_{B_q}(\mu) , \quad (177)$$

with β_0 , β_1 , γ_0 , and γ_1 defined in Eq. (97). Note, as Eq. (175) is evaluated above the bottom threshold ($m_b < \mu < m_t$), the active number of flavours here is $N_f = 5$.

Nonzero transition amplitudes result in a mass difference between the CP eigenstates of the neutral B -meson system. Writing the mass difference for a B_q^0 meson as Δm_q , its Standard Model prediction is

$$\Delta m_q = \frac{G_F^2 m_W^2 m_{B_q}}{6\pi^2} |\lambda_{tq}|^2 S_0(x_t) \eta_{2B} f_{B_q}^2 \hat{B}_{B_q}, \quad (178)$$

where λ_{tq} is defined in Eq. (174). Experimentally, the mass difference is determined from the oscillation frequency of the CP eigenstates. The frequencies are measured precisely with an error of less than a percent. Many different experiments have measured Δm_d , but the current average [64] is dominated by the LHCb experiment. For Δm_s the experimental average is again dominated by results from LHCb [64] and the precision reached is about one per mille. With

these experimental results and lattice-QCD calculations of $f_{B_q}^2 \hat{B}_{B_q}$, λ_{tq} can be determined. In lattice-QCD calculations the flavour SU(3)-breaking ratio

$$\xi^2 = \frac{f_{B_s}^2 B_{B_s}}{f_{B_d}^2 B_{B_d}} \quad (179)$$

can be obtained more precisely than the individual B_q -mixing matrix elements because statistical and systematic errors cancel in part. From ξ^2 , the ratio $|V_{td}/V_{ts}|$ can be determined and used to constrain the apex of the CKM triangle.

Neutral B -meson mixing, being loop-induced in the Standard Model, is also a sensitive probe of new physics. The most general $\Delta B = 2$ effective Hamiltonian that describes contributions to B -meson mixing in the Standard Model and beyond is given in terms of five local four-fermion operators:

$$\mathcal{H}_{\text{eff,BSM}}^{\Delta B=2} = \sum_{q=d,s} \sum_{i=1}^5 \mathcal{C}_i \mathcal{Q}_i^q, \quad (180)$$

where \mathcal{Q}_1 is defined in Eq. (172) and where

$$\begin{aligned} \mathcal{Q}_2^q &= [\bar{b}(1 - \gamma_5)q] [\bar{b}(1 - \gamma_5)q], & \mathcal{Q}_3^q &= [\bar{b}^\alpha(1 - \gamma_5)q^\beta] [\bar{b}^\beta(1 - \gamma_5)q^\alpha], \\ \mathcal{Q}_4^q &= [\bar{b}(1 - \gamma_5)q] [\bar{b}(1 + \gamma_5)q], & \mathcal{Q}_5^q &= [\bar{b}^\alpha(1 - \gamma_5)q^\beta] [\bar{b}^\beta(1 + \gamma_5)q^\alpha], \end{aligned} \quad (181)$$

with the superscripts α, β denoting colour indices, which are shown only when they are contracted across the two bilinears. There are three other basis operators in the $\Delta B = 2$ effective Hamiltonian. When evaluated in QCD, however, they give identical matrix elements to the ones already listed due to parity invariance in QCD. The short-distance Wilson coefficients \mathcal{C}_i depend on the underlying theory and can be calculated perturbatively. In the Standard Model only matrix elements of \mathcal{Q}_1^q contribute to Δm_q , while all operators do, for example, for general SUSY extensions of the Standard Model [65]. The matrix elements or bag parameters for the non-SM operators are also useful to estimate the width difference $\Delta\Gamma_q$ between the CP eigenstates of the neutral B meson in the Standard Model, where combinations of matrix elements of \mathcal{Q}_1^q , \mathcal{Q}_2^q , and \mathcal{Q}_3^q contribute to $\Delta\Gamma_q$ at $\mathcal{O}(1/m_b)$ [66, 67].

In this section, we report on results from lattice-QCD calculations for the neutral B -meson mixing parameters \hat{B}_{B_d} , \hat{B}_{B_s} , $f_{B_d}\sqrt{\hat{B}_{B_d}}$, $f_{B_s}\sqrt{\hat{B}_{B_s}}$ and the SU(3)-breaking ratios B_{B_s}/B_{B_d} and ξ defined in Eqs. (176), (177), and (179). The results are summarized in Tabs. 35 and 36 and in Figs. 23 and 24. Additional details about the underlying simulations and systematic error estimates are given in Appendix C.5.2. Some collaborations do not provide the RGI quantities \hat{B}_{B_q} , but quote instead $B_B(\mu)^{\overline{\text{MS}},\text{NDR}}$. In such cases, we convert the results using Eq. (177) to the RGI quantities quoted in Tab. 35 with a brief description for each case. More detailed descriptions for these cases are provided in FLAG13 [68]. We do not provide the B -meson-matrix elements of the other operators \mathcal{Q}_{2-5} in this report. They have been calculated in Ref. [30] for the $N_f = 2$ case, in Refs. [69, 70] for $N_f = 2 + 1$, and in Ref. [71] for $N_f = 2 + 1 + 1$. A discussion is provided on the comparison of these results in a recent review [72].

Let us mention that our averages here have no updates from the previous review [39]. The new addition to this subsection is that we review a measure of continuum-limit quality $\delta(a_{\min})$ for each result that is included in the average. We used this quantity for the continuum-limit

Collaboration	Ref.	N_f	publication status	continuum extrapolation	chiral extrapolation	finite volume	renormalization/matching	heavy-quark treatment	$f_{B_d} \sqrt{\hat{B}_{B_d}}$	$f_{B_s} \sqrt{\hat{B}_{B_s}}$	\hat{B}_{B_d}	\hat{B}_{B_s}
HPQCD 19A	[71]	2+1+1	A	○	○	★	○	✓	210.6(5.5)	256.1(5.7)	1.222(61)	1.232(53)
FNAL/MILC 16	[70]	2+1	A	★	○	★	○	✓	227.7(9.5)	274.6(8.4)	1.38(12)(6) [⊙]	1.443(88)(48) [⊙]
RBC/UKQCD 14A	[42]	2+1	A	○	○	○	○	✓	240(15)(33)	290(09)(40)	1.17(11)(24)	1.22(06)(19)
FNAL/MILC 11A	[69]	2+1	C	★	○	★	○	✓	250(23) [†]	291(18) [†]	—	—
HPQCD 09	[45]	2+1	A	○	○	▽	○	✓	216(15) [*]	266(18) [*]	1.27(10) [*]	1.33(6) [*]
HPQCD 06A	[73]	2+1	A	■	■	★	○	✓	—	281(21)	—	1.17(17)
ETM 13B	[30]	2	A	★	○	○	★	✓	216(6)(8)	262(6)(8)	1.30(5)(3)	1.32(5)(2)
ETM 12A, 12B	[50, 74]	2	C	★	○	○	★	✓	—	—	1.32(8) [⊙]	1.36(8) [⊙]

[⊙] PDG averages of decay constant f_{B^0} and f_{B_s} [75] are used to obtain these values.

[†] Reported f_B^2 at $\mu = m_b$ is converted to RGI by multiplying the 2-loop factor 1.517.

[▽] While wrong-spin contributions are not included in the HMrS χ PT fits, the effect is expected to be small for these quantities (see description in FLAG 13 [68]).

^{*} This result uses an old determination of $r_1 = 0.321(5)$ fm from Ref. [54] that has since been superseded, which however has only a small effect in the total error budget (see description in FLAG 13 [68]).

[⊙] Reported B at $\mu = m_b = 4.35$ GeV is converted to RGI by multiplying the 2-loop factor 1.521.

Table 35: Neutral B - and B_s -meson mixing matrix elements (in MeV) and bag parameters.

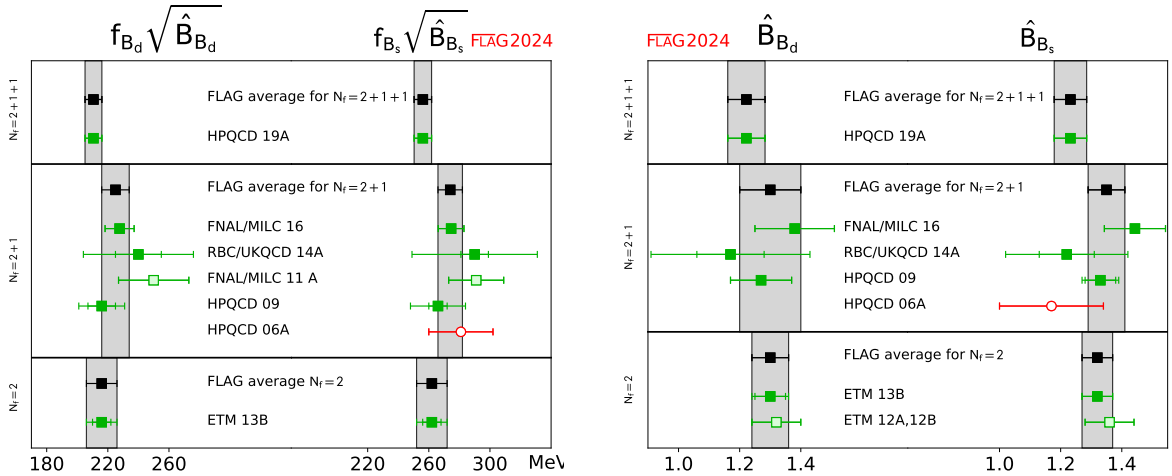


Figure 23: Neutral B - and B_s -meson-mixing matrix elements and bag parameters [values in Tab. 35 and Eqs. (182), (185), (188), (183), (186), (189)].

Collaboration	Ref.	N_f	publication status	continuum extrapolation	chiral extrapolation	finite volume	renormalization/matching	heavy-quark treatment	ξ	B_{B_s}/B_{B_d}
HPQCD 19A	[71]	2+1+1	A	○	○	★	○	✓	1.216(16)	1.008(25)
RBC/UKQCD 18A	[56]	2+1	P	★	★	★	★	✓	1.1939(67)(⁺⁹⁵ ₋₁₇₇)	0.9984(45)(⁺⁸⁰ ₋₆₃)
FNAL/MILC 16	[70]	2+1	A	★	○	★	○	✓	1.206(18)	1.033(31)(26) [⊙]
RBC/UKQCD 14A	[42]	2+1	A	○	○	○	○	✓	1.208(41)(52)	1.028(60)(49)
FNAL/MILC 12	[76]	2+1	A	○	○	★	○	✓	1.268(63)	1.06(11)
RBC/UKQCD 10C	[57]	2+1	A	■	■	■	○	✓	1.13(12)	—
HPQCD 09	[45]	2+1	A	○	○ [▽]	○	○	✓	1.258(33)	1.05(7)
ETM 13B	[30]	2	A	★	○	○	★	✓	1.225(16)(14)(22)	1.007(15)(14)
ETM 12A, 12B	[50, 74]	2	C	★	○	○	★	✓	1.21(6)	1.03(2)

[⊙] PDG average of the ratio of decay constants f_{B_s}/f_{B^0} [75] is used to obtain the value.

[▽] Wrong-spin contributions are not included in the HMrS χ PT fits. As the effect may not be negligible, these results are excluded from the average (see description in FLAG 13 [68]).

Table 36: Results for SU(3)-breaking ratios of neutral B_d - and B_s -meson-mixing matrix elements and bag parameters.

criterion for heavy-quark related quantities in FLAG 13 [68]. This time we only quote the value for information and we do not use it when calculating averages.

There are no new results for $N_f = 2$ reported after FLAG 16 [77]. In this category, one work (ETM 13B) [30] passes the quality criteria. A description of this work can be found in FLAG 13 [68] where it did not enter the average as it had not appeared in a journal. This is the only result available for $N_f = 2$, so we quote their values as our estimates

$$f_{B_d}\sqrt{\hat{B}_{b_d}} = 216(10) \text{ MeV}, \quad f_{B_s}\sqrt{\hat{B}_{B_s}} = 262(10) \text{ MeV} \quad \text{Ref. [30]}, \quad (182)$$

$$N_f = 2: \quad \hat{B}_{B_d} = 1.30(6), \quad \hat{B}_{B_s} = 1.32(5) \quad \text{Ref. [30]}, \quad (183)$$

$$\xi = 1.225(31), \quad B_{B_s}/B_{B_d} = 1.007(21) \quad \text{Ref. [30]}. \quad (184)$$

The continuum-limit measure, $\delta(a_{\min})$, cannot be estimated for the ETM 13B results for \hat{B}_{B_d} because the relevant continuum-limit information is not provided. For the other quantities of ETM 13B, $\delta(a_{\min}) \simeq 0.1$ (\hat{B}_{B_d}), 2 (ξ) and 0.7 (B_{B_s}/B_{B_d}).

For $N_f = 2+1$ the results that enter our averages for $N_f = 2+1$ are FNAL/MILC 16 [70], which had been included in the averages at FLAG 19 [1], RBC/UKQCD 14A [42], included in the averages at FLAG 16 [77], and HPQCD 09 [45] for which a description is available in

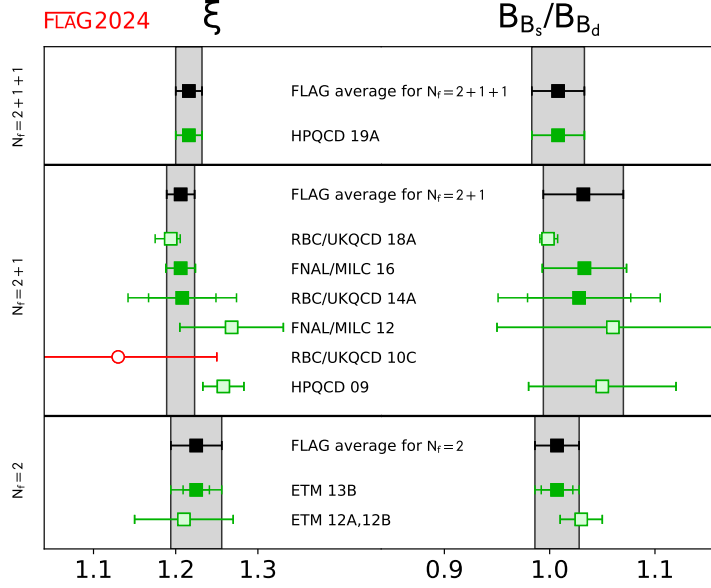


Figure 24: The SU(3)-breaking quantities ξ and B_{B_s}/B_{B_d} [values in Tab. 36 and Eqs. (184), (187), (190)].

FLAG 13 [68]. The work in RBC/UKQCD 18A [56] on the flavour SU(3)-breaking ratios, whose description can be found in FLAG 21 [39], has not been published yet and therefore do not enter into the averages. Thus, the averages for $N_f = 2 + 1$ are unchanged:

$$N_f = 2 + 1 :$$

$$f_{B_d} \sqrt{\hat{B}_{B_d}} = 225(9) \text{ MeV}, \quad f_{B_s} \sqrt{\hat{B}_{B_s}} = 274(8) \text{ MeV} \quad \text{Refs. [42, 45, 70]}, \quad (185)$$

$$\hat{B}_{B_d} = 1.30(10), \quad \hat{B}_{B_s} = 1.35(6) \quad \text{Refs. [42, 45, 70]}, \quad (186)$$

$$\xi = 1.206(17), \quad B_{B_s}/B_{B_d} = 1.032(38) \quad \text{Refs. [42, 70]}. \quad (187)$$

Here all the above equations have not been changed from FLAG 19. The averages were obtained using the nested averaging scheme described in Sec. 2.3.2, due to a nested correlation structure among the results. Details are discussed in the FLAG 19 report [1].

We estimate $\delta(a_{\min}) \simeq 2$ for both \hat{B}_{B_s} and \hat{B}_{B_d} of FNAL/MILC 16. Data are not available in FNAL/MILC 16 to estimate $\delta(a_{\min})$ for the ratio of the bag parameters. Since the $f_{B_s} \sqrt{\hat{B}_{B_s}}$, $f_{B_d} \sqrt{\hat{B}_{B_d}}$ and ξ are quantities derived using PDG estimates of the decay constants and their ratio, we do not provide an estimate of $\delta(a_{\min})$ of these quantities. For RBC/UKQCD 14A, $\delta(a_{\min}) \simeq 0.7$ ($f_{B_d} \sqrt{\hat{B}_{B_d}}$), 1.3 ($f_{B_s} \sqrt{\hat{B}_{B_s}}$), 0.3 (ξ), 0.3 (\hat{B}_{B_d}), 0.4 (\hat{B}_{B_s}) and 0 (B_{B_s}/B_{B_d}). For HPQCD 09, $\delta(a_{\min}) \simeq 0.8$ ($f_{B_d} \sqrt{\hat{B}_{B_d}}$), 3 ($f_{B_s} \sqrt{\hat{B}_{B_s}}$), 0.3 (ξ), at most 1 (\hat{B}_{B_d}), 0.8 (\hat{B}_{B_s}) and 1 (B_{B_s}/B_{B_d}).

We note that, for $N_f = 2 + 1$, there is an on-going study involving the JLQCD and

RBC/UKQCD collaborations, with initial results reported in the Lattice 2021 proceedings [78]. These results utilize coarse lattices at the physical point from RBC/UKQCD along with very fine lattices from JLQCD (up to $a^{-1} = 4.5$ GeV) with unphysical pion masses, both using domain-wall fermions.

The only result available for $N_f = 2 + 1 + 1$ is HPQCD 19A [71], which uses MILC collaboration's HISQ ensembles and NRQCD for the b quark. A detailed description can be found in the previous review [39]. We quote their values as the FLAG estimates

$$N_f = 2 + 1 + 1:$$

$$f_{B_d} \sqrt{\hat{B}_{b_d}} = 210.6(5.5) \text{ MeV}, \quad f_{B_s} \sqrt{\hat{B}_{B_s}} = 256.1(5.7) \text{ MeV} \quad \text{Ref. [71]}, \quad (188)$$

$$\hat{B}_{B_d} = 1.222(61), \quad \hat{B}_{B_s} = 1.232(53) \quad \text{Ref. [71]}, \quad (189)$$

$$\xi = 1.216(16), \quad B_{B_s}/B_{B_d} = 1.008(25) \quad \text{Ref. [71]}. \quad (190)$$

We estimate $\delta(a_{\min}) \simeq 0.1$ for \hat{B}_{B_s} , 1 for B_{B_s}/B_{B_d} and at most 1 for \hat{B}_{B_d} . The other quantities are derived ones using the estimates of decay constants in FNAL/MILC 17.

We note that the above results with the same N_f (e.g., those in Eqs. (188–190)) are all correlated with each other, due to the use of the same gauge-field ensembles for different quantities. The results are also correlated with the averages obtained in Sec. 8.1 and shown in Eqs. (162)–(164) for $N_f = 2$, Eqs. (165)–(167) for $N_f = 2 + 1$ and Eqs. (168)–(170) for $N_f = 2 + 1 + 1$. This is because the calculations of B -meson decay constants and mixing quantities are performed on the same (or on similar) sets of ensembles, and results obtained by a given collaboration use the same actions and setups. These correlations must be considered when using our averages as inputs to unitarity triangle (UT) fits. For this reason, if one were for example to estimate $f_{B_s} \sqrt{\hat{B}_s}$ from the separate averages of f_{B_s} (Eq. (166)) and \hat{B}_s (Eq. (186)) for $N_f = 2 + 1$, one would obtain a value about one standard deviation below the one quoted above in Eq. (185). While these two estimates lead to compatible results, giving us confidence that all uncertainties have been properly addressed, we do not recommend combining averages this way, as many correlations would have to be taken into account to properly assess the errors. We recommend instead using the numbers quoted above. In the future, as more independent calculations enter the averages, correlations between the lattice-QCD inputs to UT fits will become less significant.

8.3 Semileptonic form factors for B decays to light flavours

The Standard Model differential rate for the decay $B_{(s)} \rightarrow P \ell \nu$ involving a quark-level $b \rightarrow u$ transition is given, at leading order in the weak interaction, by a formula analogous to the one for D decays in Eq. (133), but with $D \rightarrow B_{(s)}$ and the relevant CKM matrix element $|V_{cq}| \rightarrow |V_{ub}|$:

$$\begin{aligned} \frac{d\Gamma(B_{(s)} \rightarrow P \ell \nu)}{dq^2} &= \frac{G_F^2 |\eta_{EW}|^2 |V_{ub}|^2 (q^2 - m_\ell^2)^2 \sqrt{E_P^2 - m_P^2}}{24\pi^3 q^4 m_{B_{(s)}}^2} \\ &\times \left[\left(1 + \frac{m_\ell^2}{2q^2} \right) m_{B_{(s)}}^2 (E_P^2 - m_P^2) |f_+(q^2)|^2 \right. \\ &\quad \left. + \frac{3m_\ell^2}{8q^2} (m_{B_{(s)}}^2 - m_P^2)^2 |f_0(q^2)|^2 \right]. \end{aligned} \quad (191)$$

Again, for $\ell = e, \mu$ the contribution from the scalar form factor f_0 can be neglected, and one has a similar expression to Eq. (135), which, in principle, allows for a direct extraction of $|V_{ub}|$ by matching theoretical predictions to experimental data. However, while for D (or K) decays the entire physical range $0 \leq q^2 \leq q_{\max}^2$ can be covered with moderate momenta accessible to lattice simulations, in $B \rightarrow \pi \ell \nu$ decays one has $q_{\max}^2 \sim 26 \text{ GeV}^2$ and only part of the full kinematic range is reachable. As a consequence, obtaining $|V_{ub}|$ from $B \rightarrow \pi \ell \nu$ is more complicated than obtaining $|V_{cd(s)}|$ from semileptonic D -meson decays.

In practice, lattice computations are restricted to large values of the momentum transfer q^2 (see Sec. 7.2) where statistical and momentum-dependent discretization errors can be controlled, which in existing calculations roughly cover the upper third of the kinematically allowed q^2 range.³ Since, on the other hand, the decay rate is suppressed by phase space at large q^2 , most of the semileptonic $B \rightarrow \pi$ events are observed in experiment at lower values of q^2 , leading to more accurate experimental results for the binned differential rate in that region.⁴ It is, therefore, a challenge to find a window of intermediate values of q^2 at which both the experimental and lattice results can be reliably evaluated.

State-of-the-art determinations of CKM matrix elements, say, $|V_{ub}|$, are obtained from joint fits to lattice and experimental results, keeping the relative normalization $|V_{ub}|^2$ as a free parameter. This requires, in particular, that both experimental and lattice data for the q^2 -dependence be parameterized by fitting data to specific ansätze, with the ultimate aim of minimizing the systematic uncertainties involved. This plays a key role in assessing the systematic uncertainties of CKM determinations, and will be discussed extensively in this section. A detailed discussion of the parameterization of form factors as a function of q^2 can be found in Appendix B.2.

8.3.1 Form factors for $B \rightarrow \pi \ell \nu$

The semileptonic decay process $B \rightarrow \pi \ell \nu$ enables the determination of the CKM matrix element $|V_{ub}|$ within the Standard Model via Eq. (191). Early results for $B \rightarrow \pi \ell \nu$ form factors came from the HPQCD [80] and FNAL/MILC [81] collaborations (HPQCD 06 and FNAL/MILC 08A).

Our 2016 review featured a significantly extended calculation of $B \rightarrow \pi \ell \nu$ from FNAL/MILC [82] (FNAL/MILC 15) and a new computation from RBC/UKQCD [83] (RBC/UKQCD 15). In 2022, the JLQCD collaboration published another new calculation using Möbius Domain Wall fermions – JLQCD 22 [84]. FNAL/MILC and RBC/UKQCD continue working on further new calculations of the $B \rightarrow \pi$ form factors and have reported on their progress at the annual Lattice conferences and the 2020 Asia-Pacific Symposium for Lattice Field Theory. The results are preliminary or blinded, so not yet ready for inclusion in this review. FNAL/MILC is using $N_f = 2 + 1 + 1$ HISQ ensembles with $a \approx 0.15, 0.12, 0.088 \text{ fm}, 0.057 \text{ fm}$, with Goldstone-pion mass down to its physical value [85, 86]. The RBC/UKQCD Collaborations have added a new Möbius-domain-wall-fermion ensemble with $a \approx 0.07 \text{ fm}$ and $m_\pi \approx 230 \text{ MeV}$ to their analysis [87]. In addition, HPQCD using MILC ensembles had published the first $N_f = 2 + 1 + 1$ results for the $B \rightarrow \pi \ell \nu$ scalar form factor, working at zero recoil ($q^2 = q_{\max}^2$) and pion masses

³The variance of hadron correlation functions at nonzero three-momentum is dominated at large Euclidean times by zero-momentum multiparticle states [79]; therefore the noise-to-signal grows more rapidly than for the vanishing three-momentum case.

⁴Upcoming data from Belle II are expected to significantly improve the precision of experimental results, in particular, for larger values of q^2 .

down to the physical value [88]; this adds to previous reports on ongoing work to upgrade their 2006 computation [89, 90]. Since this latter result has no immediate impact on current $|V_{ub}|$ determinations, which come from the vector-form-factor-dominated decay channels into light leptons, we will from now on concentrate on the $N_f = 2 + 1$ determinations of the q^2 -dependence of $B \rightarrow \pi$ form factors.

Both the HPQCD 06 and the FNAL/MILC 15 computations of $B \rightarrow \pi \ell \nu$ amplitudes use ensembles of gauge configurations with $N_f = 2 + 1$ flavours of rooted staggered quarks produced by the MILC collaboration; however, FNAL/MILC 15 makes a much more extensive use of the currently available ensembles, both in terms of lattice spacings and light-quark masses. HPQCD 06 has results at two values of the lattice spacing ($a \approx 0.12, 0.09$ fm), while FNAL/MILC 15 employs four values ($a \approx 0.12, 0.09, 0.06, 0.045$ fm). Lattice-discretization effects are estimated within heavy-meson rooted staggered chiral perturbation theory (HMrS χ PT) in the FNAL/MILC 15 computation, while HPQCD 06 quotes the results at $a \approx 0.12$ fm as central values and uses the $a \approx 0.09$ fm results to quote an uncertainty. The relative scale is fixed in both cases through the quark-antiquark potential-derived ratio r_1/a . HPQCD 06 set the absolute scale through the Υ 2S–1S splitting, while FNAL/MILC 15 uses a combination of f_π and the same Υ splitting, as described in Ref. [35]. The spatial extent of the lattices employed by HPQCD 06 is $L \simeq 2.4$ fm, save for the lightest-mass point (at $a \approx 0.09$ fm) for which $L \simeq 2.9$ fm. FNAL/MILC 15, on the other hand, uses extents up to $L \simeq 5.8$ fm, in order to allow for light-pion masses while keeping finite-volume effects under control.

Indeed, while in the HPQCD 06 work the lightest RMS pion mass is 400 MeV, the FNAL/MILC 15 work includes pions as light as 165 MeV—in both cases the bound $m_\pi L \gtrsim 3.8$ is kept. Other than the qualitatively different range of MILC ensembles used in the two computations, the main difference between HPQCD 06 and FNAL/MILC 15 lies in the treatment of heavy quarks. HPQCD 06 uses the NRQCD formalism, with a 1-loop matching of the relevant currents to the ones in the relativistic theory. FNAL/MILC 15 employs the clover action with the Fermilab interpretation, with a mostly-nonperturbative renormalization of the relevant currents, within which the overall renormalization factor of the heavy-light current is written as a product of the square roots of the renormalization factors of the light-light and heavy-heavy temporal vector currents (which are determined nonperturbatively) and a residual factor that is computed using 1-loop perturbation theory. (See Tab. 37; full details about the computations are provided in tables in Appendix C.5.3.)

The RBC/UKQCD 15 computation is based on $N_f = 2 + 1$ DWF ensembles at two values of the lattice spacing ($a \approx 0.12, 0.09$ fm), and pion masses in a narrow interval ranging from slightly above 400 MeV to slightly below 300 MeV, keeping $m_\pi L \gtrsim 4$. The scale is set using the Ω^- baryon mass. Discretization effects coming from the light sector are estimated in the 1% ballpark using HM χ PT supplemented with effective higher-order interactions to describe cutoff effects. The b quark is treated using the Columbia RHQ action, with a mostly nonperturbative renormalization of the relevant currents. Discretization effects coming from the heavy sector are estimated with power-counting arguments to be below 2%. The collaboration has also reported on progress toward an improved calculation that adds a third, finer lattice spacing [91].

The JLQCD 22 calculation is using Möbius Domain Wall fermions, including for the heavy quark, with $a \approx 0.08, 0.055$, and 0.044 fm and pion masses down to 230 MeV. The relative scales are set using the gradient-flow time $t_0^{1/2}/a$, with the absolute scale $t_0^{1/2}$ taken from

Ref. [92]. All ensembles have $m_\pi L \gtrsim 4.0$. The bare heavy-quark masses satisfy $am_Q < 0.7$ and reach from the charm mass up to 2.44 times the charm mass. The form factors are extrapolated linearly in $1/m_Q$ to the bottom mass. For the lower range of the quark masses, the vector current is renormalized using a factor $Z_{V_{qq}}$ obtained from position-space current-current correlators. For heavier quark masses, $\sqrt{Z_{V_{QQ}}Z_{V_{qq}}}$ is used, where $Z_{V_{QQ}}$ is the renormalization factor of the flavour-conserving temporal vector current, determined using charge conservation. This corresponds to mostly nonperturbative renormalization with tree-level residual matching factors, but the residual matching factors are expected to be close to 1 and approach this value exactly in the continuum limit. We therefore assign a ○ rating for renormalization.

Given the large kinematical range available in the $B \rightarrow \pi$ transition, chiral extrapolations are an important source of systematic uncertainty: apart from the eventual need to reach physical pion masses in the extrapolation, the applicability of χ PT is not guaranteed for large values of the pion energy E_π . Indeed, in all computations E_π reaches values in the 1 GeV ballpark, and chiral-extrapolation systematics is the dominant source of errors. FNAL/MILC uses SU(2) NLO HMrS χ PT for the continuum-chiral extrapolation, supplemented by NNLO analytic terms and hard-pion χ PT terms [93];⁵ systematic uncertainties are estimated through an extensive study of the effects of varying the specific fit ansatz and/or data range. RBC/UKQCD and JLQCD use SU(2) hard-pion HM χ PT to perform their combined continuum-chiral extrapolations, and obtain estimates for systematic uncertainties by varying the ansätze and ranges used in fits. HPQCD performs chiral extrapolations using HMrS χ PT formulae, and estimates systematic uncertainties by comparing the result with the ones from fits to a linear behaviour in the light-quark mass, continuum HM χ PT, and partially quenched HMrS χ PT formulae (including also data with different sea and valence light-quark masses).

FNAL/MILC 15, RBC/UKQCD 15, and JLQCD 22 describe the q^2 -dependence of f_+ and f_0 by applying a BCL parameterization to the form factors extrapolated to the continuum limit, within the range of values of q^2 covered by data. (A discussion of the various parameterizations can be found in Appendix B.2.) RBC/UKQCD 15 and JLQCD 22 generate synthetic data for the form factors at some values of q^2 (evenly spaced in z) from the continuous function of q^2 obtained from the joint chiral-continuum extrapolation, which are then used as input for the fits. After having checked that the kinematical constraint $f_+(0) = f_0(0)$ is satisfied within errors by the extrapolation to $q^2 = 0$ of the results of separate fits, this constraint is imposed to improve fit quality. In the case of FNAL/MILC 15, rather than producing synthetic data a functional method is used to extract the z -parameterization directly from the fit functions employed in the continuum-chiral extrapolation. In the case of HPQCD 06, the parameterization of the q^2 -dependence of form factors is somewhat intertwined with chiral extrapolations: a set of fiducial values $\{E_\pi^{(n)}\}$ is fixed for each value of the light-quark mass, and $f_{+,0}$ are interpolated to each of the $E_\pi^{(n)}$; chiral extrapolations are then performed at fixed E_π (i.e., m_π and q^2 are varied subject to $E_\pi = \text{constant}$). The interpolation is performed using a Ball-Zwicky (BZ) ansatz [95]. The q^2 -dependence of the resulting form factors in the chiral limit is then described by means of a BZ ansatz, which is cross-checked against Becirevic-Kaidalov (BK) [96], Richard Hill (RH) [97], and Boyd-Grinstein-Lebed (BGL) [98]

⁵It is important to stress the finding in Ref. [94] that the factorization of chiral logs in hard-pion χ PT breaks down, implying that it does not fulfill the expected requisites for a proper effective field theory. Its use to model the mass dependence of form factors can thus be questioned.

Collaboration	Ref.	N_f		publication status	continuum extrapolation	chiral extrapolation	finite volume	renormalization	heavy-quark treatment	z -parameterization
JLQCD 22	[84]	2+1	A	★	○	★	○	✓		BCL
FNAL/MILC 15	[82]	2+1	A	★	○	★	○	✓		BCL
RBC/UKQCD 15	[83]	2+1	A	○	○	○	○	✓		BCL
HPQCD 06	[80]	2+1	A	○	○	○	○	✓		n/a

Table 37: Results for the $B \rightarrow \pi \ell \nu$ semileptonic form factor.

parameterizations (see Appendix B.2), finding agreement within the quoted uncertainties. Unfortunately, the correlation matrix for the values of the form factors at different q^2 is not provided, which severely limits the possibilities of combining them with other computations into a global z -parameterization.

The different ways in which the current results are presented do not allow a straightforward averaging procedure. RBC/UKQCD 15 only provides synthetic values of f_+ and f_0 at a few values of q^2 as an illustration of their results, and FNAL/MILC 15 does not quote synthetic values at all. In both cases, full results for BCL z -parameterizations defined by Eq. (524) are quoted. In the case of HPQCD 06, unfortunately, a fit to a BCL z -parameterization is not possible, as discussed above.

In order to combine these form factor calculations, we start from sets of synthetic data for several q^2 values. HPQCD 06, RBC/UKQCD 15, and JLQCD 22 directly provide this information; FNAL/MILC 15 present only fits to a BCL z -parameterization from which we can easily generate an equivalent set of form factor values. It is important to note that in both the RBC/UKQCD 15 and JLQCD 22 synthetic data and the FNAL/MILC z -parameterization fits the kinematic constraint at $q^2 = 0$ is automatically included (in the FNAL/MILC 15 case the constraint is manifest in an exact degeneracy of the (a_n^+, a_n^0) covariance matrix). Due to these considerations, in our opinion, the most accurate procedure is to perform a simultaneous fit to all synthetic data for the vector and scalar form factors. Unfortunately, the absence of information on the correlation in the HPQCD 06 result between the vector and scalar form factors even at a single q^2 point makes it impossible to include consistently this calculation in the overall fit. In fact, the HPQCD 06 and FNAL/MILC 15 statistical uncertainties are highly correlated (because they are based on overlapping subsets of MILC $N_f = 2 + 1$ ensembles) and, without knowledge of the $f_+ - f_0$ correlation we are unable to construct the HPQCD 06-FNAL/MILC 15 off-diagonal entries of the overall covariance matrix.

In conclusion, we will present as our best result a combined vector and scalar form factor fit to the FNAL/MILC 15, RBC/UKQCD 15, and JLQCD 22 results that we treat as completely uncorrelated.

$$B \rightarrow \pi \ (N_f = 2 + 1)$$

	Central Values	Correlation Matrix				
a_0^+	0.423 (21)	1	-0.00466	-0.0749	0.402	0.0920
a_1^+	-0.507 (93)	-0.00466	1	0.498	-0.0556	0.659
a_2^+	-0.75 (34)	-0.0749	0.498	1	-0.152	0.677
a_0^0	0.561 (24)	0.402	-0.0556	-0.152	1	-0.548
a_1^0	-1.42 (11)	0.0920	0.659	0.677	-0.548	1

Table 38: Coefficients and correlation matrix for the $N^+ = N^0 = 3$ z -expansion fit of the $B \rightarrow \pi$ form factors f_+ and f_0 . The coefficient a_2^0 is fixed by the $f_+(q^2 = 0) = f_0(q^2 = 0)$ constraint. The chi-square per degree of freedom is $\chi^2/\text{dof} = 43.6/12$ and the errors on the z -parameters have been rescaled by $\sqrt{\chi^2/\text{dof}} = 1.9$. The lattice calculations that enter this fit are taken from FNAL/MILC 15 [82], RBC/UKQCD 15 [83] and JLQCD 22 [84]. The parameterizations are defined in Eqs. (524) and (525). The form factors can be reconstructed using parameterization and inputs given in Appendix B.3.2.

The resulting data set is then fitted to the BCL parameterization in Eqs. (524) and (525). We assess the systematic uncertainty due to truncating the series expansion by considering fits to different orders in z . In Fig. 25 (left), we show $(1 - q^2/m_{B^*}^2)f_+(q^2)$ and $f_0(q^2)$ versus z ; Fig. 25 (right) shows the full form factors versus q^2 . The fit has $\chi^2/\text{dof} = 43.6/12$ with $N^+ = N^0 = 3$. The poor quality of the fit is caused by tensions between the results from the different collaborations; in particular in the slopes of f_0 , which are very constrained due to strong correlations between data points. We have therefore rescaled the uncertainties of the z parameters by $\sqrt{\chi^2/\text{dof}} = 1.9$. We point out that tensions in the form factors, especially in f_0 , might be an artifact associated with the basis of form factors employed to take the continuum limit, as explained in Appendix B.2. The outcome of the five-parameter $N^+ = N^0 = 3$ BCL fit to the FNAL/MILC 15, RBC/UKQCD 15, and JLQCD 22 calculations is shown in Tab. 38.

The fit shown in Tab. 38 can therefore be used as the averaged FLAG result for the lattice-computed form factor $f_+(q^2)$. The coefficient a_3^+ can be obtained from the values for $a_0^+ - a_2^+$ using Eq. (523). The coefficient a_2^0 can be obtained from all other coefficients imposing the $f_+(q^2 = 0) = f_0(q^2 = 0)$ constraint. We emphasize that future lattice-QCD calculations of semileptonic form factors should publish their full statistical and systematic correlation matrices to enable others to use the data. It is also preferable to present a set of synthetic form-factor data equivalent to the z -fit results, since this allows for an independent analysis that avoids further assumptions about the compatibility of the procedures to arrive at a given z -parameterization.⁶ It is also preferable to present covariance/correlation matrices with enough significant digits to calculate correctly all their eigenvalues.

8.3.2 Form factors for $B \rightarrow \rho \ell \nu$

Another process sensitive to $|V_{ub}|$ is $B \rightarrow \rho \ell \nu$, with experimental data available from Babar, Belle, and Belle II [99–101]. Early lattice calculations of the $B \rightarrow \rho \ell \nu$ form factors were done

⁶Note that generating synthetic data is a trivial task, but less so is choosing the number of required points and the q^2 values that lead to an optimal description of the form factors.

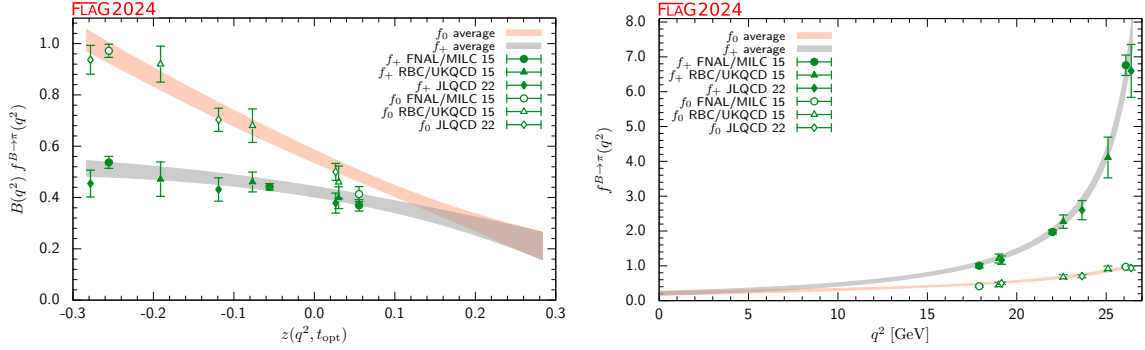


Figure 25: The form factors $f_+(q^2)$ and $f_0(q^2)$ for $B \rightarrow \pi \ell \nu$ plotted versus z (left panel) and q^2 (right panel). In the left plot, we removed the Blaschke factors. See text for a discussion of the data set. The grey and salmon bands display our preferred $N^+ = N^0 = 3$ BCL fit (five parameters).

in the quenched approximation and assumed the ρ resonance to be stable under the strong interaction [102, 103]. A proper treatment of the ρ final state requires a calculation of the $B \rightarrow \pi \pi \ell \nu$ (P wave) form factors as a function of both q^2 and $\pi\pi$ invariant mass, followed by analytic continuation to the ρ resonance pole. On the lattice, this can be done using the Lellouch-Lüscher finite-volume method [104–114]. Early lattice results for the $B \rightarrow \pi \pi \ell \nu$ P -wave vector form factor at $m_\pi \approx 320$ MeV were reported in Refs. [115, 116].

8.3.3 Form factors for $B_s \rightarrow K \ell \nu$

Similar to $B \rightarrow \pi \ell \nu$, measurements of $B_s \rightarrow K \ell \nu$ decay rates enable determinations of the CKM matrix element $|V_{ub}|$ within the Standard Model via Eq. (191). From the lattice point of view, the two channels are very similar. As a matter of fact, $B_s \rightarrow K \ell \nu$ is actually somewhat simpler, in that the kaon mass region is easily accessed by all simulations making the systematic uncertainties related to chiral extrapolation smaller. Lattice calculations of the $B_s \rightarrow K$ form factors are available from HPQCD 14 [117], RBC/UKQCD [83, 118] (RBC/UKQCD 15 and RBC/UKQCD 23), and FNAL/MILC 19 [119].

The HPQCD 14 computation uses ensembles of gauge configurations with $N_f = 2 + 1$ flavours of asqtad rooted staggered quarks produced by the MILC collaboration at two values of the lattice spacing ($a \approx 0.12, 0.09$ fm), for three and two different sea-pion masses, respectively, down to a value of 260 MeV. The b quark is treated within the NRQCD formalism, with a 1-loop matching of the relevant currents to the ones in the relativistic theory, omitting terms of $\mathcal{O}(\alpha_s \Lambda_{\text{QCD}}/m_b)$. The HISQ action is used for the valence light and s quarks. The continuum-chiral extrapolation is combined with the description of the q^2 -dependence of the form factors into a modified z -expansion (cf. Appendix B.2) that formally coincides in the continuum with the BCL ansatz. The dependence of form factors on the pion energy and quark masses is fitted to a 1-loop ansatz inspired by hard-pion χ PT [93], that factorizes out the chiral logarithms describing soft physics.

The FNAL/MILC computation (FNAL/MILC 19) coincides with HPQCD 14 in using ensembles of gauge configurations with $N_f = 2 + 1$ flavours of asqtad rooted staggered quarks produced by the MILC collaboration, but only one ensemble is shared, and a different va-

Collaboration	Ref.	N_f	publication status	continuum extrapolation	chiral extrapolation	finite volume	renormalization	heavy-quark treatment	z -parameterization
RBC/UKQCD 23*	[118]	2+1	A	★	○	★	○	✓	BGL [§]
FNAL/MILC 19	[119]	2+1	A	★	○	★	○	✓	BCL
RBC/UKQCD 15	[83]	2+1	A	○	○	○	○	✓	BCL
HPQCD 14	[117]	2+1	A	○	○	○	○	✓	BCL [†]

* Supersedes RBC/UKQCD 15.

§ Generalized as discussed in Ref. [120].

† Results from modified z -expansion.

Table 39: Summary of lattice calculations of the $B_s \rightarrow K\ell\nu$ semileptonic form factors.

lence regularization is employed; we will thus treat the two results as fully independent from the statistics point of view. FNAL/MILC 19 uses three values of the lattice spacing ($a \approx 0.12, 0.09, 0.06$ fm); only one value of the sea pion mass and the volume is available at the extreme values of the lattice spacing, while four different masses and volumes are considered at $a = 0.09$ fm. Heavy quarks are treated within the Fermilab approach. HMrS χ PT expansion is used at next-to-leading order in SU(2) and leading order in $1/M_B$, including next-to-next-to-leading-order (NNLO) analytic and generic discretization terms, to perform continuum-chiral extrapolations. Hard kaons are assumed to decouple, i.e., their effect is reabsorbed in the SU(2) LECs. Continuum- and chiral-extrapolated values of the form factors are fitted to a z -parametrization imposing the kinematical constraint $f_+(0) = f_0(0)$. See Tab. 39 and the tables in Appendix C.5.3 for full details.

The RBC/UKQCD 15 computation [83] had been published together with the $B \rightarrow \pi\ell\nu$ computation discussed in Sec. 8.3.1, all technical details being practically identical. The RBC/UKQCD 23 computation [118] (which considers $B_s \rightarrow K\ell\nu$ only) differs from RBC/UKQCD 15 by the addition of one new ensemble with a third, finer lattice spacing that also has a lower pion mass than the other ensembles, updated scale setting and updated tuning of m_s and of the RHQ parameters, and a change of the form-factor basis in which the chiral-continuum extrapolation is performed (previously: f_{\parallel} and f_{\perp} , now: f_+ and f_0). RBC/UKQCD 23 [118] furthermore uses a new method to perform extrapolations of the form factors to the full q^2 range with unitarity bounds, taking into account that the dispersive integral ranges only over an arc of the unit circle instead of the full circle [120, 121]. However, we do not use these extrapolations in performing our average and instead use the synthetic data points provided in RBC/UKQCD 23 [118]. This allows users of our average to impose their own dispersive bounds in phenomenological applications if desired, since such bounds should be imposed only once.

In order to combine the results for the q^2 -dependence of the form factors from the three

$B_s \rightarrow K$ ($N_f = 2 + 1$)

	Central Values	Correlation Matrix						
a_0^+	0.370(21)	1.	0.2781	-0.3169	-0.3576	0.6130	0.3421	0.2826
a_1^+	-0.68(10)	0.2781	1.	0.3672	0.1117	0.4733	0.8487	0.8141
a_2^+	0.55(48)	-0.3169	0.3672	1.	0.8195	0.3323	0.6614	0.6838
a_3^+	2.11(83)	-0.3576	0.1117	0.8195	1.	0.2350	0.4482	0.4877
a_0^0	0.234(10)	0.6130	0.4733	0.3323	0.2350	1.	0.6544	0.5189
a_1^0	0.135(86)	0.3421	0.8487	0.6614	0.4482	0.6544	1.	0.9440
a_2^0	0.20(35)	0.2826	0.8141	0.6838	0.4877	0.5189	0.9440	1.

Table 40: Coefficients and correlation matrix for the $N^+ = N^0 = 4$ z -expansion of the $B_s \rightarrow K$ form factors f_+ and f_0 . The coefficient a_3^0 is fixed by the $f_+(q^2 = 0) = f_0(q^2 = 0)$ constraint. The chi-square per degree of freedom is $\chi^2/\text{dof} = 3.82$ and the errors on the z -parameters have been rescaled by $\sqrt{\chi^2/\text{dof}} = 1.95$. The form factors can be reconstructed using parameterization and inputs given in Appendix B.3.3.

collaborations, we will follow a similar approach to the one adopted above for $B \rightarrow \pi \ell \nu$, and produce synthetic data from the preferred fits quoted in the papers (or use the synthetic data provided in the paper), to obtain a dataset to which a joint fit can be performed. Note that the kinematic constraint at $q^2 = 0$ is included in all three cases; we will impose it in our fit as well, since the synthetic data will implicitly depend on that fitting choice. However, it is worth mentioning that the systematic uncertainty of the resulting extrapolated value $f_+(0) = f_0(0)$ can be fairly large, the main reason being the required long extrapolation from the high- q^2 region covered by lattice data. While we stress that the average far away from the high- q^2 region has to be used carefully, it is possible that increasing the number of z coefficients beyond what is sufficient for a good description of the lattice data and using unitarity constraints to control the size of additional terms, might yield fits with a more stable extrapolation at very low q^2 . We plan to include said unitarity analysis into the next edition of the FLAG review. It is, however, important to emphasize that joint fits with experimental data, where the latter accurately map the low q^2 region, are expected to be safe.

Our fits employ a BCL ansatz with $t_+ = (M_B + M_\pi)^2$ and $t_0 = t_+ - \sqrt{t_+(t_+ - t_-)}$, with $t_- = (M_{B_s} - M_K)^2$. Our pole factors will contain a single pole in both the vector and scalar channels, for which we take the mass values $M_{B^*} = 5.32465$ GeV and $M_{B^*(0+)} = 5.68$ GeV.⁷ The constraint $f_+(0) = f_0(0)$ is imposed by expressing the coefficient $b_{N^0-1}^0$ in terms of all others. The outcome of the seven-parameter $N^+ = N^0 = 4$ BCL fit, which we quote as our preferred result, is shown in Tab. 40. The fit has a chi-square per degree of freedom $\chi^2/\text{dof} = 3.82$. Following the PDG recommendation, we rescale the whole covariance matrix by χ^2/dof : the errors on the z -parameters are increased by $\sqrt{\chi^2/\text{dof}} = 1.95$ and the correlation matrix is unaffected. The parameters shown in Tab. 40 provide the averaged FLAG results for the lattice-computed form factors $f_+(q^2)$ and $f_0(q^2)$. The coefficient a_4^+ can be obtained from the

⁷These are the values used in the FNAL/MILC 19 determination, while HPQCD 14 and RBC/UKQCD 15 use $M_{B^*(0+)} = 5.6794(10)$ GeV and $M_{B^*} = 5.63$ GeV, respectively. They also employ different values of t_+ and t_0 than employed here, which again coincide with FNAL/MILC 19's choice.

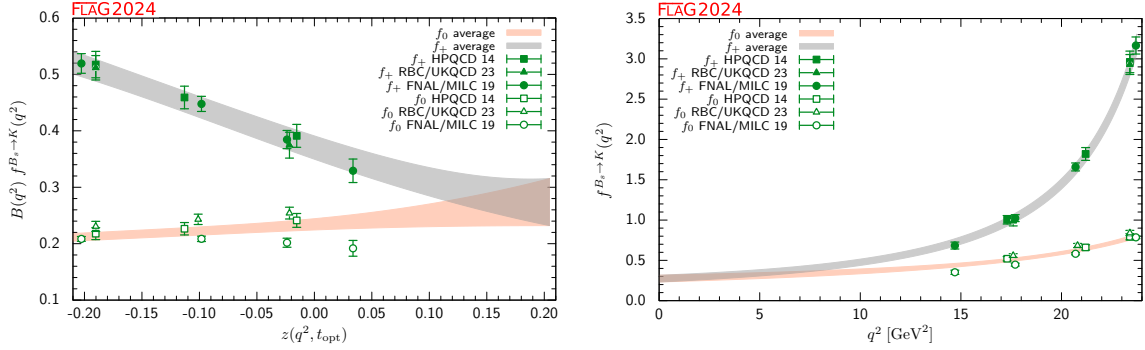


Figure 26: The form factors $f_+(q^2)$ and $f_0(q^2)$ for $B_s \rightarrow K \ell \nu$ plotted versus z (left panel) and q^2 (right panel). In the left plot, we remove the Blaschke factors. See text for a discussion of the data sets. The grey and salmon bands display our preferred $N^+ = N^0 = 4$ BCL fit (seven parameters).

values for $a_0^+ - a_3^+$ using Eq. (523). The fit is illustrated in Fig. 26.⁸ As can be seen in Fig. 26, the large value of χ^2/dof is caused by a significant tension between the lattice results from the different collaborations for f_0 . Compared to the FLAG 21 fit that used RBC/UKQCD 15, the tension has increased as the RBC/UKQCD results for f_0 have shifted upward. The tension indicates that the uncertainties have been underestimated in at least some of the calculations. One possible, at least partial, explanation was offered by the authors of RBC/UKQCD 23 [118], who found that the results for f_0 shift upward when performing the chiral/continuum extrapolation directly for f_0 and f_+ rather than f_{\parallel} and f_{\perp} as was done in RBC/UKQCD 15 and FNAL/MILC 19. Using f_0 and f_+ is argued to be the better choice because these form factors have definite J^P quantum numbers for the bound states producing poles in q^2 , and the chiral-continuum extrapolation fit functions include these poles. More details on the problems associated with taking the chiral/continuum extrapolation in the f_{\parallel} and f_{\perp} basis can be found in Appendix B.2.

A number of new calculations of the $B_s \rightarrow K$ form factors are underway. The JLQCD collaboration is using a fully-relativistic approach with Möbius domain-wall fermions [122]. FNAL/MILC is pursuing two new calculations with HISQ light quarks, one of which uses Fermilab b quarks [123] and the other uses HISQ b quarks [124].

We will conclude by pointing out progress in the application of the npHQET method to the extraction of semileptonic form factors, reported for $B_s \rightarrow K$ transitions in Ref. [125], which extends the work of Ref. [126]. This is a methodological study based on CLS $N_f = 2$ ensembles at two different values of the lattice spacing and pion masses, and full $1/m_b$ corrections are incorporated within the npHQET framework. Emphasis is on the role of excited states in the extraction of the bare form factors, which are shown to pose an impediment to reaching precisions better than a few percent.

⁸Note that in FLAG 19 [1] we had adopted the threshold $t_+ = (M_{B_s} + M_K)^2$ rather than $t_+ = (M_B + M_{\pi})^2$. This change impacted the z -range which the physical q^2 interval maps onto. We also point out that, in the FLAG 19 version of Fig. 26, the three synthetic f_0 data points from HPQCD were plotted incorrectly, but this did not affect the fit.

Collaboration	Ref.	N_f	publication status	continuum extrapolation	chiral extrapolation	finite volume	renormalization	heavy-quark treatment	z -parameterization
HPQCD 22	[132]	2+1+1	A	★	★	★	★	✓	BCL
FNAL/MILC 15D	[133]	2+1	A	★	○	★	○	✓	BCL
HPQCD 13E	[134]	2+1	A	○	○	○	○	✓	BCL

Table 41: Summary of lattice calculations of the $B \rightarrow K$ semileptonic form factors.

8.3.4 Form factors for rare and radiative B -semileptonic decays to light flavours

Lattice-QCD input is also available for some exclusive semileptonic decay channels involving neutral-current $b \rightarrow q$ transitions at the quark level, where $q = d, s$. Being forbidden at tree level in the SM, these processes allow for stringent tests of potential new physics; simple examples are $B \rightarrow K^* \gamma$, $B \rightarrow K^{(*)} \ell^+ \ell^-$, or $B \rightarrow \pi \ell^+ \ell^-$ where the B meson (and therefore the light meson in the final state) can be either neutral or charged.

The corresponding SM effective weak Hamiltonian is considerably more complicated than the one for the tree-level processes discussed above: after integrating out the top quark and the W boson, as many as ten dimension-six operators formed by the product of two hadronic currents or one hadronic and one leptonic current appear.⁹ Three of the latter, coming from penguin and box diagrams, dominate at short distances and have matrix elements that, up to small QED corrections, are given entirely in terms of $B \rightarrow (\pi, K, K^*)$ form factors. The matrix elements of the remaining seven operators can be expressed, up to power corrections whose size is still unclear, in terms of form factors, decay constants and light-cone distribution amplitudes (for the π , K , K^* and B mesons) by employing OPE arguments (at large di-lepton invariant mass) [128, 129] and results from QCD factorization (at small di-lepton invariant mass) [130]. In conclusion, the most important contributions to all of these decays are expected to come from matrix elements of current operators (vector, tensor, and axial-vector) between one-hadron states, which in turn can be parameterized in terms of a number of form factors (see Ref. [131] for a complete description).

In channels with pseudoscalar mesons in the final state, the level of sophistication of lattice calculations is similar to the $B \rightarrow \pi$ case. Early calculations of the vector, scalar, and tensor form factors for $B \rightarrow K \ell^+ \ell^-$ by HPQCD 13E [134] and FNAL/MILC 15D [133] were performed with $N_f = 2 + 1$ flavours and EFT-based heavy-quark actions. FNAL/MILC 15E also determined the form factors for $B \rightarrow \pi \ell^+ \ell^-$ [135]. Recently, HPQCD completed a new calculation of the $B \rightarrow K$ form factors with $N_f = 2 + 1 + 1$ flavours and HISQ b quarks (HPQCD 22) [132]. In the following, we present an average of the two $N_f = 2 + 1$ calculations and a comparison with HPQCD's new $N_f = 2 + 1 + 1$ results. Details of the calculations are

⁹See, e.g., Ref. [127] and references therein.

$$B \rightarrow \pi \ (N_f = 2 + 1)$$

	Central Values	Correlation Matrix			
a_0^T	0.393(17)	1.000	0.400	0.204	0.166
a_1^T	-0.65(23)	0.400	1.000	0.862	0.806
a_2^T	-0.6(1.5)	0.204	0.862	1.000	0.989
a_3^T	0.1(2.8)	0.166	0.806	0.989	1.000

Table 42: Coefficients and correlation matrix for the $N^T = 4$ z -expansion of the $B \rightarrow \pi$ form factor f_T . Results taken from Table II of Ref. [135].

provided in Tab. 41 and in Appendix C.5.4.

The $N_f = 2 + 1$ calculations both employ MILC asqtad ensembles. HPQCD 13E [136] and FNAL/MILC 15D [137] have also companion papers in which they calculate the Standard Model predictions for the differential branching fractions and other observables and compare to experiment. The HPQCD computation employs NRQCD b quarks and HISQ valence light quarks, and parameterizes the form factors over the full kinematic range using a model-independent z -expansion as in Appendix B.2, including the covariance matrix of the fit coefficients. In the case of the (separate) FNAL/MILC computations, both of them use Fermilab b quarks and asqtad light quarks, and a BCL z -parameterization of the form factors.

FNAL/MILC 15E [135] includes results for the tensor form factor for $B \rightarrow \pi \ell^+ \ell^-$ not included in previous publications on the vector and scalar form factors (FNAL/MILC 15) [82]. Nineteen ensembles from four lattice spacings are used to control continuum and chiral extrapolations. The results for $N_z = 4$ z -expansion of the tensor form factor and its correlations with the expansions for the vector and scalar form factors presented in Table II of Ref. [135], which we consider the FLAG estimate, are shown in Tab. 42. Partial decay widths for decay into light leptons or $\tau^+ \tau^-$ are presented as a function of q^2 . The former is compared with results from LHCb [138], while the latter is a prediction.

The averaging of the HPQCD 13E and FNAL/MILC 15D $N_f = 2 + 1$ results for the $B \rightarrow K$ form factors is similar to our treatment of the $B \rightarrow \pi$ and $B_s \rightarrow K$ form factors. In this case, even though the statistical uncertainties are partially correlated because of some overlap between the adopted sets of MILC ensembles, we choose to treat the two calculations as independent. The reason is that, in $B \rightarrow K$, statistical uncertainties are subdominant and cannot be easily extracted from the results presented by HPQCD 13E and FNAL/MILC 15D. Both collaborations provide only the outcome of a simultaneous z -fit to the vector, scalar and tensor form factors, that we use to generate appropriate synthetic data. We then impose the kinematic constraint $f_+(q^2 = 0) = f_0(q^2 = 0)$ and fit to a ($N^+ = N^0 = N^T = 3$) BCL parameterization. The functional forms of the form factors that we use are identical to those adopted in Ref. [137].¹⁰ The results of the fit are presented in Tab. 43. The fit is illustrated in Fig. 27. Note that the average for the f_T form factor appears to prefer the FNAL/MILC 15D synthetic data. This happens because we perform a correlated fit of the three form factors simultaneously (both FNAL/MILC 15D and HPQCD 13E present covariance matrices that include correlations between all form factors). We checked that the average for the f_T form

¹⁰Note in particular that not much is known about the sub-threshold poles for the scalar form factor. FNAL/MILC 15D includes one pole at the B_{s0}^* mass as taken from the calculation in Ref. [139].

$B \rightarrow K$ ($N_f = 2 + 1$)

	Central Values	Correlation Matrix							
a_0^+	0.471 (14)	1	0.513	0.128	0.773	0.594	0.613	0.267	0.118
a_1^+	-0.74 (16)	0.513	1	0.668	0.795	0.966	0.212	0.396	0.263
a_2^+	0.32 (71)	0.128	0.668	1	0.632	0.768	-0.104	0.0440	0.187
a_0^0	0.301 (10)	0.773	0.795	0.632	1	0.864	0.393	0.244	0.200
a_1^0	0.40 (15)	0.594	0.966	0.768	0.864	1	0.235	0.333	0.253
a_0^T	0.455 (21)	0.613	0.212	-0.104	0.393	0.235	1	0.711	0.608
a_1^T	-1.00 (31)	0.267	0.396	0.0440	0.244	0.333	0.711	1	0.903
a_2^T	-0.9 (1.3)	0.118	0.263	0.187	0.200	0.253	0.608	0.903	1

Table 43: Coefficients and correlation matrix for the $N^+ = N^0 = N^T = 3$ z -expansion of the $B \rightarrow K$ form factors f_+ , f_0 and f_T for $N_f = 2 + 1$. The coefficient a_2^0 is fixed by the $f_+(q^2 = 0) = f_0(q^2 = 0)$ constraint. The chi-square per degree of freedom is $\chi^2/\text{dof} = 1.86$ and the errors on the z -parameters have been rescaled by $\sqrt{\chi^2/\text{dof}} = 1.36$. The form factors can be reconstructed using parameterization and inputs given in Appendix B.3.4.

factor, obtained neglecting correlations with f_0 and f_+ , is a little lower and lies in between the two data sets. There is still a noticeable tension between the FNAL/MILC 15D and HPQCD 13E data for the tensor form factor; indeed, a standalone fit to these data results in $\chi_{\text{red}}^2 = 7.2/3 = 2.4$, while a similar standalone joint fit to f_+ and f_0 has $\chi_{\text{red}}^2 = 9.2/7 = 1.3$. Finally, the global fit that is shown in the figure has $\chi_{\text{red}}^2 = 18.6/10 = 1.86$.

The new $N_f = 2 + 1 + 1$ HPQCD 22 calculation of the $B \rightarrow K$ form factors [132] uses the HISQ action for all quarks including the b quark, which allows the determination of the vector- and axial-vector-current renormalization factors using Ward identities. The tensor current is renormalized using RI-SMOM [140]. The calculation is performed for multiple lighter-than-physical values of the heavy-quark mass and six different lattice spacings down to 0.044 fm; at the finest lattice spacing, the heavy-light pseudoscalar mass reaches approximately $0.94M_{B,\text{phys}}$. Three of the eight ensembles used have an approximately physical pion mass. The form factors in the physical limit are extracted from a modified BCL z -expansion fit with terms incorporating dependence on the heavy-quark mass, light and strange-quark masses, lattice spacing, and cover the entire q^2 range. The paper [132] includes supplemental files with the form-factor parameters and a Python code that can be used to reconstruct the form factors. The form factors are shown in Fig. 27 with the dark-shaded bands and are seen to be consistent with our average of the older $N_f = 2 + 1$ results. The $N_f = 2 + 1 + 1$ form factors are substantially more precise at low q^2 and somewhat less precise at high q^2 . Standard-Model predictions $B \rightarrow K\ell^+\ell^-$ and $B \rightarrow K\nu\bar{\nu}$ using these form factors are presented in a separate paper [141].

Lattice computations of form factors in channels with a vector meson in the final state face extra challenges with respect to the case of a pseudoscalar meson: the state is unstable, and the extraction of the relevant matrix element from correlation functions is significantly more complicated; χ PT cannot be used as a guide to extrapolate results at unphysically-heavy pion masses to the chiral limit. While field-theory procedures to take resonance effects into account are available [104–114], they have not yet been implemented in the available computations of

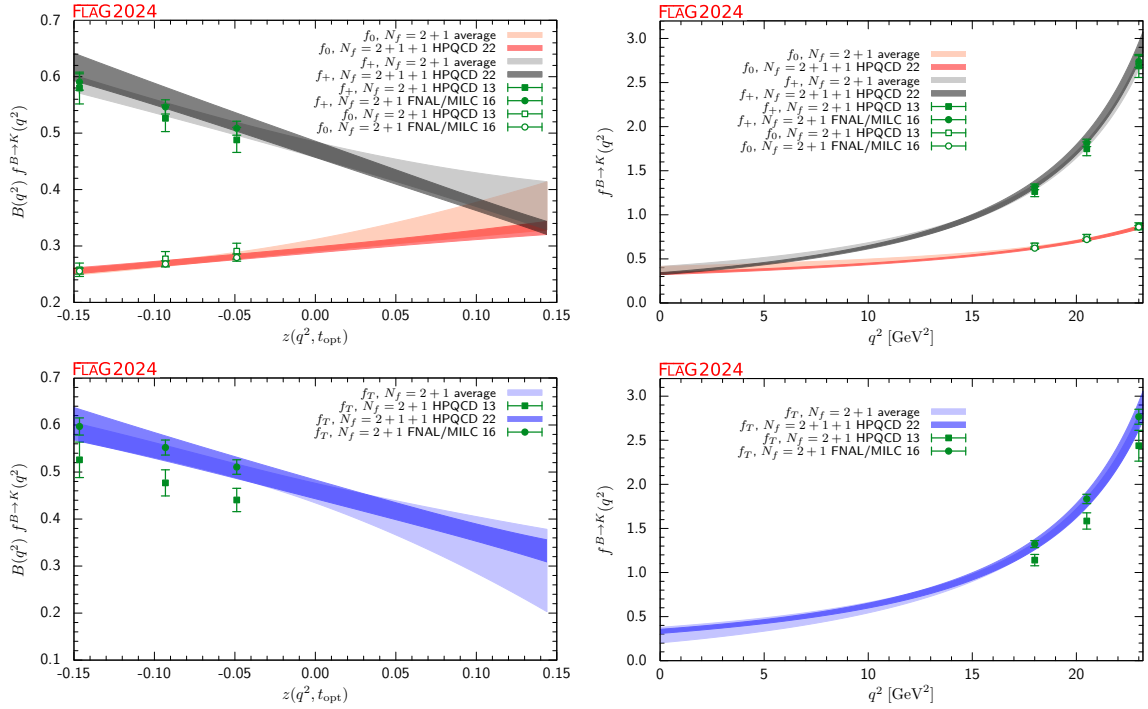


Figure 27: The $B \rightarrow K$ form factors $f_+(q^2)$, $f_0(q^2)$ and $f_T(q^2)$ plotted versus z (left panels) and q^2 (right panels). In the plots as a function of z , we remove the Blaschke factors. See text for a discussion of the data sets. The light-shaded grey, salmon and blue bands display our preferred $N^+ = N^0 = N^T = 3$ BCL fit (eight parameters) to the $N_f = 2 + 1$ lattice results. The dark-shaded grey, salmon and blue bands display the $N_f = 2 + 1 + 1$ HPQCD 22 results [132].

$B \rightarrow K^*$ and similar form factors, which therefore suffer from uncontrolled systematic errors (however, new calculations using these procedures are underway [116]).¹¹

As a consequence of the complexity of the problem, the level of maturity of these computations is significantly below the one present for pseudoscalar form factors. Therefore, we only provide a short guide to the existing results. Horgan *et al.* have obtained the seven form factors governing $B \rightarrow K^* \ell^+ \ell^-$ (as well as those for $B_s \rightarrow \phi \ell^+ \ell^-$ and for the charged-current decay $B_s \rightarrow K^* \ell \nu$) in Ref. [142] using NRQCD b quarks and asqtad staggered light quarks. In this work, they use a modified z -expansion to simultaneously extrapolate to the physical light-quark masses and fit the q^2 -dependence. As discussed above, the unstable nature of the vector mesons was not taken into account. Horgan *et al.* use their form-factor results to calculate the differential branching fractions and angular distributions and discuss the implications for phenomenology in a companion paper [143]. An update of the form factor fits that enforces endpoint relations and also provides the full correlation matrices can be found in Ref. [144]. Finally, preliminary results on $B \rightarrow K^* \ell^+ \ell^-$ and $B_s \rightarrow \phi \ell^+ \ell^-$ by RBC/UKQCD have been reported in Refs. [145–147].

8.4 Semileptonic form factors for $B_{(s)} \rightarrow D_{(s)} \ell \nu$ and $B_{(s)} \rightarrow D_{(s)}^* \ell \nu$

The semileptonic processes $B_{(s)} \rightarrow D_{(s)} \ell \nu$ and $B_{(s)} \rightarrow D_{(s)}^* \ell \nu$ have been studied extensively by experimentalists and theorists over the years. They allow for the determination of the CKM matrix element $|V_{cb}|$, an extremely important parameter of the Standard Model. The matrix element V_{cb} appears in many quantities that serve as inputs to CKM unitarity-triangle analyses and reducing its uncertainties is of paramount importance. For example, when ϵ_K , the measure of indirect CP violation in the neutral kaon system, is written in terms of the parameters ρ and η that specify the apex of the unitarity triangle, a factor of $|V_{cb}|^4$ multiplies the dominant term. As a result, the errors coming from $|V_{cb}|$ (and not those from B_K) are now the dominant uncertainty in the Standard Model (SM) prediction for this quantity.

8.4.1 $B_{(s)} \rightarrow D_{(s)}$ decays

The decay rate for $B \rightarrow D \ell \nu$ can be parameterized in terms of vector and scalar form factors in the same way as, e.g., $B \rightarrow \pi \ell \nu$ (see Sec. 8.3). The quantities directly studied are the form factors h_{\pm} defined by

$$\frac{\langle D(p_D) | i \bar{c} \gamma_{\mu} b | B(p_B) \rangle}{\sqrt{m_D m_B}} = h_+(w)(v_B + v_D)_{\mu} + h_-(w)(v_B - v_D)_{\mu}, \quad (192)$$

which are related to the standard vector and scalar form factors by

$$f_+(q^2) = \frac{1+r}{2\sqrt{r}} \left[h_+(w) - \frac{1-r}{1+r} h_-(w) \right] \equiv \frac{1+r}{2\sqrt{r}} \mathcal{G}(q^2), \quad (193)$$

$$f_0(q^2) = \sqrt{r} \left[\frac{1+w}{1+r} h_+(w) + \frac{1-w}{1-r} h_-(w) \right], \quad (194)$$

where $r = m_D/m_B$, $q^2 = (p_B - p_D)^2$, $v_A^{\mu} = p_A^{\mu}/m_A$ ($A = D, B$) are the four-velocities of the heavy mesons and $w = v_B \cdot v_D = (m_B^2 + m_D^2 - q^2)/(2m_B m_D)$.

¹¹In cases such as $B \rightarrow D^*$ transitions, that will be discussed below, this is much less of a practical problem due to the very narrow nature of the resonance.

The differential decay rate can then be written as

$$\frac{d\Gamma_{B^- \rightarrow D^0 \ell^- \bar{\nu}}}{dw} = \frac{G_F^2 m_D^3}{48\pi^3} (m_B + m_D)^2 (w^2 - 1)^{3/2} |\eta_{EW}|^2 |V_{cb}|^2 |\mathcal{G}(w)|^2, \quad (195)$$

where $\eta_{EW} = 1.0066$ is the 1-loop electroweak correction [148]. This formula does not include terms that are proportional to the lepton mass squared, which can be neglected for $\ell = e, \mu$.

Until recently, most unquenched lattice calculations for $B \rightarrow D\ell\nu$ decays focused on the form factor at zero recoil $\mathcal{G}^{B \rightarrow D}(1)$, which can then be combined with experimental input to extract $|V_{cb}|$. The main reasons for concentrating on the zero-recoil point are that (i) the decay rate then depends on a single form factor, and (ii) there are no $\mathcal{O}(\Lambda_{QCD}/m_Q)$ contributions due to Luke's theorem [149]. Since HQET sets $\lim_{m_Q \rightarrow \infty} \mathcal{G}^{B \rightarrow D}(1) = 1$ [150–152], high precision calculations of $\mathcal{G}^{B \rightarrow D}(1)$ are possible [153–155]. The application of these HQET developments to lattice calculations leads to a better control of the systematic errors, especially at zero recoil [156, 157]. In particular, the zero-recoil form factor can be computed via a double ratio in which most of the current renormalization cancels and heavy-quark discretization errors are suppressed by an additional power of Λ_{QCD}/m_Q [158].

Early computations of the form factors for $B \rightarrow D\ell\nu$ decays include $N_f = 2 + 1$ results by FNAL/MILC 04A and FNAL/MILC 13B [167, 168] for $\mathcal{G}^{B \rightarrow D}(1)$ and the $N_f = 2$ study by Atoui *et al.* [169], that in addition to providing $\mathcal{G}^{B \rightarrow D}(1)$ explored the $w > 1$ region. This latter work also provided the first results for $B_s \rightarrow D_s \ell \nu$ amplitudes, again including information about the momentum-transfer dependence. In 2014 and 2015, full results for $B \rightarrow D\ell\nu$ at $w \geq 1$ were published by FNAL/MILC 15C [161] and HPQCD 15 [159]. These works also provided full results for the scalar form factor, allowing analysis of the decay with a final-state τ . In FLAG 19 [1], we included new results for $B_s \rightarrow D_s \ell \nu$ form factors over the full kinematic range for $N_f = 2 + 1$ from HPQCD (HPQCD 17 [160] and Ref. [170]). Recently, HPQCD published new calculations of the $B_s \rightarrow D_s$ form factors in the full kinematic range [162] (HPQCD 19), now using MILC's HISQ $N_f = 2 + 1 + 1$ ensembles and using the HISQ action also for the b quark, reaching up to $m_b = 4m_c$ (unrenormalized mass) in their finest ensemble.¹² This calculation has recently been used by LHCb to determine $|V_{cb}|$ [171, 172], as discussed further in Sec. 8.9.

In the discussion below, we mainly concentrate on the latest generation of results, which allows for an extraction of $|V_{cb}|$ that incorporates information about the q^2 -dependence of the decay rate (cf. Sec. 8.9).

We will first discuss the $N_f = 2 + 1$ computations of $B \rightarrow D\ell\nu$ by FNAL/MILC 15C and HPQCD 15, both based on MILC asqtad ensembles. Full details about all the computations are provided in Tab. 44 and in the tables in Appendix C.5.5.

The FNAL/MILC 15C study [161] employs ensembles at four values of the lattice spacing ranging between approximately 0.045 fm and 0.12 fm, and several values of the light-quark mass corresponding to pions with RMS masses ranging between 260 MeV and 670 MeV (with just one ensemble with $M_\pi^{\text{RMS}} \simeq 330$ MeV at the finest lattice spacing). The b and c quarks are treated using the Fermilab approach.

¹²The ratio showed here is the ratio between the bare masses, which are inputs of the lattice action. The ratio between the renormalized masses of the quarks is usually very different from the ratio of bare masses. In order to tune the bare heavy-quark masses so they result in physical values of the renormalized quark masses, one normally tries to find out the value of the bare mass that results in a heavy meson with the right physical mass.

Collaboration	Ref.	N_f	publication status	continuum extrapolation	chiral extrapolation	finite volume	renormalization	heavy-quark treatment	$w = 1$ form factor / ratio	
HPQCD 15, HPQCD 17[159, 160]		2+1	A	○	○	○	○	✓	$\mathcal{G}^{B \rightarrow D}(1)$	1.035(40)
FNAL/MILC 15C	[161]	2+1	A	★	○	★	○	✓	$\mathcal{G}^{B \rightarrow D}(1)$	1.054(4)(8)
HPQCD 19	[162]	2+1+1	A	★	★	○*	★	✓	$\mathcal{G}^{B_s \rightarrow D_s}(1)$	1.071(37)
HPQCD 15, HPQCD 17[159, 160]		2+1	A	○	○	○	○	✓	$\mathcal{G}^{B_s \rightarrow D_s}(1)$	1.068(40)
FNAL/MILC 21	[163]	2+1	A	★	○	★	○	✓	$\mathcal{F}^{B \rightarrow D^*}(1)$	0.909(17)
JLQCD 23	[164]	2+1	A	★	○	★	○	✓	$\mathcal{F}^{B \rightarrow D^*}(1)$	0.887 (14)
HPQCD 23	[165]	2+1+1	A	★	★	★	★	✓	$\mathcal{F}^{B \rightarrow D^*}(1)$	0.903(14)
HPQCD 23	[165]	2+1+1	A	★	★	★	★	✓	$\mathcal{F}^{B_s \rightarrow D_s^*}(1)$	0.8970(92)
HPQCD 15, HPQCD 17[159, 160]		2+1	A	○	○	○	○	✓	$\mathcal{G}^{B_s \rightarrow D_s}(1)$	1.068(40)
HPQCD 20B	[166]	2+1+1	A	★	○	★	★	✓	n/a	n/a
HPQCD 15, HPQCD 17[159, 160]		2+1	A	○	○	○	○	✓	$R(D)$	0.300(8)
FNAL/MILC 15C	[161]	2+1	A	★	○	★	○	✓	$R(D)$	0.299(11)
FNAL/MILC 21	[163]	2+1	A	★	○	★	○	✓	$R(D^*)$	0.265(13)
JLQCD 23	[164]	2+1	A	★	○	★	○	✓	$R(D^*)$	0.252(22)
HPQCD 23	[165]	2+1+1	A	★	★	★	★	✓	$R(D^*)$	0.273(15)
HPQCD 23	[165]	2+1+1	A	★	★	★	★	✓	$R(D_s^*)$	0.266(9)

* The rationale for assigning a ○ rating is discussed in the text.

Table 44: Lattice results for mesonic processes involving $b \rightarrow c$ transitions. The form factor \mathcal{G} is defined in Eqs. (192, 193), the form factor \mathcal{F} is defined in Eqs. (202, 212), and the ratios R are defined in Eq. (221). Note that the results for $\mathcal{F}^{B \rightarrow D^*}(1)$, $\mathcal{F}^{B_s \rightarrow D_s^*}(1)$, $R(D^*)$ and $R(D_s^*)$ have been obtained using the results of the BGL fits described in the text and do not necessarily coincide with the results presented by the individual collaborations.

The hadronic form factor relevant for experiment, $\mathcal{G}(w)$, is then obtained from the relation $\mathcal{G}(w) = \sqrt{4r} f_+(q^2)/(1+r)$. The form factors are obtained from double ratios of three-point functions in which the flavour-conserving current renormalization factors cancel. The remaining matching factor to the flavour-changing normalized current is estimated with 1-loop lattice perturbation theory. In order to obtain $h_{\pm}(w)$, a joint continuum-chiral fit is performed to an ansatz that contains the light-quark mass and lattice-spacing dependence predicted by next-to-leading order HMrS χ PT, and the leading dependence on m_c predicted by the heavy-quark expansion ($1/m_c^2$ for h_+ and $1/m_c$ for h_-). The w -dependence, which allows for an interpolation in w , is given by analytic terms up to $(1-w)^2$, as well as a contribution from the logarithm proportional to $g_{D^*D\pi}^2$. The total resulting systematic error, determined as a function of w and quoted at the representative point $w = 1.16$ as 1.2% for f_+ and 1.1% for f_0 , dominates the final error budget for the form factors. After f_+ and f_0 have been determined as functions of w within the interval of values of q^2 covered by the computation, synthetic data points are generated to be subsequently fitted to a z -expansion of the BGL form, cf. Sec. 8.3, with pole factors set to unity. This in turn enables one to determine $|V_{cb}|$ from a joint fit of this z -expansion and experimental data. The value of the zero-recoil form factor resulting from the z -expansion is

$$\mathcal{G}^{B \rightarrow D}(1) = 1.054(4)_{\text{stat}}(8)_{\text{sys}}. \quad (196)$$

The HPQCD computations HPQCD 15 and HPQCD 17 [159, 160] use ensembles at two values of the lattice spacing, $a = 0.09, 0.12$ fm, and two and three values of light-quark masses, respectively. The b quark is treated using NRQCD, while for the c quark the HISQ action is used. The form factors studied, extracted from suitable three-point functions, are

$$\langle D_{(s)}(p_{D(s)}) | V^0 | B_{(s)} \rangle = \sqrt{2M_{B(s)}} f_{\parallel}^{(s)}, \quad \langle D_{(s)}(p_{D(s)}) | V^k | B_{(s)} \rangle = \sqrt{2M_{B(s)}} p_{D(s)}^k f_{\perp}^{(s)}, \quad (197)$$

where V_{μ} is the relevant vector current and the $B_{(s)}$ rest frame is chosen. The standard vector and scalar form factors are retrieved as

$$f_+^{(s)} = \frac{1}{\sqrt{2M_{B(s)}}} \left[f_{\parallel}^{(s)} + (M_{B(s)} - E_{D(s)}) f_{\perp}^{(s)} \right], \quad (198)$$

$$f_0^{(s)} = \frac{\sqrt{2M_{B(s)}}}{M_{B(s)}^2 - M_{D(s)}^2} \left[(M_{B(s)} - E_{D(s)}) f_{\parallel}^{(s)} + (M_{B(s)}^2 - E_{D(s)}^2) f_{\perp}^{(s)} \right]. \quad (199)$$

The currents in the effective theory are matched at 1-loop to their continuum counterparts. Results for the form factors are then fitted to a modified BCL z -expansion ansatz [98], that takes into account simultaneously the lattice spacing, light-quark masses, and q^2 -dependence. For the mass dependence, NLO chiral logarithms are included, in the form obtained in hard-pion χ PT (see footnote 40). As in the case of the FNAL/MILC 15C computation, once f_+ and f_0 have been determined as functions of q^2 , $|V_{cb}|$ can be determined from a joint fit of this z -expansion and experimental data. The papers quote for the zero-recoil vector form factor the result

$$\mathcal{G}^{B \rightarrow D}(1) = 1.035(40) \quad \mathcal{G}^{B_s \rightarrow D_s}(1) = 1.068(40). \quad (200)$$

The HPQCD 15 and FNAL/MILC 15C results for $B \rightarrow D$ differ by less than half a standard deviation (assuming they are uncorrelated, which they are not as some of the ensembles are

common) primarily because of lower precision of the former result. The dominant source of errors in the $|V_{cb}|$ determination by HPQCD 15 are discretization effects and the systematic uncertainty associated with the perturbative matching.

In order to combine the form-factor determination of HPQCD 15 and the one of FNAL/MILC 15C into a lattice average, we proceed in a similar way as with $B \rightarrow \pi \ell \nu$ and $B_s \rightarrow K \ell \nu$ above. FNAL/MILC 15C quotes synthetic values for each form factor at three values of w (or, alternatively, q^2) with a full correlation matrix, which we take directly as input. In the case of HPQCD 15, we use their preferred modified z -expansion parameterization to produce synthetic values of the form factors at five different values of q^2 (three for f_+ and two for f_0). This leaves us with a total of six (five) data points in the kinematical range $w \in [1.00, 1.11]$ for the form factor f_+ (f_0). As in the case of $B \rightarrow \pi \ell \nu$, we conservatively assume a 100% correlation of statistical uncertainties between HPQCD 15 and FNAL/MILC 15C. We then fit this data set to a BCL ansatz, using $t_+ = (M_{B^0} + M_{D^\pm})^2 \simeq 51.12 \text{ GeV}^2$ and $t_0 = (M_{B^0} + M_{D^\pm})(\sqrt{M_{B^0}} - \sqrt{M_{D^\pm}})^2 \simeq 6.19 \text{ GeV}^2$. In our fits, pole factors have been set to unity, i.e., we do not take into account the effect of sub-threshold poles, which is then implicitly absorbed into the series coefficients. The reason for this is our imperfect knowledge of the relevant resonance spectrum in this channel, which does not allow us to decide the precise number of poles needed.¹³ This, in turn, implies that unitarity bounds do not rigorously apply, which has to be taken into account when interpreting the results (cf. Appendix B.2).

With a procedure similar to what we adopted for the $B \rightarrow \pi$ and $B_s \rightarrow K$ cases, we impose the kinematic constraint at $q^2 = 0$ by expressing the $a_{N^0-1}^0$ coefficient in the z -expansion of f_0 in terms of all the other coefficients. As mentioned above, FNAL/MILC 15C provides synthetic data for f_+ and f_0 including correlations; HPQCD 15 presents the result of simultaneous z -fits to the two form factors including all correlations, thus enabling us to generate a complete set of synthetic data for f_+ and f_0 . Since both calculations are based on MILC ensembles, we then reconstruct the off-diagonal HPQCD 15-FNAL/MILC 15C entries of the covariance matrix by conservatively assuming that statistical uncertainties are 100% correlated. The FNAL/MILC 15C (HPQCD 15) statistical error is 58% (31%) of the total error for every f_+ value, and 64% (49%) for every f_0 one. Using this information we can easily build the off-diagonal block of the overall covariance matrix (e.g., the covariance between $[f_+(q_1^2)]_{\text{FNAL}}$ and $[f_0(q_2^2)]_{\text{HPQCD}}$ is $(\delta[f_+(q_1^2)]_{\text{FNAL}} \times 0.58) (\delta[f_0(q_2^2)]_{\text{HPQCD}} \times 0.49)$, where δf is the total error).

For our central value, we choose an $N^+ = N^0 = 3$ BCL fit, shown in Tab. 45. The coefficient a_3^+ can be obtained from the values for $a_0^+ - a_2^+$ using Eq. (523). We find $\chi^2/\text{dof} = 4.6/6 = 0.77$. The fit, which is dominated by the FNAL/MILC 15C calculation, is illustrated in Fig. 28.

Let us finally discuss the most recent results for $B_s \rightarrow D_s$ form factors, obtained by the HPQCD collaboration using MILC's $N_f = 2 + 1 + 1$ ensembles in Ref. [162] (HPQCD 19). Three values of the lattice spacing are used, including a very fine ensemble at $a \simeq 0.044 \text{ fm}$; the pion mass is kept fixed at around 300 MeV, and in addition at the coarser $a \simeq 0.09 \text{ fm}$ lattice an ensemble with the physical pion mass is included. The scalar current needs no renormalization because of the Partial Conservation of the Vector Current (PCVC) relation, while the vector current is nonperturbatively normalized by imposing a condition based on

¹³As noted above, this is the same approach adopted by FNAL/MILC 15C in their fits to a BGL ansatz. HPQCD 15, meanwhile, uses one single pole in the pole factors that enter their modified z -expansion, using their spectral studies to fix the value of the relevant resonance masses.

$B \rightarrow D (N_f = 2 + 1)$

a_n^i	Central Values	Correlation Matrix				
a_0^+	0.896 (10)	1	0.423	-0.231	0.958	0.596
a_1^+	-7.94 (20)	0.423	1	0.325	0.498	0.919
a_2^+	51.4 (3.2)	-0.231	0.325	1	-0.146	0.317
a_0^0	0.7821 (81)	0.958	0.498	-0.146	1	0.593
a_1^0	-3.28 (20)	0.596	0.919	0.317	0.593	1

Table 45: Coefficients and correlation matrix for the $N^+ = N^0 = 3$ z -expansion of the $B \rightarrow D$ form factors f_+ and f_0 . The chi-square per degree of freedom is $\chi^2/\text{dof} = 4.6/6 = 0.77$. The lattice calculations that enter this fit are taken from FNAL/MILC 15C [161] and HPQCD 15 [159]. The form factors can be reconstructed using parameterization and inputs given in Appendix B.3.5.

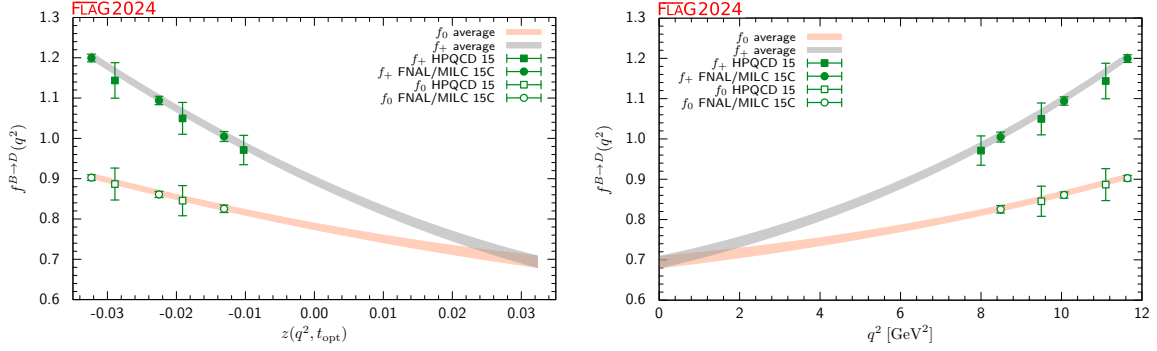


Figure 28: The form factors $f_+(q^2)$ and $f_0(q^2)$ for $B \rightarrow D\ell\nu$ plotted versus z (left panel) and q^2 (right panel). See text for a discussion of the data sets. The grey and salmon bands display our preferred $N^+ = N^0 = 3$ BCL fit (five parameters).

the PCVC relation at zero recoil. Heavy quarks are treated in a fully relativistic fashion through the use of the HISQ regularization, employing bare values of the quark mass up to $am_h = 0.8$ for the extrapolation to the physical b point.

Results for the form factors are fitted to a modified z -expansion ansatz, based on a BCL ansatz with a Blaschke factor containing one sub-threshold pole, tuned to reproduce the lattice-spacing and heavy-quark-mass-dependent mass of the corresponding resonance. The final error budget is equally dominated by statistics and the combined effect of the continuum and heavy quark mass extrapolations, which correspond to 1.1% and 1.2% uncertainties, respectively, for the scalar form factor at zero recoil. The total uncertainty of f_0 is thus below 2%, which remains true in the whole q^2 range. The uncertainty of f_+ is somewhat larger, starting at around 2% at $q^2 = 0$ and increasing up to around 3.5% at zero recoil.

One important matter of concern with this computation is the use of the $a \simeq 0.044$ fm ensemble with periodic boundary conditions, which suffers from severe topology freezing. Other than possible implications for statistical uncertainties, the lack of topology fluctuations are expected to significantly enhance finite-volume effects, which are no longer exponential

$B_s \rightarrow D_s$ ($N_f = 2 + 1 + 1$)

a_n^i	Central Values	Correlation Matrix					
a_0^0	0.666(12)	1	0.62004	0.03149	1	0.03973	0.00122
a_1^0	-0.26(25)	0.62004	1	0.36842	0.62004	0.12945	0.00002
a_2^0	-0.1(1.8)	0.03149	0.36842	1	0.03149	0.22854	-0.00168
a_0^+	0.666(12)	1	0.62004	0.03149	1	0.03973	0.00122
a_1^+	-3.24(45)	0.03973	0.12945	0.22854	0.03973	1	0.11086
a_2^+	-0.1(2.0)	0.00122	0.00002	-0.00168	0.00122	0.11086	1

Table 46: Coefficients and correlation matrix for the z -expansion of the $B_s \rightarrow D_s$ form factors f_+ and f_0 . These results are a reproduction of Table VIII of Ref. [162] (HPQCD 19). The form factors can be reconstructed using parameterization and inputs given in Appendix B.3.6.

in $m_\pi L$, but become power-like in the spatial volume. The authors neglect the impact of finite-volume effects in the computation, with a twofold argument: for the two coarser lattice spacings, the impact of pion-mass-related corrections on the heavy-meson states involved is presumably negligible; and, for the finest ensemble, the estimate of finite-volume effects on the D_s decay constant obtained in Ref. [173] turns out to be very small, a result which is presumed to extend to form factors. It is however unclear whether the latter argument would really hold, since the computation in Ref. [173] does show that the expected effect is heavily observable-dependent, reaching, e.g., more than 1% for f_D . We have, therefore, concluded that our standard criteria for finite-volume effects cannot be applied at the finest lattice spacing, and opted to assign \circ rating to them.

We thus proceed to quote the final result of HPQCD 19 as the FLAG estimate for the $N_f = 2 + 1 + 1$ $B_s \rightarrow D_s$ form factors. The preferred fit is a constrained BCL form with the imposition of the kinematical constraint $f_+(0) = f_0(0)$, carried through z^2 for f_0 and z^3 for f_+ . Both form factors contain just one sub-threshold pole, to which the masses $M_{B_c^*} = 6.329$ GeV and $M_{B_{c0}} = 6.704$ GeV, respectively, have been assigned. The fit parameters and covariance matrix, quoted in Table VIII of Ref. [162], are reproduced in Tab. 46.

There are ongoing efforts in these channels from several collaborations. The JLQCD collaboration is working on a $B \rightarrow D$ analysis at nonzero recoil using the domain-wall action for heavy and light quarks [174]. The FNAL/MILC collaborations are working on two parallel calculations of the form factors of the $B_{(s)} \rightarrow D_{(s)}$ channels sharing the same light-quark action, but with different heavy-quark actions [124].

8.4.2 $B_{(s)} \rightarrow D_{(s)}^*$ decays

The community has been focusing on the decays with final vector states, $B_{(s)} \rightarrow D_{(s)}^*$, because of increasing availability of high-quality experimental data. The decay rate for $B \rightarrow D^* \ell \nu$ involves a spin-1 hadron in the final-state whose vector and axial-vector current matrix elements

require the introduction of four form factors:

$$\frac{\langle D^* | V_\mu | B \rangle}{\sqrt{m_B m_{D^*}}} = h_V(w) \varepsilon_{\mu\nu\alpha\beta} \epsilon^{*\nu} v_{D^*}^\alpha v_B^\beta, \quad (201)$$

$$\frac{\langle D^* | A_\mu | B \rangle}{i\sqrt{m_B m_{D^*}}} = h_{A_1}(w)(1+w)\epsilon^{*\mu} - h_{A_2}(w)\epsilon^* \cdot v_B v_{B\mu} - h_{A_3}(w)\epsilon^* \cdot v_B v_{D^*\mu}. \quad (202)$$

where $w = v_B \cdot v_{D^*} = (m_B^2 + m_{D^*}^2 - q^2)/(2m_B m_{D^*})$. As has become customary, we further express the four form factors h_{V,A_1,A_2,A_3} in terms of the form factors g, f, F_1 and F_2 as follows (see, for instance, Eq. (31) of Ref. [165]):

$$g = \frac{h_V}{m_B \sqrt{r}}, \quad (203)$$

$$f = m_B \sqrt{r} (1+w) h_{A_1}, \quad (204)$$

$$F_1 = m_B^2 \sqrt{r} (1+w) \left[(w-r) h_{A_1} - (w-1)(r h_{A_2} + h_{A_3}) \right], \quad (205)$$

$$F_2 = \frac{1}{\sqrt{r}} \left[(1+w) h_{A_1} + (rw-1) h_{A_2} + (r-w) h_{A_3} \right]. \quad (206)$$

One can then write the differential decay rate as [175, 176]

$$\begin{aligned} \frac{d\Gamma_{\bar{B} \rightarrow D^* \ell \bar{\nu}}}{dw dc_v dc_l d\chi} &= \frac{\eta_{\text{EW}}^2 3m_B m_{D^*}}{4(4\pi)^4} \sqrt{w^2 - 1} (1 - 2wr + r^2) G_F^2 |V_{cb}|^2 \\ &\times \left[(1 - c_l)^2 s_v^2 H_+^2 + (1 + c_l)^2 s_v^2 H_-^2 + 4s_l^2 c_v^2 H_0^2 - 2s_l^2 s_v^2 \cos(2\chi) H_+ H_- \right. \\ &\quad \left. - 4s_l(1 - c_l) s_v c_v \cos \chi H_+ H_0 + 4s_l(1 + c_l) s_v c_v \cos \chi H_- H_0 \right], \end{aligned} \quad (207)$$

where $c_v \equiv \cos \theta_v$, $s_v \equiv \sin \theta_v$, $c_l \equiv \cos \theta_l$, $s_l \equiv \sin \theta_l$. The angles θ_v , θ_l and χ parameterize the kinematics of the three-body final state (see, for instance, Fig. 3 of Ref. [177]). The helicity amplitudes $H_{\pm,0}$ have simple expressions in terms of the form factors g, f and F_1 (see, for instance, Eq. (13) of Ref. [177]):

$$H_0 = \frac{F_1}{\sqrt{q^2}}, \quad (208)$$

$$H_{\pm} = f \mp m_B m_{D^*} \sqrt{w^2 - 1} g. \quad (209)$$

For the calculation of the ratio of the semileptonic rates in the τ and $\ell = e, \mu$ channels, it is necessary to consider the differential $d\Gamma/dw$ decay rate for nonzero lepton mass:¹⁴

$$\begin{aligned} \frac{d\Gamma_{\bar{B} \rightarrow D^* \ell \bar{\nu}}}{dw} &= |V_{cb}|^2 G_F^2 \eta_{\text{EW}}^2 \frac{m_B^3}{48\pi^3} r^2 \sqrt{w^2 - 1} \left(1 - \frac{m_\ell^2}{q^2} \right)^2 \\ &\times \left[\left(1 + \frac{m_\ell^2}{2q^2} \right) \frac{q^2}{m_B^2} (H_+^2 + H_-^2 + m_B^2 H_0^2) + \frac{3}{2} r^2 \frac{m_B^2}{q^2} m_\ell^2 (w^2 - 1) F_2^2 \right]. \end{aligned} \quad (210)$$

In the limit of vanishing lepton mass, Eq. (210) reduces to

$$\frac{d\Gamma_{B^- \rightarrow D^{*0} \ell^- \bar{\nu}}}{dw} = \frac{G_F^2 m_{D^*}^3}{4\pi^3} (m_B - m_{D^*})^2 (w^2 - 1)^{1/2} |\eta_{\text{EW}}|^2 |V_{cb}|^2 \chi(w) |\mathcal{F}(w)|^2. \quad (211)$$

¹⁴This formula can be found, for instance, in Eq. (7) of Ref. [163]. Note that in Ref. [163] the normalizations of the helicity amplitudes $H_{\pm,0}$ differ from those adopted here.

The function $\chi(w)$ in Eq. (211) depends on the recoil w and the meson masses, and reduces to unity at zero recoil [127]. In particular, the normalization factor $\chi(w)$ [127] is defined in such a way that at zero recoil

$$\mathcal{F}(1) = h_{A_1}(1) = \frac{f(1)}{2\sqrt{m_B m_{D^*}}} . \quad (212)$$

Unquenched lattice calculations for $B \rightarrow D^* \ell \nu$ decays have focused on the form factors at zero recoil $\mathcal{F}^{B \rightarrow D^*}(1)$ until a few years ago (see, for instance, FNAL/MILC 08 [178], FNAL/MILC 14 [179], HPQCD 17B [180, 181]); these can then be combined with experimental input to extract $|V_{cb}|$. The situation mirrors that of the channel $B \rightarrow D \ell \nu$: at the zero-recoil point a single form factor is enough to calculate the decay rate and Luke's theorem [149] guarantees the absence of $\mathcal{O}(\Lambda_{QCD}/m_Q)$ corrections. By heavy-quark symmetry, $\lim_{m_Q \rightarrow \infty} \mathcal{F}^{B \rightarrow D^*}(1) = 1$ [150–152], since in that limit there is no distinction between heavy quarks. The calculation of higher-order corrections to this value has been systematically addressed in several publications [153–155, 182], and also applied to lattice calculations [156, 157]. On the lattice, the zero recoil form factor of this channel can also be computed via a double ratio, cancelling most of the current renormalization and suppressing heavy-quark discretization errors by an additional power of Λ_{QCD}/m_Q [183]. The situation has dramatically improved recently, and now data away from the zero-recoil region is available from several sources. For that reason, we mainly concentrate on the latest generation of results in the discussion below, which allows for an extraction of $|V_{cb}|$ that incorporates information about the q^2 -dependence of the decay rate (cf. Sec. 8.9).

Extraction of the form factors away from the zero-recoil point is quite challenging. The polarization of the D^* plays a key role in the correlation functions, as shown in Eq. (202). One can build the following double ratio:

$$\mathcal{R}_{A_1}(\mathbf{p}) = \frac{\langle D^*(\mathbf{p}, \varepsilon_\perp) | \bar{c} \gamma_\perp \gamma_5 b | \bar{B}(\mathbf{0}) \rangle \langle \bar{B}(\mathbf{0}) | \bar{b} \gamma_\perp \gamma_5 c | D^*(\mathbf{p}, \varepsilon_\perp) \rangle}{\langle D^*(\mathbf{0}) | \bar{c} \gamma_4 c | D^*(\mathbf{0}) \rangle \langle \bar{B}(\mathbf{0}) | \bar{b} \gamma_4 b | \bar{B}(\mathbf{0}) \rangle} \propto |h_{A_1}(w)|^2, \quad (213)$$

which is proportional to $|h_{A_1}(w)|^2$, as long as the D^* is transversally polarized (the spatial components of ε_\perp are perpendicular to \mathbf{p}) and parallel to the axial current, which displays only spatial components (γ_\perp is parallel to the spatial components of ε_\perp). At zero recoil, Eq. (213) greatly simplifies to give

$$\mathcal{R}_{A_1}(\mathbf{0}) = |h_{A_1}(1)|^2. \quad (214)$$

Hence, an alternative to directly computing Eq. (213) is to evaluate Eq. (214), and then compute the following ratio

$$\mathcal{Q}_{A_1} = \frac{\langle D^*(\mathbf{p}, \varepsilon_\perp) | \bar{c} \gamma_\perp \gamma_5 b | \bar{B}(\mathbf{0}) \rangle}{\langle D^*(\mathbf{0}, \varepsilon) | \bar{c} \gamma_j \gamma_5 b | \bar{B}(\mathbf{0}) \rangle}, \quad (215)$$

which gives $h_{A_1}(w)/h_{A_1}(1)$ times extra factors that must be removed. Other form factors can be extracted by considering other polarizations and components of the axial current in Eq. (202), as well as the vector current. Normally, all the form factors are referenced to $h_{A_1}(w)$, therefore any systematics associated to the extraction of $h_{A_1}(w)$ are carried over to the remaining form factors.

Currently, there are two $N_f = 2+1$ calculations of the $B \rightarrow D^* \ell \nu$ form factors. One comes from the FNAL/MILC collaborations [163] (FNAL/MILC 21). It uses 15 MILC $N_f = 2+1$ ensembles generated with asqtad staggered quarks in the sea. The bottom and charm quarks are simulated using the clover action with the Fermilab interpretation, and they are tuned to their physical masses by using the D_s and the B_s mesons as references. This implies that the renormalization cannot be fully nonperturbative. The collaboration employs a clever scheme that computes ratios where the largest component of the renormalization factors cancels out, leaving a small component that is computed perturbatively. The MILC ensembles employed span five lattice spacings, ranging from $a \approx 0.15$ fm to $a \approx 0.045$ fm, and as many as five values of the light-quark masses per ensemble (though just one at the finest lattice spacing). Results are then extrapolated to the physical, continuum/chiral, limit employing staggered, heavy-light meson χ PT.

The D^* meson is not a stable particle in QCD and decays predominantly into a D plus a pion. Nevertheless, heavy-light meson χ PT can be applied to extrapolate lattice simulation results for the $B \rightarrow D^* \ell \nu$ form factor to the physical light-quark mass. The D^* width is quite narrow, 0.083(2) MeV for the $D^{*\pm}$ (2010) and less than 2.1 MeV for the D^{*0} (2007) [15], making this system much more stable and long lived than the ρ or the K^* systems. Therefore it is appropriate to consider the D^* as a stable particle on the lattice, at the current level of precision. The fact that the $D^* - D$ mass difference is close to the pion mass leads to the well-known “cusp” in \mathcal{R}_{A_1} just above the physical pion mass [183–185]. This cusp makes the chiral extrapolation sensitive to values used in the χ PT formulas for the $D^* D \pi$ coupling $g_{D^* D \pi}$. In order to take this sensitivity into account, the FNAL/MILC collaboration includes this coupling in their fits as an input prior $g_{D^* D \pi} = 0.53 \pm 0.08$, but they do not analyze the impact of such a prior in the final result. By looking at their previous calculation at zero recoil [179] (FNAL/MILC 14), which used the same ensembles and statistics, we estimate a subpercent increase in the total uncertainty for $h_{A_1}(1)$.

The final result presented in Ref. [163] (FNAL/MILC 21) is provided as synthetic data points for the four form factors in the HQET basis, $\{h_{A_1}, h_{A_2}, h_{A_3}, h_V\}$, at three different values of the recoil parameter, and a full covariance matrix. The result at zero recoil is

$$N_f = 2+1: \mathcal{F}^{B \rightarrow D^*}(1) = 0.909(17) \quad [\text{FNAL/MILC 21 [163]}] \quad (216)$$

making up a total error of 1.9%. The largest systematic uncertainty comes from discretization errors followed by effects of higher-order corrections in the chiral perturbation theory ansatz.

The JLQCD collaboration has published the other $N_f = 2+1$ study of the $B \rightarrow D^* \ell \nu$ form factors away from the zero recoil point – JLQCD 23 [164]. Their calculation is based on nine $N_f = 2+1$ Möbius domain-wall ensembles, using the same action for the valence, heavy quarks b and c . The ensembles cover three different lattice spacings, starting from 0.080 fm down to 0.044 fm, and several pion masses ranging from ~ 230 MeV to ~ 500 MeV. The charm-quark mass is always physical, whereas the largest value of the bottom-quark mass reached is $\approx 3m_c$ (unrenormalized mass) in their finest ensemble. Each ensemble features at least 3 different values of the bottom-quark mass, but in the coarsest ensemble only $m_Q \approx 1.5m_c$ is reached. In terms of lattice units, the bottom-quark mass never exceeds $am_Q \lesssim 0.7$, and the final result does not significantly change if only data with $am_Q \lesssim 0.5$ (or equivalently $m_Q \lesssim 2.0m_c$) is employed. The three-point functions leading to the form factors are evaluated for four source-sink separations to properly control the excited-states contamination, and also the effects of possible topological freezing are carefully analyzed to

rule out finite-volume effects. The renormalization scheme employed to renormalize the axial and vector currents is equivalent to a mostly nonperturbative renormalization scheme at tree level. However, the properties of the Domain-Wall action establish that $Z_A \approx Z_V$ at finite lattice spacing. Hence, we expect large cancellations of renormalization factors in ratios like Eq. (213). Also, discretization errors in the coefficients are expected to behave better than $O(a)$ for the same reason.

Physical data is obtained after performing combined chiral-continuum and heavy-quark-mass extrapolations, which employs an approximate estimator for the covariance matrix, due to the low statistics of the input data and the large number of parameters involved (heavy- and light-quark masses, and lattice spacings). The ansatz for the extrapolation is motivated by heavy-light meson χ PT and HQET, and the collaboration uses the same value for the $D^*D\pi$ coupling $g_{D^*D\pi}$ as the FNAL/MILC collaboration, $g_{D^*D\pi} = 0.53 \pm 0.08$, but instead of including it as a prior in the fit, they estimate the systematics associated to the coupling by shifting the central value by $\pm\sigma$. The uncertainty arising from this choice is not provided, although it is explicitly stated that it is small.

The collaboration provides three synthetic data points per form factor in the BGL basis, $\{g, f, F_1, F_2\}$ as their final result of their extrapolation, along with a full covariance matrix. The result at zero recoil is not directly provided, but their BGL fit results in the following value,

$$N_f = 2 + 1: \mathcal{F}^{B \rightarrow D^*}(1) = 0.887(14) \quad [\text{JLQCD 23 [164]}]. \quad (217)$$

For $N_f = 2 + 1 + 1$ there is only one calculation away from the zero-recoil point, by the HPQCD collaboration [165] – HPQCD 23. They use five MILC HISQ ensembles and the HISQ action for both the light and the heavy quarks, reaching up to $m_b = 4m_c$ (unrenormalized mass) in their finest ensemble. The lattice spacings range from 0.090 fm down to 0.044 fm, and the pion masses are physical in two of the ensembles, whereas the rest use values $m_\pi \approx 320$ MeV. They calculate the form factors for three or four bare values of the heavy-quark mass, depending on the ensemble, topping at $am_Q \leq 0.8$. For the three-point functions, three different source-sink separations are evaluated, and the currents are renormalized nonperturbatively using the PCAC/PCVC relations and, for the tensor current, the RI-SMOM scheme [140]. The renormalization factors are interpolated for some correlators in one of the coarsest ensembles, and they are estimated for the finest ensemble with a physical pion mass, adding a conservative 1% error. As in previous analyses of HPQCD with a similar setup, the impact of fixing the topological charge in the finest ensembles is not discussed; nonetheless, it has been pointed out that the impact on the form factors of MILC ensembles with nonequilibrated topological charge is below 0.1% [186]. An important difference of this analysis from the $N_f = 2 + 1$ ones is the inclusion of twisted boundary conditions to reach larger values of the recoil parameter. As a result, HPQCD 23 offers data in the whole recoil range, as opposed to the other analyses, which are limited to the range $w \in [1.0, 1.2]$. The constraint between the form factors at maximum recoil then is naturally satisfied with great precision without any need to impose it. This feature also allows them to include higher powers of $(w - 1)$ in the chiral-continuum extrapolation to model the recoil parameter dependence. Using BGL-inspired priors, the collaboration includes terms up to $(w - 1)^{10}$, stemming from a z expansion up to z^4 .

HPQCD 23 provides five synthetic data points per form factor, of which only three are completely independent, in the HQET basis, along with the full covariance matrix. The

zero-recoil value of the decay amplitude is

$$N_f = 2 + 1 + 1: \mathcal{F}^{B \rightarrow D^*}(1) = 0.903(14) \quad [\text{FLAG average, HPQCD 23 [165]}], \quad (218)$$

in agreement with the value from FNAL/MILC 21, but with a slightly smaller total error, 1.6%. The largest systematic uncertainty comes from the treatment of the heavy quark.

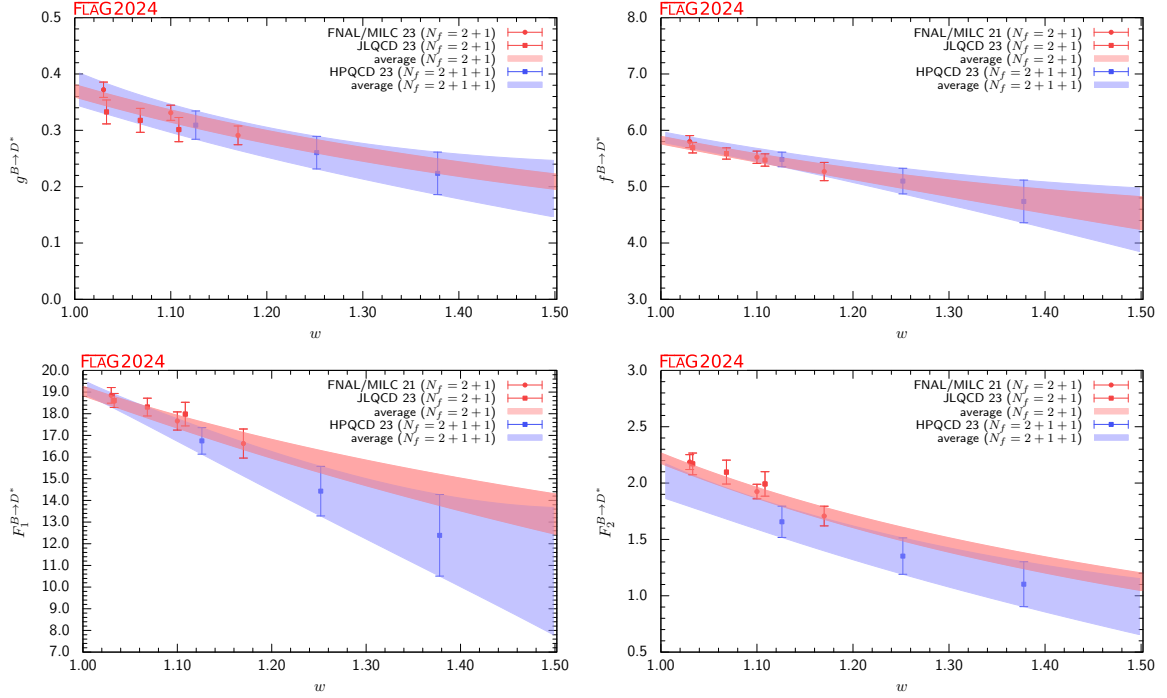


Figure 29: The form factors g , f , F_1 and F_2 for $B \rightarrow D^* \ell \nu$ as a function of w . The red band displays our preferred $(N_g, N_f, N_{F_1}, N_{F_2}) = (2, 3, 3, 2)$ BGL fit (eight parameters) to $N_f = 2 + 1$ lattice data. The constraints at zero and maximum recoil are imposed exactly. No use of unitarity constraints and priors has been made. The blue band is obtained using directly the $N_f = 2 + 1 + 1$ HPQCD 23 [165] results.

We use synthetic data points provided by FNAL/MILC 21 [163] and JLQCD 23 [164] and HPQCD 23 [165] to fit the form factors g , f , F_1 , and F_2 using a BGL parameterization. We adopt the same outer functions, poles, and z definition as in Sec. 5.1 of Ref. [163]. In particular, we impose the kinematic constraints at zero and maximal recoil (see Eqs.(72, 73) of Ref. [163]) by eliminating the coefficients $a_0^{F_1}$ and $a_0^{F_2}$. We also do not adopt priors for any of the coefficients and do not impose unitarity constraints. We found that a fit with $(N_g, N_f, N_{F_1}, N_{F_2}) = (2, 3, 3, 2)$ provides an adequate description of the lattice data.¹⁵ The results of the fits are presented in Tab. 47 and in Fig. 29. The two $N_f = 2 + 1$ calculations of FNAL/MILC 21 [163] and JLQCD 23 [164] are quite compatible and the combined fit yields

¹⁵Adequate in the sense that the coefficients do not change much when adding more terms in the z expansion, but any extra coefficient becomes unphysically large with equally large errors. Hence, our choice is the maximum number of coefficients that can be reasonably determined with the given data without including extra information, like unitarity constraints.

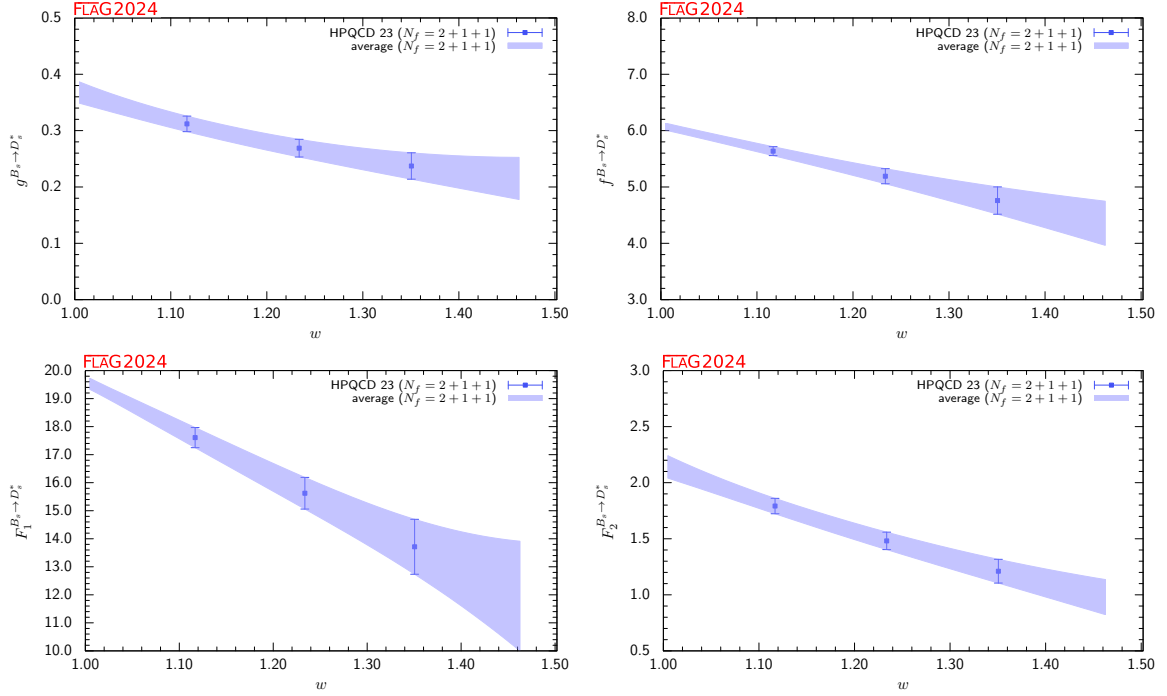


Figure 30: The form factors g , f , F_1 , and F_2 for $B_s \rightarrow D_s^* \ell \nu$ as a function of w . The blue band is obtained using directly the $N_f = 2 + 1 + 1$ HPQCD 23 [165] results.

$\chi^2_{\min}/\text{dof} = 15.0/16$. In Fig. 29, we present also the $N_f = 2 + 1 + 1$ form factors obtained directly from results of the $N_f = 2 + 1 + 1$ HPQCD 23 [165] calculation in order to allow for a direct comparison between the $N_f = 2 + 1$ and $N_f = 2 + 1 + 1$ determinations. For completeness, we present the result for $\mathcal{F}^{B \rightarrow D^*}(1)$ as extracted from the fits in Tab. 47:

$$N_f = 2 + 1: \mathcal{F}^{B \rightarrow D^*}(1) = 0.894(10) \quad [\text{FLAG average, Refs. [163, 164]}]. \quad (219)$$

Calculations in the $B_s \rightarrow D_s^*$ channel are relatively recent. The first calculations at zero recoil were done by the HPQCD collaboration in 2017 and 2019 [181, 187] (HPQCD 17B and HPQCD 19B). In 2021, the same collaboration published the first study of the form factors of this channel at nonzero recoil [188] (HPQCD 21B), using four $N_f = 2 + 1 + 1$ MILC ensembles and the HISQ regularization for both sea and valence quarks, including the b quark. The lattice spacings range from 0.090 fm to 0.044 fm, and one of the coarsest ensembles features a physical pion mass, whereas the rest are generated with $m_\pi \approx 320$ MeV. Correlators are generated for each ensemble at three/four values of the bare-quark mass, never exceeding $am_Q \leq 0.8$, and the maximum heavy-quark mass simulated is $m_Q \approx 4m_c$ (nonrenormalized). Momentum is injected using twisted boundary conditions, which allows them to calculate the form factors directly at large values of the recoil parameter. This calculation was recently superseded by a combined study of the $B_{(s)} \rightarrow D_{(s)}^*$ channels by HPQCD 23 [165], adding one more ensemble and increasing statistics. The details have already been outlined earlier in this section. Since there is only one available result (see Fig. 30), we set our $N_f = 2 + 1 + 1$

$B \rightarrow D^* (N_f = 2 + 1)$									
coeff	Central Values	Correlation Matrix							
a_0^g	0.03132(93)	1	0.1331	0.1786	0.03800	0.006578	0.06997	0.1061	0.03250
a_1^g	-0.057(26)	0.1331	1	0.001304	0.2425	0.1505	0.1342	0.1966	0.2331
a_0^f	0.01208(14)	0.1786	0.001304	1	-0.02370	0.09098	0.04710	0.1573	0.1161
a_1^f	0.0135(72)	0.03800	0.2425	-0.02370	1	-0.3968	0.6172	-0.01165	0.5136
a_2^f	-0.08(27)	0.006578	0.1505	0.09098	-0.3968	1	-0.2518	0.1880	-0.05661
$a_1^{F_1}$	-0.0032(18)	0.06997	0.1342	0.04710	0.6172	-0.2518	1	-0.1105	0.6653
$a_2^{F_1}$	-0.014(25)	0.1061	0.1966	0.1573	-0.01165	0.1880	-0.1105	1	0.5974
$a_1^{F_2}$	-0.188(44)	0.03250	0.2331	0.1161	0.5136	-0.05661	0.6653	0.5974	1

Table 47: Coefficients and correlation matrix for the $(N_g, N_f, N_{F_1}, N_{F_2}) = (2, 3, 3, 2)$ BGL fit to the $B \rightarrow D^*$ form factors g , f , F_1 and F_2 for $N_f = 2 + 1$. The form factors can be reconstructed using parameterization and inputs given in Appendix B.3.7.

average to the HPQCD 23 value [165],

$$N_f = 2 + 1 + 1: \mathcal{F}^{B_s \rightarrow D_s^*}(1) = 0.8970(92) \quad [\text{FLAG average, Ref. [165]}]. \quad (220)$$

There are still ongoing efforts on both the $B \rightarrow D^*$ and the $B_s \rightarrow D_s^*$ channels, and we can expect improvements in the coming years. The FNAL/MILC collaborations are working in two different calculations in parallel for $B \rightarrow D^*$, mainly differing on the heavy-quark action: one calculation uses Fermilab heavy quarks, whereas the other uses the HISQ action for the c and the b quarks. Both calculations employ the HISQ action for the light sector [124]. The LANL-SWME collaboration is working on a different calculation, using MILC HISQ ensembles and the Oktay-Kronfeld action for the heavy sector [189].

8.4.3 Lepton-flavour-universality ratios $R(D^{(*)})$ and $R(D_s^{(*)})$

The availability of results for the scalar form factor f_0 for $B \rightarrow D\ell\nu$ amplitudes allows us to study interesting observables that involve the decay in the τ channel. One such quantity is the ratio

$$R(D_{(s)}^{(*)}) = \frac{\mathcal{B}(B \rightarrow D_{(s)}^{(*)}\tau\nu)}{\mathcal{B}(B \rightarrow D_{(s)}^{(*)}\ell\nu)} \quad \text{with } \ell = e, \mu, \quad (221)$$

which, in the Standard Model, depends only on the form factors and hadron and lepton masses. Indeed, the recent availability of experimental results for $R(D)$ has made this quantity particularly relevant in the search for possible physics beyond the Standard Model. The most recent HFLAV average reads (see Ref. [190] and the Moriond 2024 update):

$$R(D)_{\text{exp}} = 0.342(26). \quad (222)$$

Using the FLAG average of the $B \rightarrow D$ form factors discussed above and presented in Table 45, we find $R(D)_{\text{lat}}^{\text{FLAG}} = 0.2938(38)$. The ratio $R(D)$ requires the integral of the branching ratios for $\ell = e, \mu, \tau$ over the whole phase space. Since lattice simulations are sensitive mostly to relatively large q^2 values, lattice-only calculations of $R(D)$ rely on the extrapolation of the form factors to low q^2 and are especially sensitive to the choice of parameterization. In order to estimate this source of systematics, we repeated the fit using the parameterization adopted by HPQCD in Ref. [159]. The main difference with respect to our default parameterization is the inclusion of Blaschke factors for the form factors f_+ and f_0

located at $M_+ = M_{B_c^*} = 6.330(9)$ GeV and $M_0 = 6.420(9)$ GeV $\sim M_{B_{c0}}$ ¹⁶; additionally, the parameter t_0 is set to $(m_B - m_D)^2$. Using five coefficients ($a_{1,2,3}^+$ and $a_{1,2}^0$ with a_3^0 fixed by the $f_+(q^2 = 0) = f_0(q^2 = 0)$ condition) we find $R(D)_{\text{lat}}^{\text{HPQCD}} = 0.3009(38)$ which deviates from $R(D)_{\text{lat}}^{\text{FLAG}}$ by 1.4σ . To take this potential source of systematic uncertainty into account we rescale accordingly the uncertainty of our default fit and obtain:

$$N_f = 2 + 1: R(D)_{\text{lat}} = 0.2938(54) \quad [\text{FLAG average, Refs. [159, 161]}]. \quad (223)$$

This result is about 1.5σ lower than the current experimental average [190] for this quantity. It has to be stressed that achieving this level of precision critically depends on the reliability with which the low- q^2 region is controlled by the parameterizations of the form factors.

HPQCD 17 also computes values for $R(D_s)$, the analog of $R(D)$ with both heavy-light mesons containing a strange quark. The earlier calculation using NRQCD b quarks gives

$$N_f = 2 + 1: R(D_s)_{\text{lat}} = 0.301(6) \quad [160]. \quad (224)$$

The newer calculation with HISQ b quarks, HPQCD 19, yields the somewhat more precise value

$$N_f = 2 + 1 + 1: R(D_s)_{\text{lat}} = 0.2987(46) \quad [162]. \quad (225)$$

A similar ratio $R(D^*)$ can be considered for $B \rightarrow D^*$ transitions. As a matter of fact, the experimental value of $R(D^*)$ is significantly more precise than the one of $R(D)$. The most recent HFLAV average reads (see Ref. [190] and the Moriond 2024 update):

$$R(D^*)_{\text{exp}} = 0.287(12). \quad (226)$$

The recent developments in decays with vector products have yielded a variety of new lattice results for this LFU ratio. For $N_f = 2 + 1$ in the sea, the Fermilab lattice and MILC collaborations (FNAL/MILC 21) report the value

$$N_f = 2 + 1: R(D^*)_{\text{lat}} = 0.265(13) \quad [163], \quad (227)$$

which is around 1.5σ lower than the current experimental average [190].

The JLQCD collaboration has obtained the following value (JLQCD 23)

$$N_f = 2 + 1: R(D^*)_{\text{lat}} = 0.252(22) \quad [164]. \quad (228)$$

Their result is compatible with the FNAL/MILC 21 value, but it increases the tension with the experimental average up to 1.6σ , in spite of the larger error.

The HPQCD collaboration has also computed this ratio using $N_f = 2+1+1$ configurations, obtaining (HPQCD 23)

$$N_f = 2 + 1 + 1: R(D^*)_{\text{lat}} = 0.273(15) \quad [\text{FLAG average, [165]}], \quad (229)$$

which is closer to the current HFLAV average, but still lower by 1.3σ .

Using the results of the $N_f = 2 + 1$ (FNAL/MILC 21 and JLQCD 23) [163, 164] fit summarized in Tab. 47, we calculate the following value for the ratio $R(D^*)$:

$$N_f = 2 + 1: R(D^*)_{\text{lat}} = 0.2582(51) \quad [\text{FLAG average, Refs. [163, 164]}]. \quad (230)$$

The HPQCD 23 analysis also covered the $B_s \rightarrow D_s^*$ channel, and for the first time a result for the $R(D_s^*)$ ratio is provided:

$$N_f = 2 + 1 + 1: R(D_s^*)_{\text{lat}} = 0.266(9) \quad [\text{FLAG average, Ref. [165]}]. \quad (231)$$

¹⁶The value of $M_{B_{c0}}$ is not known from experiment and here we adopted the value used by HPQCD in Ref. [159].

8.4.4 Fragmentation fraction ratio f_s/f_d

Another area of immediate interest in searches for physics beyond the Standard Model is the measurement of $B_s \rightarrow \mu^+ \mu^-$ decays, recently studied at the LHC. One of the inputs required by the LHCb analysis is the ratio of B_q meson ($q = d, s$) fragmentation fractions f_s/f_d , where f_q is the probability that a q quark hadronizes into a B_q . This ratio can be measured by writing it as a product of ratios that involve experimentally measurable quantities, cf. Refs. [191, 192]. One of the factors is the ratio $f_0^{(s)}(M_\pi^2)/f_0^{(d)}(M_K^2)$ of scalar form factors for the corresponding semileptonic meson decay, which is where lattice input becomes useful.

A dedicated $N_f = 2 + 1$ study, FNAL/MILC 12C [193] addresses the ratios of scalar form factors $f_0^{(q)}(q^2)$,¹⁷ and quotes:

$$f_0^{(s)}(M_\pi^2)/f_0^{(d)}(M_K^2) = 1.046(44)(15), \quad f_0^{(s)}(M_\pi^2)/f_0^{(d)}(M_\pi^2) = 1.054(47)(17), \quad (232)$$

where the first error is statistical and the second systematic. The more recent results from HPQCD 17 [160] are:

$$f_0^{(s)}(M_\pi^2)/f_0^{(d)}(M_K^2) = 1.000(62), \quad f_0^{(s)}(M_\pi^2)/f_0^{(d)}(M_\pi^2) = 1.006(62). \quad (233)$$

Results from both groups lead to fragmentation fraction ratios f_s/f_d that are consistent with LHCb's measurements via other methods [192].

8.5 Semileptonic form factors for $B_c \rightarrow (\eta_c, J/\psi) \ell \nu$ decays

In a recent publication, HPQCD 20B [166] provided the first full determination of $B_c \rightarrow J/\psi$ form factors, extending earlier preliminary work that also covered $B_c \rightarrow \eta_c$, Refs. [194, 195]. While the latter employed both NRQCD and HISQ actions for the valence b quark, and the HISQ action for the c quark, in HPQCD 20B the HISQ action is used throughout for all flavours. The setup is the same as for the $B_s \rightarrow D_s$ computation discussed above, HPQCD 19; we refer to the entries for the latter paper in summary tables for details. The flavour-singlet nature of the final state means that there are contributions to the relevant three-point functions from disconnected Wick contractions, which are not discussed in the paper.

Both the J/ψ and the η_c are unstable resonances, and the correct approach on the lattice would involve treating the J/ψ and the η_c as such. However, as in the case of the D^* meson, their widths are very narrow (93(2) keV for the J/ψ and 30.5(5) keV for the η_c). Hence, we can consider them as stable particles on the lattice.

In the J/ψ case, since the hadron in the final state has vector quantum numbers, the description of the hadronic amplitude requires four independent form factors, which in Ref. [166]

¹⁷This work also provided a value for $R(D)$, now superseded by FNAL/MILC 15C [161].

have been chosen as

$$\begin{aligned}
\langle J/\psi(p', \lambda) | \bar{c} \gamma^\mu b | B_c^-(p) \rangle &= \frac{2iV(q^2)}{M_{B_c} + M_{J/\psi}} \varepsilon^{\mu\nu\rho\sigma} \epsilon_\nu^*(p', \lambda) p'_\rho p_\sigma, \\
\langle J/\psi(p', \lambda) | \bar{c} \gamma^\mu \gamma^5 b | B_c^-(p) \rangle &= 2M_{J/\psi} A_0(q^2) \frac{\epsilon^*(p', \lambda) \cdot q}{q^2} q^\mu \\
&\quad + (M_{B_c} + M_{J/\psi}) A_1(q^2) \left[\epsilon^{*\mu}(p', \lambda) - \frac{\epsilon^*(p', \lambda) \cdot q}{q^2} q^\mu \right] \\
&\quad - A_2(q^2) \frac{\epsilon^*(p', \lambda) \cdot q}{M_{B_c} + M_{J/\psi}} \left[p^\mu + p'^\mu - \frac{M_{B_c}^2 - M_{J/\psi}^2}{q^2} q^\mu \right],
\end{aligned} \tag{234}$$

where ϵ_μ is the polarization vector of the J/ψ state. The computed form factors are fitted to a z -parameterization-inspired ansatz, where coefficients are modified to model the lattice-spacing and the heavy- and light-mass dependences, for a total of 280 fit parameters. In the continuum and at physical kinematics only 16 parameters survive, as each form factor is parameterized by an expression of the form

$$F(q^2) = \frac{1}{P(q^2)} \sum_{n=0}^3 a_n z^n, \tag{235}$$

where the pole factor is given by

$$P(q^2) = \prod_k z(q^2, M_k^2), \tag{236}$$

with $\{M_k\}$ a different set of pole energies below the BD^* threshold for each set of J^P quantum numbers, taken from a mixture of experimental results, lattice determinations, and model estimates. The values used (in GeV) are

$$\begin{aligned}
0^- &: 6.275, 6.872, 7.25; \\
1^- &: 6.335, 6.926, 7.02, 7.28; \\
1^+ &: 6.745, 6.75, 7.15, 7.15.
\end{aligned} \tag{237}$$

The outcome of the fit, that we quote as a FLAG estimate, is

	a_0	a_1	a_2	a_3
V	0.1057(55)	-0.746(92)	0.10(98)	0.006(1.000)
A_0	0.1006(37)	-0.731(72)	0.30(90)	-0.02(1.00)
A_1	0.0553(19)	-0.266(40)	0.31(70)	0.11(99)
A_2	0.0511(91)	-0.22(19)	-0.36(82)	-0.05(1.00)

The correlation matrix for the coefficients is provided in Tables XIX–XXVII of Ref. [166]. Using these form factors, the following Standard-Model prediction for the lepton-flavour ratio $R(J/\psi)$ is obtained:

$$R(J/\psi)_{\text{lat}} = \frac{\Gamma(B_c^+ \rightarrow J/\psi \tau^+ \nu_\tau)}{\Gamma(B_c^+ \rightarrow J/\psi \mu^+ \nu_\mu)} = 0.2582(38), \quad N_f = 2 + 1 + 1 \text{ [196]}. \tag{238}$$

8.6 Semileptonic form factors for $\Lambda_b \rightarrow (p, \Lambda_c^{(*)}) \ell \bar{\nu}$ decays

The $b \rightarrow c \ell \bar{\nu}$ and $b \rightarrow u \ell \bar{\nu}$ transitions can also be probed in decays of Λ_b baryons. With the LHCb experiment, the final state of $\Lambda_b \rightarrow p \mu \bar{\nu}$ is easier to identify than that of $B \rightarrow \pi \mu \bar{\nu}$ [197], and the first determination of $|V_{ub}|/|V_{cb}|$ at the Large Hadron Collider was performed using a ratio of $\Lambda_b \rightarrow p \mu \bar{\nu}$ and $\Lambda_b \rightarrow \Lambda_c \mu \bar{\nu}$ decay rates [198] (cf. Sec. 8.10).

The amplitudes of the decays $\Lambda_b \rightarrow p \ell \bar{\nu}$ and $\Lambda_b \rightarrow \Lambda_c \ell \bar{\nu}$ receive contributions from both the vector and the axial-vector components of the current in the matrix elements $\langle p | \bar{u} \gamma^\mu (\mathbf{1} - \gamma_5) b | \Lambda_b \rangle$ and $\langle \Lambda_c | \bar{c} \gamma^\mu (\mathbf{1} - \gamma_5) b | \Lambda_b \rangle$. The matrix elements split into three form factors f_+ , f_0 , f_\perp mediated by the vector component of the current, and another three form factors g_+ , g_0 , g_\perp mediated by the axial-vector component—see, e.g., Ref. [199] for a complete description. Given the sensitivity to all Dirac structures, measurements of the baryonic decay rates also provides useful complementary constraints on right-handed couplings beyond the Standard Model [198].

To date, only one unquenched lattice-QCD computation of the $\Lambda_b \rightarrow p$ and $\Lambda_b \rightarrow \Lambda_c$ form factors with physical heavy-quark masses has been published: Detmold 15 [200]. This computation uses RBC/UKQCD $N_f = 2 + 1$ DWF ensembles, and treats the b and c quarks within the Columbia RHQ approach. The renormalization of the currents is carried out using a mostly nonperturbative method, with residual matching factors computed at one loop. Two values of the lattice spacing ($a \approx 0.11, 0.085$ fm) are considered, with the absolute scale set from the $\Upsilon(2S)$ – $\Upsilon(1S)$ splitting. Sea-pion masses lie in a narrow interval ranging from slightly above 400 MeV to slightly below 300 MeV, keeping $m_\pi L \gtrsim 4$; however, lighter pion masses are considered in the valence DWF action for the u, d quarks. The lowest valence-valence pion mass is 227(3) MeV, which leads to a ■ rating of finite-volume effects. Results for the form factors are obtained from suitable three-point functions, and fitted to a modified z -expansion ansatz that combines the q^2 -dependence with the chiral and continuum extrapolations. The main results of the paper are the predictions (errors are statistical and systematic, respectively)

$$\zeta_{p\mu\bar{\nu}}(15\text{GeV}^2) \equiv \frac{1}{|V_{ub}|^2} \int_{15\text{ GeV}^2}^{q_{\text{max}}^2} \frac{d\Gamma(\Lambda_b \rightarrow p \mu^- \bar{\nu}_\mu)}{dq^2} dq^2 = 12.31(76)(77) \text{ ps}^{-1}, \quad (239)$$

$$\zeta_{\Lambda_c\mu\bar{\nu}}(7\text{GeV}^2) \equiv \frac{1}{|V_{cb}|^2} \int_{7\text{ GeV}^2}^{q_{\text{max}}^2} \frac{d\Gamma(\Lambda_b \rightarrow \Lambda_c \mu^- \bar{\nu}_\mu)}{dq^2} dq^2 = 8.37(16)(34) \text{ ps}^{-1}, \quad (240)$$

$$\frac{\zeta_{p\mu\bar{\nu}}(15\text{GeV}^2)}{\zeta_{\Lambda_c\mu\bar{\nu}}(7\text{GeV}^2)} = 1.471(95)(109), \quad (241)$$

which are the input for the LHCb analysis. Predictions for the total rates in all possible lepton channels, as well as for ratios similar to $R(D)$ (cf. Sec. 8.4) between the τ and light-lepton channels are also available, in particular,

$$R(\Lambda_c) = \frac{\Gamma(\Lambda_b \rightarrow \Lambda_c \tau^- \bar{\nu}_\tau)}{\Gamma(\Lambda_b \rightarrow \Lambda_c \mu^- \bar{\nu}_\mu)} = 0.3328(74)(70). \quad (242)$$

Datta 2017 [201] additionally includes results for the $\Lambda_b \rightarrow \Lambda_c$ tensor form factors h_+ , h_\perp , \tilde{h}_+ , \tilde{h}_\perp , based on the same lattice computation as Detmold 15 [200]. The main focus of Datta 2017 is the phenomenology of the $\Lambda_b \rightarrow \Lambda_c \tau \bar{\nu}_\tau$ decay and how it can be used to constrain contributions from beyond the Standard Model physics. Unlike in the case of the vector and axial-vector currents, the residual matching factors of the tensor currents are set to their

tree-level value. While the matching systematic uncertainty is augmented to take this fact into account, the procedure implies that the tensor current retains an uncanceled logarithmic divergence at $\mathcal{O}(\alpha_s)$.

Progress with next-generation lattice calculations of the $\Lambda_b \rightarrow p$ and $\Lambda_b \rightarrow \Lambda_c$ form factors was reported in Ref. [202].

Recently, first lattice calculations have also been completed for Λ_b semileptonic decays to negative-parity baryons in the final state. Such calculations are substantially more challenging and have not yet reached the same level of precision. Meinel 21 [203], which was updated in Meinel 21B [204], considers the decays $\Lambda_b \rightarrow \Lambda_c^*(2595)\ell\bar{\nu}$ and $\Lambda_b \rightarrow \Lambda_c^*(2625)\ell\bar{\nu}$, where the $\Lambda_c^*(2595)$ and $\Lambda_c^*(2625)$ are the lightest charm baryons with isospin 0 and $J^P = \frac{1}{2}^-$ and $J^P = \frac{3}{2}^-$, respectively. These decay modes may eventually provide new opportunities to test lepton-flavour universality at the LHC, but are also very interesting from a theoretical point of view. The lattice results for the form factors may help tighten dispersive constraints in global analyses of $b \rightarrow c$ semileptonic decays [205], and may provide new insights into the internal structure of the negative-parity heavy baryons and their description in heavy-quark-effective-theory [206, 207]. The $\Lambda_c^*(2595)$ and $\Lambda_c^*(2625)$ are very narrow resonances decaying through the strong interaction into $\Lambda_c\pi\pi$. The strong decays are neglected in Meinel 21 and Meinel 21B [203, 204]. The calculation was performed using the same lattice actions as previously for $\Lambda_b \rightarrow \Lambda_c$, albeit with newly tuned RHQ parameters. Only three ensembles are used, with $a \approx 0.11, 0.08$ fm and pion masses in the range from approximately 300 to 430 MeV, with valence-quark masses equal to the sea-quark masses. Chiral-continuum extrapolations linear in m_π^2 and a^2 are performed, with systematic uncertainties estimated using higher-order fits. Finite-volume effects and effects associated with the strong decays of the Λ_c^* 's are not quantified. The calculation is done in the Λ_c^* rest frame, where the cubic symmetry is sufficient to avoid mixing with unwanted lower-mass states. As a consequence, the calculation is limited to a small kinematic region near the zero-recoil point $w = 1$. On each ensemble, lattice data were produced for two values of $w - 1$ of approximately 0.01 and 0.03. The final results for the form factors are parameterized as linear functions of $w - 1$ and can be found in Meinel 21B [204] and associated supplemental files.

8.7 Semileptonic form factors for $\Lambda_b \rightarrow \Lambda^{(*)}\ell\ell$

The decays $\Lambda_b \rightarrow \Lambda\ell^+\ell^-$ are mediated by the same underlying $b \rightarrow s\ell^+\ell^-$ FCNC transition as, for example, $B \rightarrow K\ell^+\ell^-$ and $B \rightarrow K^*\ell^+\ell^-$, and can therefore provide additional information on the hints for physics beyond the Standard Model seen in the meson decays. The Λ baryon in the final state decays through the weak interaction into $p\pi^-$ (or $n\pi^0$), leading to a wealth of angular observables even for unpolarized Λ_b . When including the effects of a nonzero Λ_b polarization, $\Lambda_b \rightarrow \Lambda(\rightarrow p\pi^-)\ell^+\ell^-$ decays are characterized by five angles leading to 34 angular observables [208], which have been measured by LHCb in the bin $q^2 \in [15, 20]$ GeV² [209]. Given that the Λ is stable under the strong interactions, the $\Lambda_b \rightarrow \Lambda$ form factors parametrizing the matrix elements of local $\bar{s}\Gamma b$ currents can be calculated on the lattice with high precision using standard methods. Of course, the process $\Lambda_b \rightarrow \Lambda\ell^+\ell^-$ also receives contributions from nonlocal matrix elements of four-quark and quark-gluon operators in the weak effective Hamiltonian combined with the electromagnetic current. As with the mesonic $b \rightarrow s\ell^+\ell^-$ decays, these contributions cannot easily be calculated on the lattice and one relies on other theoretical tools for them, including the local OPE at high q^2 and a light-cone OPE / QCD factorization at low q^2 .

Following an early calculation with static b quarks [210], Detmold 16 [211] provides results for all ten relativistic $\Lambda_b \rightarrow \Lambda$ form factors parametrizing the matrix elements of the local vector, axial-vector and tensor $b \rightarrow s$ currents. The lattice setup is identical to that used in the 2015 calculation of the $\Lambda_b \rightarrow p$ form factors in Detmold 15 [200], and similar considerations as in the previous section thus apply. The lattice data cover the upper 60% of the q^2 range, and the form factors are extrapolated to the full q^2 range using BCL z -expansion fits. This extrapolation is done simultaneously with the chiral and continuum extrapolations. The caveat regarding the renormalization of the tensor currents also applies here. Progress with next-generation lattice calculations of the $\Lambda_b \rightarrow \Lambda$ form factors was reported in Ref. [202].

Reference [212] uses the lattice results for the $\Lambda_b \rightarrow \Lambda$ form factors together with the experimental results for $\Lambda_b \rightarrow \Lambda(\rightarrow p\pi^-)\mu^+\mu^-$ from LHCb [209, 213] to perform fits of the $b \rightarrow s\mu^+\mu^-$ Wilson coefficients and of the Λ_b polarization parameter. Given the uncertainties (which are still dominated by experiment), the results for the Wilson coefficients are presently consistent both with the Standard-Model values and with the deviations seen in global fits that include all mesonic decays [16, 214].

As with the $b \rightarrow c$ semileptonic form factors, a first lattice calculation, Meinel 2020 [215] (updated in Meinel 21B [204]), was also completed for a $b \rightarrow s$ transition to a negative-parity baryon in the final state, in this case the $\Lambda^*(1520)$ with $J^P = \frac{3}{2}^-$ (no calculation has yet been published for the strange $J^P = \frac{1}{2}^-$ final states, which would be the broader and even more challenging $\Lambda^*(1405)/\Lambda^*(1380)$ [64]). The $\Lambda^*(1520)$ decays primarily to $pK^-/n\bar{K}^0$, $\Sigma\pi$, and $\Lambda\pi\pi$ with a total width of 15.6 ± 1.0 MeV [64]. The analysis of the lattice data again neglects the strong decays and does not quantify finite-volume effects, and is again limited to a small kinematic region near q_{max}^2 . The results of Meinel 2020 are superseded by Meinel 21B [204], in which the fits to the lattice data were improved by including exact endpoint relations in the form-factor parametrizations.

Process	Collaboration	Ref.	N_f	publication status	continuum extrapolation	chiral extrapolation	finite volume	renormalization	heavy-quark treatment
$\Lambda_b \rightarrow \Lambda_c^*(2625) \ell^- \bar{\nu}_\ell$	Meinel 21B	[204]	2+1	A	○	○	■	○	✓
$\Lambda_b \rightarrow \Lambda_c^*(2595) \ell^- \bar{\nu}_\ell$	Meinel 21B	[204]	2+1	A	○	○	■	○	✓
$\Lambda_b \rightarrow \Lambda_c^*(2625) \ell^- \bar{\nu}_\ell$	Meinel 21	[203]	2+1	A	○	○	■	○	✓
$\Lambda_b \rightarrow \Lambda_c^*(2595) \ell^- \bar{\nu}_\ell$	Meinel 21	[203]	2+1	A	○	○	■	○	✓
$\Lambda_b \rightarrow \Lambda^*(1520) \ell^+ \ell^-$	Meinel 21B	[204]	2+1	A	○	○	■	○	✓
$\Lambda_b \rightarrow \Lambda^*(1520) \ell^+ \ell^-$	Meinel 20	[215]	2+1	A	○	○	■	○	✓
$\Lambda_b \rightarrow \Lambda \ell^+ \ell^-$	Detmold 16	[211]	2+1	A	○	○	■	○	✓
$\Lambda_b \rightarrow p \ell^- \bar{\nu}_\ell$	Detmold 15	[200]	2+1	A	○	○	■	○	✓
$\Lambda_b \rightarrow \Lambda_c \ell^- \bar{\nu}_\ell$	Detmold 15, Datta 17	[200, 201]	2+1	A	○	○	■	○	✓

Table 48: Summary of computations of bottom-baryon semileptonic form factors (see also Refs. [210, 216] for calculations with static b quarks). The rationale for the ■ rating of finite-volume effects in Meinel 20, Meinel 21, and Meinel 21B (despite meeting the ○ criterion based on the minimum pion mass) is that the unstable nature of the final-state baryons was neglected in the analysis.

8.8 Determination of $|V_{ub}|$

We now use the lattice-determined Standard Model transition amplitudes for leptonic (Sec. 8.1) and semileptonic (Sec. 8.3) B -meson decays to obtain exclusive determinations of the CKM matrix element $|V_{ub}|$. In this section, we describe the aspect of our work that involves experimental input for the relevant charged-current exclusive decay processes. The relevant formulae are Eqs. (155) and (191). Among leptonic channels the only input comes from $B \rightarrow \tau \nu_\tau$, since the rates for decays to e and μ have not yet been measured. In the semileptonic case, we only consider $B \rightarrow \pi \ell \nu$ transitions (experimentally measured for $\ell = e, \mu$).

We first investigate the determination of $|V_{ub}|$ through the $B \rightarrow \tau \nu_\tau$ transition. The experimental measurements of the branching fraction of this channel, $B(B^- \rightarrow \tau^- \bar{\nu})$, have not been updated since the publication of FLAG 16 [77]. The status of the experimental results for this branching fraction, summarized in Tab. 49, is unchanged from FLAG 16 [77]. Our corresponding values of $|V_{ub}|$ are unchanged from FLAG 19 [1].

It is obvious that all the measurements listed in Tab. 49 have significance smaller than 5σ , and the large uncertainties are dominated by statistical errors. These measurements lead to the averages of experimental measurements for $B(B^- \rightarrow \tau \bar{\nu})$ [2, 3],

$$B(B^- \rightarrow \tau \bar{\nu}) \times 10^4 = 0.91 \pm 0.22 \text{ from Belle,} \quad (243)$$

$$= 1.79 \pm 0.48 \text{ from BaBar,} \quad (244)$$

$$= 1.06 \pm 0.33 \text{ average,} \quad (245)$$

Collaboration	Tagging method	$B(B^- \rightarrow \tau^- \bar{\nu}) \times 10^4$
Belle [217]	Hadronic	$0.72^{+0.27}_{-0.25} \pm 0.11$
Belle [3]	Semileptonic	$1.25 \pm 0.28 \pm 0.27$
BaBar [2]	Hadronic	$1.83^{+0.53}_{-0.49} \pm 0.24$
BaBar [218]	Semileptonic	$1.7 \pm 0.8 \pm 0.2$

Table 49: Experimental measurements for $B(B^- \rightarrow \tau^- \bar{\nu})$. The first error on each result is statistical, while the second error is systematic.

where, following our standard procedure, we perform a weighted average and rescale the uncertainty by the square root of the reduced chi-squared. Note that the Particle Data Group [15] did not inflate the uncertainty in the calculation of the averaged branching ratio.

Combining the results in Eqs. (243–245) with the experimental measurements of the mass of the τ -lepton and the B -meson lifetime and mass we get

$$|V_{ub}|f_B = 0.72 \pm 0.09 \text{ MeV from Belle,} \quad (246)$$

$$= 1.01 \pm 0.14 \text{ MeV from BaBar,} \quad (247)$$

$$= 0.77 \pm 0.12 \text{ MeV average,} \quad (248)$$

which can be used to extract $|V_{ub}|$ using the averages in Eqs. (162), (165) and (168), viz.,

$$|V_{ub}| = 3.83(14)(48) \times 10^{-3} \quad [B \rightarrow \tau \nu_\tau, \text{ Belle}], \quad (249)$$

$$N_f = 2: |V_{ub}| = 5.37(20)(74) \times 10^{-3} \quad [B \rightarrow \tau \nu_\tau, \text{ Babar}], \quad (250)$$

$$|V_{ub}| = 4.10(15)(64) \times 10^{-3} \quad [B \rightarrow \tau \nu_\tau, \text{ average}], \quad (251)$$

$$|V_{ub}| = 3.75(8)(47) \times 10^{-3} \quad [B \rightarrow \tau \nu_\tau, \text{ Belle}], \quad (252)$$

$$N_f = 2 + 1: |V_{ub}| = 5.26(12)(73) \times 10^{-3} \quad [B \rightarrow \tau \nu_\tau, \text{ Babar}], \quad (253)$$

$$|V_{ub}| = 4.01(9)(63) \times 10^{-3} \quad [B \rightarrow \tau \nu_\tau, \text{ average}], \quad (254)$$

$$|V_{ub}| = 3.79(3)(47) \times 10^{-3} \quad [B \rightarrow \tau \nu_\tau, \text{ Belle}], \quad (255)$$

$$N_f = 2 + 1 + 1: |V_{ub}| = 5.32(4)(74) \times 10^{-3} \quad [B \rightarrow \tau \nu_\tau, \text{ Babar}], \quad (256)$$

$$|V_{ub}| = 4.05(3)(64) \times 10^{-3} \quad [B \rightarrow \tau \nu_\tau, \text{ average}], \quad (257)$$

where the first error comes from the uncertainty in f_B and the second comes from experiment. The experimental branching fractions do not yet meet the five-sigma discovery threshold and the relative uncertainties are significantly larger than the radiative electroweak corrections. Therefore, in line with the Particle Data Group [15] and in contrast to the $D_{(s)}$ decays, we do not include in these results the electroweak corrections.

Let us now turn our attention to semileptonic decays. The experimental value of $|V_{ub}|f_+(q^2)$ can be extracted from the measured branching fractions for $B^0 \rightarrow \pi^\pm \ell \nu$ or $B^\pm \rightarrow \pi^0 \ell \nu$ by applying Eq. (191).¹⁸ We then determine $|V_{ub}|$ by performing fits to the constrained BCL

¹⁸Since $\ell = e, \mu$ the contribution from the scalar form factor in Eq. (191) is negligible.

$B \rightarrow \pi \ell \nu$ ($N_f = 2 + 1$)

	Central Values	Correlation Matrix					
$ V_{ub} \times 10^3$	3.61 (16)	1	-0.812	-0.108	0.128	-0.326	-0.151
a_0^+	0.425 (15)	-0.812	1	-0.188	-0.309	0.409	0.00926
a_1^+	-0.441 (39)	-0.108	-0.188	1	-0.498	-0.0343	0.150
a_2^+	-0.52 (13)	0.128	-0.309	-0.498	1	-0.190	0.128
a_0^0	0.560 (17)	-0.326	0.409	-0.0343	-0.190	1	-0.772
a_1^0	-1.346 (53)	-0.151	0.00926	0.150	0.128	-0.772	1

Table 50: Value of $|V_{ub}|$, coefficients for the $N^+ = N^0 = N^T = 3$ z -expansion of the $B \rightarrow \pi$ form factors f_+ and f_0 , and their correlation matrix. The chi-square per degree of freedom is $\chi^2/\text{dof} = 116.7/62 = 1.88$ and the errors on the fit parameters have been rescaled by $\sqrt{\chi^2/\text{dof}} = 1.37$. The lattice calculations that enter this fit are taken from FNAL/MILC 15 [82], RBC/UKQCD 15 [83] and JLQCD 22 [84]. The experimental inputs are taken from BaBar [99, 219] and Belle [100, 220]. The form factors can be reconstructed using parameterization and inputs given in Appendix B.3.2.

z -parameterization of the form factor $f_+(q^2)$ given in Eq. (524). This can be done in two ways: one option is to perform separate fits to lattice and experimental results, and extract the value of $|V_{ub}|$ from the ratio of the respective a_0 coefficients; a second option is to perform a simultaneous fit to lattice and experimental data, leaving their relative normalization $|V_{ub}|$ as a free parameter. We adopt the second strategy, because it combines the lattice and experimental input in a more efficient way, leading to a smaller uncertainty on $|V_{ub}|$.

The available state-of-the-art experimental input consists of five data sets: three untagged measurements by BaBar (6-bin [99] and 12-bin [219]) and Belle [220], all of which assume isospin symmetry and provide combined $B^0 \rightarrow \pi^-$ and $B^+ \rightarrow \pi^0$ data; and the two tagged Belle measurements of $\bar{B}^0 \rightarrow \pi^+$ (13-bin) and $B^- \rightarrow \pi^0$ (7-bin) [100]. Including all of them, along with the available information about cross-correlations, will allow us to obtain a meaningful final error estimate.¹⁹ The lattice input data set will be that discussed in Sec. 8.3.

We perform a constrained BCL fit of the vector and scalar form factors (this is necessary in order to take into account the $f_+(q^2 = 0) = f_0(q^2 = 0)$ constraint) together with the combined experimental data sets. We find that the error on $|V_{ub}|$ stabilizes for $N^+ = N^0 = 3$. The result of the combined fit is presented in Tab. 50. The fit has a chi-square per degree of freedom $\chi^2/\text{dof} = 116.7/62 = 1.88$. Following the PDG recommendation, we rescale the whole covariance matrix by χ^2/dof : the errors on the z -parameters are increased by $\sqrt{\chi^2/\text{dof}} = 1.37$ and the correlation matrix is unaffected. The value of $|V_{ub}|$ which we obtain is:

$$N_f = 2 + 1: |V_{ub}| = (3.61 \pm 0.16) \times 10^{-3} \\ [B \rightarrow \pi \ell \nu, \text{FLAG average, Refs. [82–84, 99, 100, 219, 220]]]. \quad (258)$$

In Fig. 31, we show both the lattice and experimental data for $(1 - q^2/m_{B^*}^2)f_+(q^2)$ as a function of $z(q^2)$, together with our preferred fit; experimental data has been rescaled by the

¹⁹See, e.g., Sec. V.D of Ref. [82] for a detailed discussion.

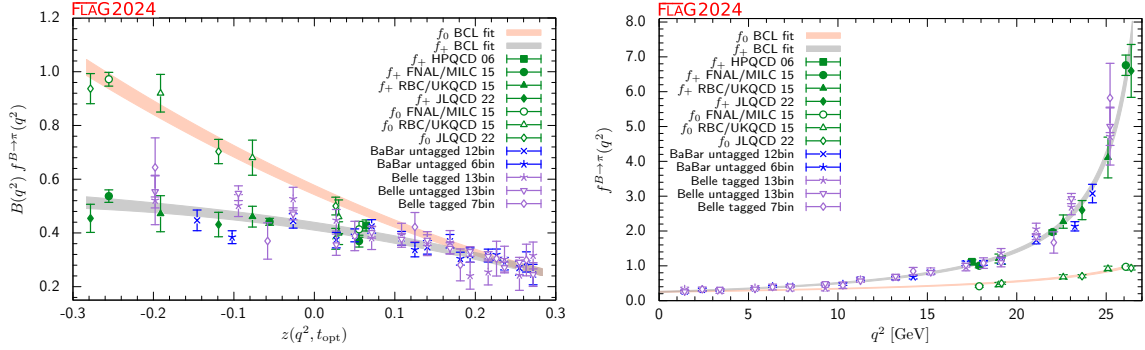


Figure 31: Lattice and experimental data for $f_+^{B \rightarrow \pi}(q^2)$ and $f_0^{B \rightarrow \pi}(q^2)$ versus z (left panel) and q^2 (right panel). Experimental data has been rescaled by the value for $|V_{ub}|$ found from the joint fit. Green symbols denote lattice-QCD points included in the fit, while blue and indigo points show experimental data divided by the value of $|V_{ub}|$ obtained from the fit. The grey and orange bands display the preferred $N^+ = N^0 = 3$ BCL fit (five z -parameters and $|V_{ub}|$).

resulting value for $|V_{ub}|^2$. It is worth noting the good consistency between the form-factor shapes from lattice and experimental data. This can be quantified, e.g., by computing the ratio of the two leading coefficients in the constrained BCL parameterization: the fit to lattice form factors yields $a_1^+/a_0^+ = -1.20(23)$ (cf. the results presented in Sec. 8.3.1), while the above lattice+experiment fit yields $a_1^+/a_0^+ = -1.039(94)$.

Finally we combine the $N_f = 2 + 1$ determinations of $|V_{ub}|$ from $B \rightarrow \tau \nu$ and $B \rightarrow \pi \ell \nu$ in Eqs. (254) and (259) and obtain:

$$N_f = 2 + 1: |V_{ub}| = (3.63 \pm 0.16) \times 10^{-3} \\ [B \rightarrow (\pi \ell \nu, \tau \nu), \text{FLAG average,} \\ \text{Refs. [2, 3, 32, 35, 37, 42, 44, 82–84, 99, 100, 219, 220]}]. \quad (259)$$

Our results are summarized in Tab. 51 and will be displayed after our discussion of $|V_{cb}|$. In that figure we also show the PDG inclusive determination $|V_{ub}|_{\text{incl}} = (4.13 \pm 0.12_{\text{exp}} \pm {}^{+0.13}_{-0.14_{\text{theo}}} \pm 0.18_{\Delta_{\text{model}}}) \times 10^{-3}$ [15] (the Δ_{model} error has been added in Ref. [15] to account for the spread in results obtained using different theoretical models).

8.9 Determination of $|V_{cb}|$

We now combine the lattice-QCD results for the $B \rightarrow D^{(*)}$ form factors with all available experimental information on $B \rightarrow D^{(*)} \ell \nu$ ($\ell = e, \mu$) semileptonic decays to obtain determinations of the CKM matrix element $|V_{cb}|$ in the Standard Model.

For $B \rightarrow D$ we perform a joint fit to the available lattice data, i.e., the $N_f = 2 + 1$ FNAL/MILC 15C [161] and HPQCD 15 [159] calculations discussed in Sec. 8.4, and state-of-the-art experimental determinations. We combine the Belle measurement [221], which provides partial integrated decay rates in 10 bins in the recoil parameter w , with the 2010 BaBar data set in Ref. [222], which quotes the value of $\mathcal{G}^{B \rightarrow D}(w) \eta_{\text{EW}} |V_{cb}|$ for 10 values of

	from	$ V_{ub} \times 10^3$
FLAG average for $N_f = 2 + 1$	$B \rightarrow \pi \ell \nu$	3.61(16)
FLAG average for $N_f = 2 + 1$	$B \rightarrow \tau \nu$	4.01(64)
FLAG average for $N_f = 2 + 1$	$B \rightarrow (\pi \ell \nu, \tau \nu)$	3.63(16)
FLAG average for $N_f = 2 + 1 + 1$	$B \rightarrow \tau \nu$	4.05(64)
PDG 24	$B \rightarrow X_u \ell \nu$	4.13(26)

Table 51: Results for $|V_{ub}|$. The averages involving $B \rightarrow \pi \ell \nu$ and $B \rightarrow \tau \nu$ can be found in Eqs. (258), (254), (259) and (257); all uncertainties have been added in quadrature. The inclusive average is taken from PDG 24 [15]. The lattice calculations for the $B \rightarrow \pi$ form factors are taken from Refs. [82–84], for f_B at $N_f = 2 + 1$ from Refs. [32, 35, 37, 42, 44] and for f_B at $N_f = 2 + 1 + 1$ from Refs. [31, 34, 36, 40].

w .²⁰ The fit is dominated by the more precise Belle data. Given this, and the fact that only partial correlations among systematic uncertainties are to be expected, we will treat both data sets as uncorrelated.²¹ The formula for the differential $B \rightarrow D \ell \nu$ branching ratio is given in Eq. (195).

A constrained ($N^+ = N^0 = 3$) BCL fit using the same ansatz as for lattice-only data in Sec. 8.4 yields our average:

$$N_f = 2 + 1: |V_{cb}| = 40.0(1.0) \times 10^{-3} \\ [B \rightarrow D \ell \nu, \text{FLAG average, Refs. [159, 161, 221, 222]}]. \quad (260)$$

The fit has a chi-square per degree of freedom $\chi^2/\text{dof} = 20.0/25 = 0.80$. The result of the full fit, including the correlation matrix between $|V_{cb}|$ and the BCL coefficients is presented in Tab. 52 and illustrated in Fig. 32. In passing, we note that, if correlations between the FNAL/MILC and HPQCD calculations are neglected, the $|V_{cb}|$ central value rises to 40.3×10^{-3} in nice agreement with the results presented in Ref. [223].

Finally, using the fit results in Tab. 52, we extract a value for $R(D)$ which includes both lattice and experimental information:

$$N_f = 2 + 1: R(D)_{\text{lat+exp}} = 0.2955(32) \\ [\text{FLAG average, Refs. [159, 161, 221, 222]}]. \quad (261)$$

Note that we do not need to rescale the uncertainty on $R(D)_{\text{lat+exp}}$ because, after the inclusion of experimental $B \rightarrow D \ell \nu$ ($\ell = e, \mu$) results, the shift in central value caused by using a different parameterization is negligible (see the discussion above Eq. (223)). For $B \rightarrow D^*$, we perform a joint fit to all available lattice and experimental data. On the lattice side, we consider separately the two $N_f = 2 + 1$ calculations FNAL/MILC 21 [163] and JLQCD 23 [164] and the single $N_f = 2 + 1 + 1$ HPQCD 23 [165] calculation. On the experimental side, the situation is more complicated because we need to combine the following results.

²⁰We thank Marcello Rotondo for providing the 10 bins result of the BaBar analysis.

²¹We have checked that results using just one experimental data set are compatible within 1σ . In the case of BaBar, we have taken into account the introduction of some EW corrections in the data.

$B \rightarrow D\ell\nu$ ($N_f = 2 + 1$)

	Central Values	Correlation Matrix					
$ V_{cb} \times 10^3$	40.0 (1.0)	1.00	-0.525	-0.339	0.0487	-0.521	-0.433
a_0^+	0.8946 (94)	-0.525	1.00	0.303	-0.351	0.953	0.529
a_1^+	-8.03 (16)	-0.339	0.303	1.00	0.203	0.375	0.876
a_2^+	50.1 (3.1)	0.0487	-0.351	0.203	1.00	-0.276	0.196
a_0^0	0.7804 (75)	-0.521	0.953	0.375	-0.276	1.0	0.502
a_1^0	-3.38 (16)	-0.433	0.529	0.876	0.196	0.502	1.0

Table 52: Value of $|V_{cb}|$, coefficients for the $N^+ = N^0$ z -expansion of the $B \rightarrow D$ form factors f_+ and f_0 , and their correlation matrix. The coefficient a_2^0 is fixed by the $f_+(q^2 = 0) = f_0(q^2 = 0)$ constrain. The chi-square per degree of freedom is $\chi^2/\text{dof} = 20.0/25 = 0.80$. The lattice calculations that enter this fit are taken from FNAL/MILC 15C [161] and HPQCD 15 [159]. The experimental inputs are taken from BaBar [222] and Belle [221]. The form factors can be reconstructed using parameterization and inputs given in Appendix B.3.5.

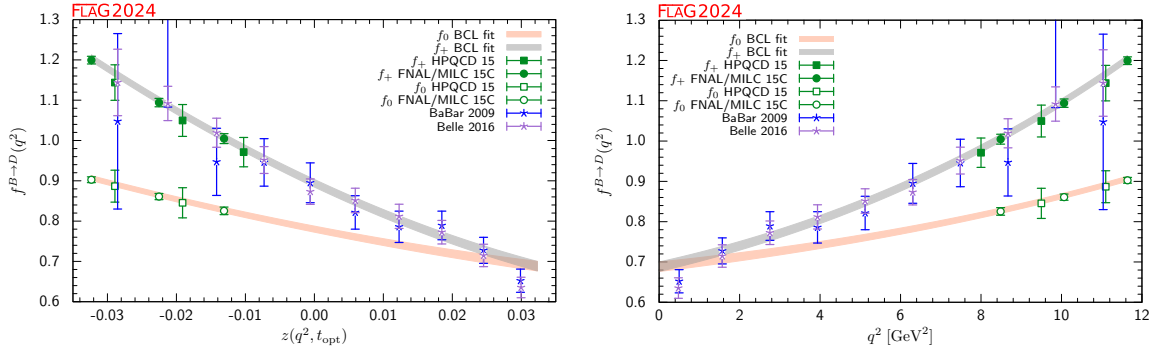


Figure 32: Lattice and experimental data for $f_+^{B \rightarrow D}(q^2)$ and $f_0^{B \rightarrow D}(q^2)$ versus z (left panel) and q^2 (right panel). Green symbols denote lattice-QCD points included in the fit, while blue and indigo points show experimental data divided by the value of $|V_{cb}|$ obtained from the fit. The grey and orange bands display the preferred $N^+ = N^0 = 3$ BCL fit (five z -parameters and $|V_{cb}|$).

- The Belle untagged measurement [177] of the differential $B^0 \rightarrow D^{*-}\ell^+\nu_\ell$ partial width.
- The Belle tagged measurement [224] of the *normalized* differential $B \rightarrow D^*\ell\nu_\ell$ partial width (averaged over the B^- and \bar{B}^0 modes).
- The Belle II tagged measurement [225] of the *normalized* differential $\bar{B}^0 \rightarrow D^{*+}\ell^-\bar{\nu}_\ell$ partial width.
- The Belle II tagged branching ratio measurement $\text{BR}(\bar{B}^0 \rightarrow D^{*+}\ell^-\bar{\nu}_\ell) = (4.922 \pm 0.023 \pm 0.220)\%$ [225].
- A modified HFLAV world average for the branching ratio of $\bar{B}^0 \rightarrow D^{*+}\ell^-\bar{\nu}_\ell$ mode

in which the contributions from the Belle untagged [177] (already included in the differential results we use) and Belle II tagged [226] (superseded by the Belle II tagged result [225] which we include separately) measurements have been removed. Using the results from Table 69 of Ref. [190], we calculate $\text{BR}(\bar{B}^0 \rightarrow D^{*+} \ell^- \bar{\nu}_\ell) = (5.12 \pm 0.19)\%$ where a PDG rescaling factor 1.36 has been applied.

- The HFLAV world average $\text{BR}(B^- \rightarrow D^{*0} \ell^- \bar{\nu}_\ell) = (5.58 \pm 0.07_{\text{stat}} \pm 0.21_{\text{syst}})\%$ [190] (which is not included in the Belle tagged shape-only measurement).

The theoretical predictions for the differential $B \rightarrow D^* \ell \nu$ rate binned over the variables w , $\cos \theta_v$, $\cos \theta_l$ and χ are obtained easily via direct integration of Eq. (210). One small subtlety is the inclusion of the so-called Coulomb factor $(1 + \alpha\pi)$ for final states involving two charged particles, i.e., only for $\text{BR}(\bar{B}^0 \rightarrow D^{*+} \ell^- \bar{\nu}_\ell)$. Regarding the fit methodology, we chose not to use any prior nor to impose unitarity constraints on the BGL coefficients. The Belle untagged analysis [177] presents the data in 10 bins of each kinematical variable; since the integral over the bins in each of the four distributions are identical, we remove the last bin in each of the three angular distributions. Moreover, we marginalize over N_{B^0} , the number of B^0 mesons in the data sample, thus properly correlating its impact over all the distributions and over the electron and muon modes.

The results of this global fit are presented in Tab. 53. The chi-square per degree of freedom of the two fits are $\chi^2/\text{dof} = 216/160 = 1.35$ for $N_f = 2 + 1$ and $\chi^2/\text{dof} = 200/148 = 1.35$ for $N_f = 2 + 1 + 1$ (the difference in the degrees of freedom is simply due to the presence of two sets of lattice synthetic data, each comprised of 12 points, for the $N_f = 2 + 1$ case). Note that we have rescaled all the errors by $\sqrt{\chi^2/\text{dof}}$ following the standard PDG recipe. In particular, we find:

$$N_f = 2 + 1: |V_{cb}| = 39.23(65) \times 10^{-3} \\ [B \rightarrow D^* \ell \nu, \text{FLAG average, Refs. [163, 164, 177, 190, 224, 225]}], \quad (262)$$

$$N_f = 2 + 1 + 1: |V_{cb}| = 39.44(89) \times 10^{-3} \\ [B \rightarrow D^* \ell \nu, \text{FLAG average, Refs. [165, 177, 190, 224, 225]}]. \quad (263)$$

In Fig. 33, we show the form factors obtained from combining lattice and experimental results. In Fig. 34, we present a comparison of the four *normalized* differential distributions extracted from the experimental data, from the individual lattice results and from the combined lattice plus experiment fit.²² The top (bottom) four panels correspond to $N_f = 2 + 1$ ($2 + 1 + 1$). Direct inspection of these distributions shows quite a good agreement (as already evidenced by the relatively good chi-square per degree of freedom of the fits) albeit with some tensions in some of the shapes. In particular, the normalized distributions extracted from $N_f = 2 + 1$ and $N_f = 2 + 1 + 1$ results tend to deviate from the measured ones along similar patterns: deficit at large w , excess at large $\cos \theta_v$, flatter distribution in $\cos \theta_\ell$. The tensions in the $N_f = 2 + 1 + 1$ are only apparently more pronounced because of the larger lattice uncertainties.

Finally, using the fit results in Tab. 53, we extract a value for $R(D^*)$ which includes both

²²For the Belle untagged case [177] we produce the normalized binned distributions by inverting the electron and muon response matrices and averaging over the leptons. Note that these distributions are presented for illustrative purpose only.

$B \rightarrow D^* (N_f = 2 + 1)$										
coeff	Central Values	Correlation Matrix								
$ V_{cb} \times 10^3$	39.23(65)	1	-0.3552	-0.1269	-0.6672	-0.3260	0.2331	-0.2412	0.1118	-0.08658
a_0^g	0.03036(72)	-0.3552	1	-0.4976	0.3645	-0.0009317	-0.02169	0.1026	-0.02327	-0.09817
a_1^g	-0.083(21)	-0.1269	-0.4976	1	0.02961	0.1874	-0.2543	0.08161	-0.03930	0.1177
a_0^f	0.01213(15)	-0.6672	0.3645	0.02961	1	-0.08990	0.07897	-0.08767	0.07594	-0.09589
a_1^f	0.0234(64)	-0.3260	-0.0009317	0.1874	-0.08990	1	-0.8384	0.4660	-0.2491	0.3552
a_2^f	-0.59(16)	0.2331	-0.02169	-0.2543	0.07897	-0.8384	1	-0.2414	0.07961	-0.2880
$a_1^{F_1}$	0.00141(97)	-0.2412	0.1026	0.08161	-0.08767	0.4660	-0.2414	1	-0.9135	-0.06385
$a_2^{F_1}$	-0.005(17)	0.1118	-0.02327	-0.03930	0.07594	-0.2491	0.07961	-0.9135	1	0.2820
$a_1^{F_1}$	-0.093(17)	-0.08658	-0.09817	0.1177	-0.09589	0.3552	-0.2880	-0.06385	0.2820	1

$B \rightarrow D^* (N_f = 2 + 1 + 1)$										
coeff	Central Values	Correlation Matrix								
$ V_{cb} \times 10^3$	39.44(89)	1	-0.1717	-0.06581	-0.7257	-0.4981	0.4426	-0.2473	0.08156	-0.2155
a_0^g	0.0311(21)	-0.1717	1	-0.9267	0.1121	-0.004683	0.1735	0.1230	-0.003372	0.07094
a_1^g	-0.125(75)	-0.06581	-0.9267	1	0.09615	0.1018	-0.2899	-0.03844	-0.03789	-0.03009
a_0^f	0.01207(21)	-0.7257	0.1121	0.09615	1	0.01430	-0.04137	-0.03342	0.02486	0.07847
a_1^f	0.023(12)	-0.4981	-0.004683	0.1018	0.01430	1	-0.9267	0.2522	0.03052	0.3601
a_2^f	-0.55(31)	0.4426	0.1735	-0.2899	-0.04137	-0.9267	1	-0.06981	-0.1655	-0.3503
$a_1^{F_1}$	0.0016(14)	-0.2473	0.1230	-0.03844	-0.03342	0.2522	-0.06981	1	-0.9270	-0.1678
$a_2^{F_1}$	-0.008(27)	0.08156	-0.003372	-0.03789	0.02486	0.03052	-0.1655	-0.9270	1	0.3148
$a_1^{F_1}$	-0.090(48)	-0.2155	0.07094	-0.03009	0.07847	0.3601	-0.3503	-0.1678	0.3148	1

Table 53: $|V_{cb}|$, coefficients and correlation matrix for the $(N_g, N_f, N_{F_1}, N_{F_2}) = (2, 3, 3, 2)$ BGL fit to the $B \rightarrow D^*$ form factors g , f , F_1 and F_2 for $N_f = 2 + 1$ and $N_f = 2 + 1 + 1$. The form factors can be reconstructed using parameterization and inputs given in Appendix B.3.7.

lattice and experimental information:

$$N_f = 2 + 1: R(D^*)_{\text{lat+exp}} = 0.2505(11) \quad [\text{FLAG average, Refs. [163, 164, 177, 190, 224, 225]}], \quad (264)$$

$$N_f = 2 + 1 + 1: R(D^*)_{\text{lat+exp}} = 0.2506(17) \quad [\text{FLAG average, Refs. [165, 177, 190, 224, 225]}]. \quad (265)$$

Before discussing the combination of the above $|V_{cb}|$ results, we note that the LHCb Collaboration recently reported the first determination of $|V_{cb}|$ at the Large Hadron Collider using $B_s \rightarrow D_s^- \mu^+ \nu_\mu$ and $B_s \rightarrow D_s^{*-} \mu^+ \nu_\mu$ decays [171, 172]. The differential decay rates, in combination with the $N_f = 2 + 1 + 1$ HPQCD 19 [162] and HPQCD 19B [187] lattice results for $f_+^{B_s \rightarrow D_s}$ and $\mathcal{F}^{B_s \rightarrow D_s^*}(1)$, were analyzed using either the CLN or BGL form-factor parameterizations. The result for $|V_{cb}|$ from the BGL fit is [172]

$$N_f = 2 + 1 + 1: |V_{cb}| = (41.7 \pm 0.8 \pm 0.9 \pm 1.1) \times 10^{-3} \quad [B_s \rightarrow D_s^{(*)-} \mu^+ \nu_\mu, \text{LHCb}], \quad (266)$$

where the first two uncertainties are the statistical and systematic experimental uncertainties, and the third is due to the external inputs used, including the lattice inputs.

The LHCb analysis used ratios to the reference decay modes $B^0 \rightarrow D^- \mu^+ \nu_\mu$ and $B^0 \rightarrow D^{*-} \mu^+ \nu_\mu$, whose branching fractions are used as input in the form of the Particle Data Group averages of measurements by other experiments [227]. The result (266) is therefore correlated with the determinations of $|V_{cb}|$ from $B \rightarrow D$ and $B \rightarrow D^*$ semileptonic decays. Given the challenges involved in performing our own fit to the LHCb data, we do not, at present, include the LHCb results for $B_s \rightarrow D_s^- \mu^+ \nu_\mu$ and $B_s \rightarrow D_s^{*-} \mu^+ \nu_\mu$ in our combination of $|V_{cb}|$.

We now proceed to combine the two $N_f = 2 + 1$ determinations of $|V_{cb}|$ from exclusive $B \rightarrow D$ and $B \rightarrow D^*$ semileptonic decays. To this end, we include an estimate of the correlation

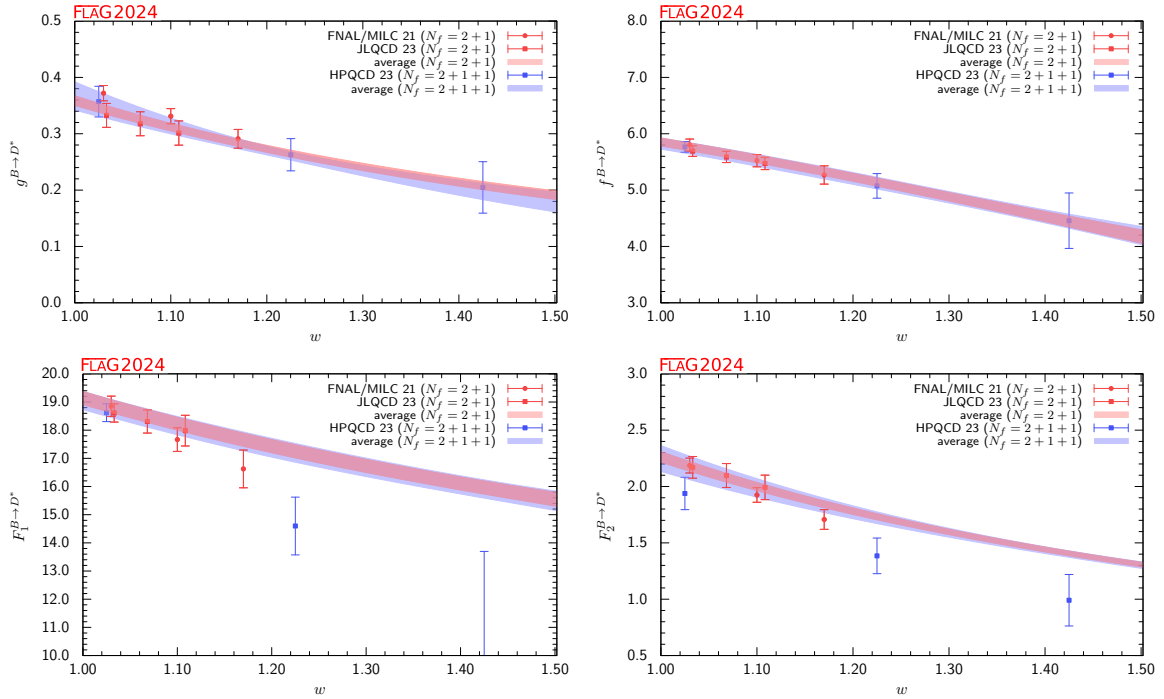


Figure 33: The form factors $g(q^2)$, $f(q^2)$, $F_1(q^2)$, and $F_2(q^2)$ for $B \rightarrow D^* \ell \nu$ plotted as a function of w . The red (blue) band displays our preferred $(N_g, N_f, N_{F_1}, N_{F_2}) = (2, 3, 3, 2)$ BGL fit (eight parameters) to experimental and $N_f = 2 + 1$ ($2 + 1 + 1$) lattice data. The constraints at zero and maximum recoil are imposed exactly. No use of unitarity constraints and priors has been made.

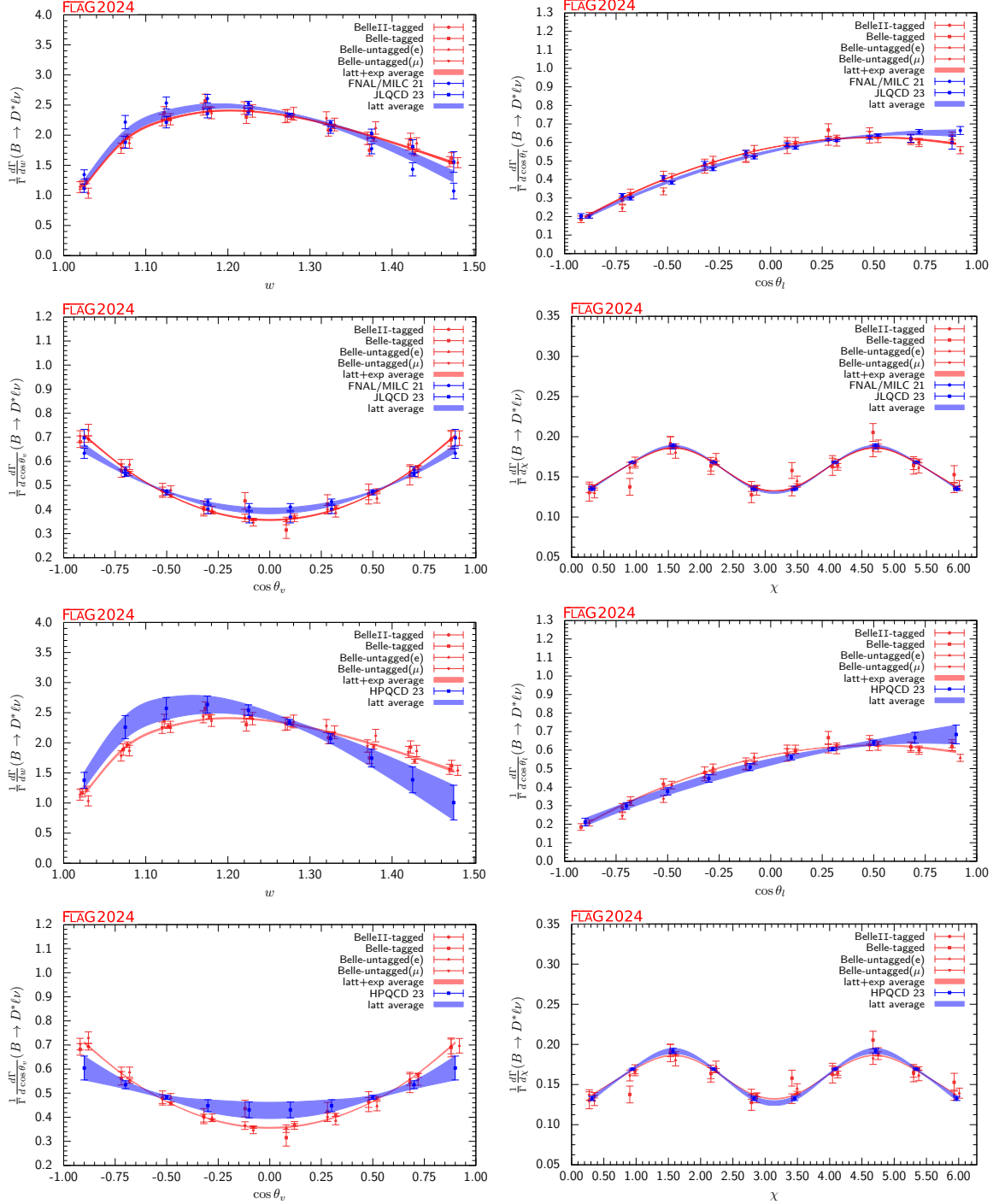


Figure 34: Normalized differential decay rates with respect to the variables w , $\cos \theta_l$, $\cos \theta_v$ and χ . The red (blue) band displays our preferred $(N_g, N_f, N_{F_1}, N_{F_2}) = (2, 3, 3, 2)$ BGL fit (eight parameters) obtained from lattice calculations with (without) the inclusion of experimental data. The constraints at zero and maximum recoil are imposed exactly. No use of unitarity constraints and priors has been made. The top and bottom four distributions are obtained using $N_f = 2 + 1$ and $N_f = 2 + 1 + 1$ lattice calculations, respectively.

	from	$ V_{cb} \times 10^3$
FLAG average for $N_f = 2 + 1$	$B \rightarrow D^* \ell \nu$	39.23(65)
FLAG average for $N_f = 2 + 1$	$B \rightarrow D \ell \nu$	40.0(1.0)
FLAG average for $N_f = 2 + 1$	$B \rightarrow (D, D^*) \ell \nu$	39.45(56)
FLAG average for $N_f = 2 + 1 + 1$	$B \rightarrow D^* \ell \nu$	39.44(89)
LHCb result for $N_f = 2 + 1 + 1$ (BGL)	$B_s \rightarrow D_s^{(*)} \ell \nu$	41.7(0.8)(0.9)(1.1)
Bordone et al.	$B \rightarrow X_c \ell \nu$	42.16(51)

Table 54: Results for $|V_{cb}|$. The lattice calculations for the $B \rightarrow D$ form factors at $N_f = 2 + 1$ are taken from FNAL/MILC 15 [82], RBC/UKQCD 15 [83] and JLQCD 22 [84]; for the $B \rightarrow D^*$ form factors at $N_f = 2 + 1$ from FNAL/MILC 21 [163] and JLQCD 23 [164]; for the $B \rightarrow D^*$ form factors at $N_f = 2 + 1 + 1$ from HPQCD 23 [165]. The LHCb result using $B_s \rightarrow D_s^{(*)} \ell \nu$ decays [162, 171, 172, 187], as well as the inclusive average obtained in the kinetic scheme from Ref. [228] are shown for comparison. In the LHCb result, the first two uncertainties are the statistical and systematic experimental uncertainties, and the third is due to the external inputs used, including the lattice inputs.

between the statistical lattice uncertainties on $|V_{cb}|_{B \rightarrow D}^{N_f=2+1}$ (FNAL/MILC and HPQCD) and $|V_{cb}|_{B \rightarrow D^*}^{N_f=2+1}$ (FNAL/MILC), because they are based on the same MILC configurations (albeit on different subsets). An estimate of this correlation is complicated due to the difficulty of disentangling lattice and experimental sources of uncertainties in a global BGL fit. Here we follow an approximate procedure which relies on estimating these correlations by looking at the $B \rightarrow D$ and $B \rightarrow D^*$ form factors at zero recoil, $\mathcal{G}^{B \rightarrow D}(1)$ and $\mathcal{F}^{B \rightarrow D^*}(1)$. The inclusion of these correlations has a very small impact on the average, thus providing an *a posteriori* justification for this approximate method. We obtain:

$$\begin{aligned}
N_f = 2 + 1: |V_{cb}| &= 39.45(56) \times 10^{-3} \\
&[B \rightarrow (D, D^*) \ell \nu, \text{ FLAG average,} \\
&\text{Refs. [159, 161, 163, 164, 177, 190, 221, 222, 224, 225]}].
\end{aligned} \tag{267}$$

Our results are summarized in Tab. 54, which also shows the inclusive determination of $|V_{cb}| = 42.16(51) \times 10^{-3}$ [228] for comparison, and are illustrated in Fig. 35.²³

8.10 Determination of $|V_{ub}/V_{cb}|$ from Λ_b decays

In 2015, the LHCb Collaboration reported a measurement of the ratio [198]

$$R_{\text{BF}}(\Lambda_b) = \frac{\int_{15 \text{ GeV}^2}^{q_{\text{max}}^2} \frac{d\mathcal{B}(\Lambda_b \rightarrow p \mu^- \bar{\nu}_\mu)}{dq^2} dq^2}{\int_{7 \text{ GeV}^2}^{q_{\text{max}}^2} \frac{d\mathcal{B}(\Lambda_b \rightarrow \Lambda_c \mu^- \bar{\nu}_\mu)}{dq^2} dq^2}, \tag{268}$$

²³This determination of $|V_{cb}|$ is also adopted by the PDG [15].

which, combined with the lattice QCD prediction from Ref. [200] (Detmold 15) discussed in Sec. 8.6 yields a determination of $|V_{ub}/V_{cb}|$. The LHCb analysis uses the decay $\Lambda_c \rightarrow pK\pi$ to reconstruct the Λ_c and requires the branching fraction $\mathcal{B}(\Lambda_c \rightarrow pK\pi)$ of this decay as an external input. Using the latest world average of $\mathcal{B}(\Lambda_c \rightarrow pK\pi) = (6.28 \pm 0.32)\%$ [64] to update the LHCb measurement gives [229]

$$R_{\text{BF}}(\Lambda_b) = (0.92 \pm 0.04 \pm 0.07) \times 10^{-2}, \quad (269)$$

and, combined with the lattice QCD prediction for $\frac{\zeta_{p\mu\nu}(15\text{GeV}^2)}{\zeta_{\Lambda_c\mu\nu}(7\text{GeV}^2)}$ discussed in Sec. 8.6,

$$|V_{ub}/V_{cb}| = 0.079 \pm 0.004_{\text{lat.}} \pm 0.004_{\text{exp.}}. \quad (270)$$

We remind the reader that the lattice calculation for the form factor ratio currently has a ■ rating; thus we will not use the result in Eq. (270) in the global $[V_{ub}, V_{cb}]$ fit.

8.11 Determination of $|V_{ub}/V_{cb}|$ from B_s decays

More recently, LHCb reported the measurements [230]

$$\begin{aligned} R_{\text{BF}}(B_s, \text{low}) &= \frac{\int_{q_{\min}^2=m_\mu^2}^{7\text{GeV}^2} \frac{d\mathcal{B}(B_s \rightarrow K^- \mu^+ \nu_\mu)}{dq^2} dq^2}{\mathcal{B}(B_s \rightarrow D_s^- \mu^+ \nu_\mu)} \\ &= (1.66 \pm 0.12) \times 10^{-3}, \end{aligned} \quad (271)$$

$$\begin{aligned} R_{\text{BF}}(B_s, \text{high}) &= \frac{\int_{7\text{GeV}^2}^{q_{\max}^2=(m_{B_s}-m_K)^2} \frac{d\mathcal{B}(B_s \rightarrow K^- \mu^+ \nu_\mu)}{dq^2} dq^2}{\mathcal{B}(B_s \rightarrow D_s^- \mu^+ \nu_\mu)} \\ &= (3.25 \pm 0.28) \times 10^{-3}, \end{aligned} \quad (272)$$

$$\begin{aligned} R_{\text{BF}}(B_s, \text{all}) &= \frac{\mathcal{B}(B_s \rightarrow K^- \mu^+ \nu_\mu)}{\mathcal{B}(B_s \rightarrow D_s^- \mu^+ \nu_\mu)} \\ &= (4.89 \pm 0.33) \times 10^{-3}. \end{aligned} \quad (273)$$

Using our average of the $B_s \rightarrow K$ form factors from lattice QCD as discussed in Sec. 8.3.3, we obtain the Standard-Model predictions

$$\frac{1}{|V_{ub}|^2} \int_{q_{\min}^2=m_\mu^2}^{7\text{GeV}^2} \frac{d\Gamma(B_s \rightarrow K^- \mu^+ \nu_\mu)}{dq^2} = (2.51 \pm 0.62) \text{ ps}^{-1}, \quad (274)$$

$$\frac{1}{|V_{ub}|^2} \int_{7\text{GeV}^2}^{q_{\max}^2=(m_{B_s}-m_K)^2} \frac{d\Gamma(B_s \rightarrow K^- \mu^+ \nu_\mu)}{dq^2} = (4.02 \pm 0.51) \text{ ps}^{-1}, \quad (275)$$

$$\frac{1}{|V_{ub}|^2} \Gamma(B_s \rightarrow K^- \mu^+ \nu_\mu) = (6.5 \pm 1.1) \text{ ps}^{-1}. \quad (276)$$

For the denominator, we use the $B_s \rightarrow D_s$ form factors from Ref. [162] (HPQCD 19), which yields

$$\frac{1}{|V_{cb}|^2} \Gamma(B_s \rightarrow D_s^- \mu^+ \nu_\mu) = (9.15 \pm 0.37) \text{ ps}^{-1}. \quad (277)$$

Since the form factor shape is most reliably constrained by the lattice data only at high- q^2 , the most reliable determination of the ratio $|V_{ub}/V_{cb}|$ is obtained by using LHCb measurements limited to the high- q^2 region. The result which we obtain and which is used in the combination presented in Sec. 8.12, reads:

$$\frac{|V_{ub}|}{|V_{cb}|}(\text{high}) = 0.0861 \pm 0.0057_{\text{lat.}} \pm 0.0038_{\text{exp.}}. \quad (278)$$

For reference, the corresponding CKM ratio obtained at low- q^2 and in the whole q^2 regions are, $|V_{ub}|/|V_{cb}|(\text{low}) = 0.0779 \pm 0.0098_{\text{lat.}} \pm 0.0028_{\text{exp.}}$ and $|V_{ub}|/|V_{cb}|(\text{all}) = 0.0828 \pm 0.0070_{\text{lat.}} \pm 0.0028_{\text{exp.}}$, respectively.

8.12 Summary: $|V_{ub}|$ and $|V_{cb}|$

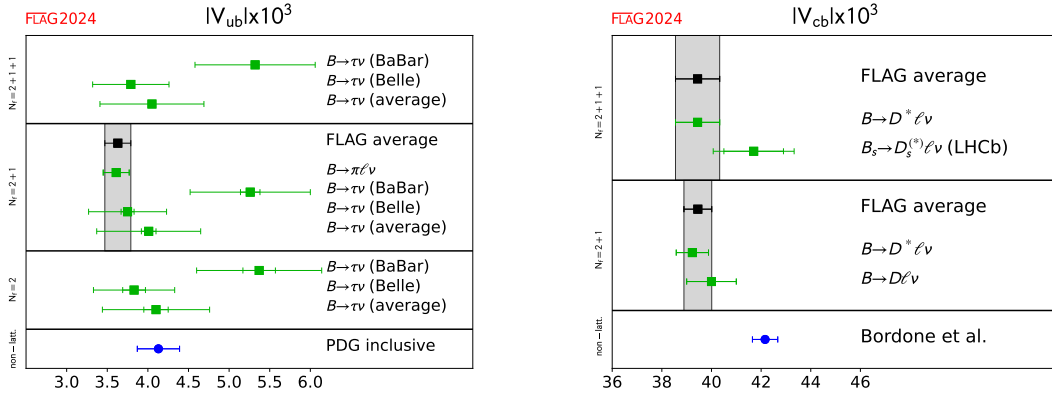


Figure 35: Left: Summary of $|V_{ub}|$ determined using: i) the B -meson leptonic decay branching fraction, $B(B^- \rightarrow \tau^- \bar{\nu})$, measured at the Belle and BaBar experiments, and our averages for f_B from lattice QCD; and ii) the various measurements of the $B \rightarrow \pi \ell \nu$ decay rates by Belle and BaBar, and our averages for lattice determinations of the relevant vector form factor $f_+(q^2)$. The inclusive result is taken from PDG [15]. Right: Same for determinations of $|V_{cb}|$ using semileptonic decays. The inclusive result is taken from Ref. [228].

In Fig. 36, we present a summary of determinations of $|V_{ub}|$ and $|V_{cb}|$ from $B \rightarrow (\pi, D^{(*)})\ell\nu$, $B_s \rightarrow (K, D_s)\ell\nu$ (high q^2 only), $B \rightarrow \tau\nu$ and $\Lambda_b \rightarrow (p, \Lambda_c)\ell\nu$, as well as the results from inclusive $B \rightarrow X_{u,c}\ell\nu$ decays. Currently, the determinations of V_{cb} from $B \rightarrow D^*$ and $B \rightarrow D$ decays are quite compatible; however, a sizeable tension involving the extraction of V_{cb} from inclusive decays remains. Note that constraints on $|V_{ub}/V_{cb}|$ from baryon modes are displayed but, in view of the rating in Tab. 48, are not included in the global fit. As discussed in Sec. 8.9, experimental inputs used in the extraction of $|V_{cb}|$ from $B_s \rightarrow D_s^{(*)}\ell\nu$ decays [171, 172] given in Eq. (266) are highly correlated with those entering the global $(|V_{ub}|, |V_{cb}|)$ fit described in this section. Given these correlations and the challenges in reproducing the LHCb analysis, for the time being we do not include the result Eq. (266) into the global fit.

In the global fit we include an estimate of the correlations between the $|V_{ub}|$ and $|V_{cb}|$ determinations from semileptonic B decays. We conservatively assume 100% correlation between the statistical lattice uncertainties on (1) $|V_{ub}|$ (FNAL/MILC), $|V_{cb}|_{B \rightarrow D}$ (FNAL/MILC

and HPQCD) and $|V_{cb}|_{B \rightarrow D^*}$ (FNAL/MILC) and (2) $|V_{ub}|$ (JLQCD) and $|V_{cb}|_{B \rightarrow D}$ (JLQCD). Due to the difficulty of disentangling statistical lattice uncertainties in the three BGL fits for $B \rightarrow (\pi, D, D^*)$, we follow the same approximate procedure described at the end of Sec. 8.9 and estimate the correlations by looking at the zero-recoil form factors $f_+(0)$, $\mathcal{F}^{B \rightarrow D}(1)$ and $\mathcal{F}^{B \rightarrow D^*}(1)$. The results of the fit are

$$|V_{cb}| = 39.46(53) \times 10^{-3}, \quad (279)$$

$$|V_{ub}| = 3.60(14) \times 10^{-3}, \quad (280)$$

$$p\text{-value} = 0.66, \quad (281)$$

with a 0.36 correlation coefficient. For reference, the fit without the inclusion of any correlation between the various lattice calculations yield $|V_{cb}| = 39.50(51) \times 10^{-3}$, $|V_{ub}| = 3.60(13) \times 10^{-3}$ with a 0.09 correlation coefficient (the latter does not vanish because of the inclusion of $|V_{ub}/V_{cb}|$ from $B_s \rightarrow (K, D_s)\ell\nu$ decays).

The inclusive determinations read $|V_{cb}|_{\text{incl}} = (42.16 \pm 0.51) \times 10^{-3}$ [231] and $|V_{ub}|_{\text{incl}} = (4.13 \pm 0.12_{\text{exp}} \pm {}^{+0.13}_{-0.14}_{\text{theo}} \pm 0.18_{\Delta\text{model}}) \times 10^{-3}$ [15].

References

- [1] [FLAG 19] S. Aoki et al., *FLAG Review 2019: Flavour Lattice Averaging Group (FLAG)*, *Eur. Phys. J. C* **80** (2020) 113 [1902.08191].
- [2] BABAR collaboration, *Evidence of $B \rightarrow \tau\nu$ decays with hadronic B tags*, *Phys.Rev.* **D88** (2013) 031102 [1207.0698].
- [3] BELLE collaboration, *Measurement of the branching fraction of $B^+ \rightarrow \tau^+\nu_\tau$ decays with the semileptonic tagging method*, *Phys. Rev.* **D92** (2015) 051102 [1503.05613].
- [4] T. Inami and C.S. Lim, *Effects of superheavy quarks and leptons in low-energy weak processes $K_L \rightarrow \mu\bar{\mu}$, $K^+ \rightarrow \pi^+\nu\bar{\nu}$ and $K^0 \leftrightarrow \bar{K}^0$* , *Prog. Theor. Phys.* **65** (1981) 297.
- [5] G. Buchalla and A.J. Buras, *QCD corrections to rare K and B decays for arbitrary top quark mass*, *Nucl.Phys.* **B400** (1993) 225.
- [6] LHCb collaboration, *First evidence for the decay $B_s \rightarrow \mu^+\mu^-$* , *Phys.Rev.Lett.* **110** (2013) 021801 [1211.2674].
- [7] LHCb, CMS collaboration, *Observation of the rare $B_s^0 \rightarrow \mu^+\mu^-$ decay from the combined analysis of CMS and LHCb data*, *Nature* **522** (2015) 68 [1411.4413].
- [8] ATLAS collaboration, *Study of the rare decays of B_s^0 and B^0 mesons into muon pairs using data collected during 2015 and 2016 with the ATLAS detector*, *JHEP* **04** (2019) 098 [1812.03017].
- [9] CMS collaboration, *Measurement of properties of $B_s^0 \rightarrow \mu^+\mu^-$ decays and search for $B^0 \rightarrow \mu^+\mu^-$ with the CMS experiment*, *JHEP* **04** (2020) 188 [1910.12127].
- [10] LHCb collaboration, *Measurement of the $B_s^0 \rightarrow \mu^+\mu^-$ branching fraction and effective lifetime and search for $B^0 \rightarrow \mu^+\mu^-$ decays*, *Phys. Rev. Lett.* **118** (2017) 191801 [1703.05747].

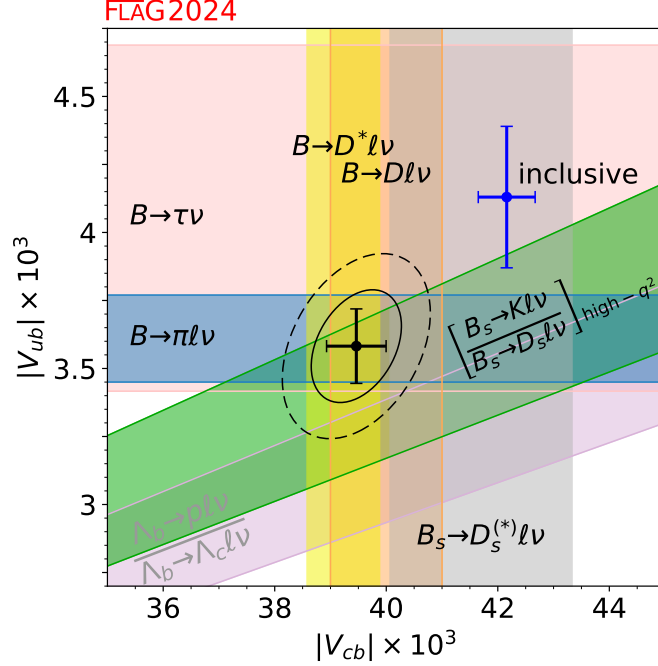


Figure 36: Summary of $|V_{ub}|$ and $|V_{cb}|$ determinations. The black solid and dashed lines correspond to 68% and 95% C.L. contours, respectively. The result of the global fit (which does not include $|V_{ub}/V_{cb}|$ from baryon modes nor $|V_{cb}|$ from $B_s \rightarrow D_s^{(*)} \ell \nu$) is $(|V_{cb}|, |V_{ub}|) = (39.46 \pm 0.53, 3.60 \pm 0.14) \times 10^{-3}$ with a p -value of 0.66. The lattice and experimental results that contribute to the various contours are the following. $B \rightarrow \pi \ell \nu$: lattice (FNAL/MILC 15 [82], RBC/UKQCD 15 [83], and JLQCD 22 [84]) and experiment (BaBar [99, 219] and Belle [100, 220]). $B \rightarrow D \ell \nu$: lattice (FNAL/MILC 15C [161] and HPQCD 15 [159]) and experiment (BaBar [222] and Belle [221]). $B \rightarrow D^* \ell \nu$: lattice (FNAL/MILC 21 [163], JLQCD 23 [164], HPQCD 23 [165]) and experiment (Belle [177, 224], Belle II [225], HFLAV [190]). $B \rightarrow \tau \nu$: lattice ($N_f = 2 + 1 + 1$ determination of f_B in Eq. (168) [31, 34, 36, 40]) and experiment (BaBar [3] and Belle [2]). $B_s \rightarrow K \ell \nu / B_s \rightarrow D_s \ell \nu$: lattice (HPQCD 14 [117], RBC/UKQCD 23 [118], FNAL/MILC 19 [119], HPQCD 19 [162]) and experiment (LHCb [230]). $\Lambda_b \rightarrow p \ell \nu / \Lambda_b \rightarrow \Lambda_c \ell \nu$: lattice (Detmold 15 [200]) and experiment (LHCb [198]). $B_s \rightarrow D_s^* \ell \nu / B_s \rightarrow D_s \ell \nu$: lattice (HPQCD 19 [162] and HPQCD 19B [187]) and experiment (LHCb [171, 172]). The inclusive determinations are taken from Refs. [64, 228, 229] and read $(|V_{cb}|, |V_{ub}|)_{\text{incl}} = (42.16 \pm 0.51, 4.13 \pm 0.26) \times 10^{-3}$.

[11] ATLAS collaboration, *Combination of the ATLAS, CMS and LHCb results on the $B_{(s)}^0 \rightarrow \mu^+ \mu^-$ decays.*, 2020. LHCb-CONF-2020-002, CMS PAS BPH-20-003, ATLAS-CONF-2020-049.

[12] M. Beneke, C. Bobeth and R. Szafron, *Power-enhanced leading-logarithmic QED corrections to $B_q \rightarrow \mu^+ \mu^-$* , *JHEP* **10** (2019) 232 [1908.07011].

[13] LHCb collaboration, *Measurement of the $B_s^0 \rightarrow \mu^+ \mu^-$ decay properties and search*

- for the $B^0 \rightarrow \mu^+\mu^-$ and $B_s^0 \rightarrow \mu^+\mu^-\gamma$ decays, *Phys. Rev. D* **105** (2022) 012010 [[2108.09283](#)].
- [14] CMS collaboration, *Measurement of the $B_S^0 \rightarrow \mu^+\mu^-$ decay properties and search for the $B^0 \rightarrow \mu^+\mu^-$ decay in proton-proton collisions at $\sqrt{s} = 13$ TeV*, *Phys. Lett. B* **842** (2023) 137955 [[2212.10311](#)].
- [15] PARTICLE DATA GROUP collaboration, *Review of particle physics*, *Phys. Rev. D* **110** (2024) 030001.
- [16] W. Altmannshofer and P. Stangl, *New Physics in Rare B Decays after Moriond 2021*, *Eur. Phys. J. C* **81** (2021) 952 [[2103.13370](#)].
- [17] LHCb collaboration, *Analysis of Neutral B-Meson Decays into Two Muons*, *Phys. Rev. Lett.* **128** (2022) 041801 [[2108.09284](#)].
- [18] T. Janowski, B. Pullin and R. Zwicky, *Charged and neutral $\overline{B}_{u,d,s} \rightarrow \gamma$ form factors from light cone sum rules at NLO*, *JHEP* **12** (2021) 008 [[2106.13616](#)].
- [19] A. Kozachuk, D. Melikhov and N. Nikitin, *Rare FCNC radiative leptonic $B_{s,d} \rightarrow \gamma l^+ l^-$ decays in the standard model*, *Phys. Rev. D* **97** (2018) 053007 [[1712.07926](#)].
- [20] I. Belov, A. Berezhnoy and D. Melikhov, *Nonfactorizable charming-loop contribution to FCNC $B_s \rightarrow \gamma l^+ l^-$ decay*, *Phys. Rev. D* **109** (2024) 114012 [[2404.01222](#)].
- [21] D. Guadagnoli, C. Normand, S. Simula and L. Vittorio, *From $D_s \rightarrow \gamma$ in lattice QCD to $B_s \rightarrow \mu\mu\gamma$ at high q^2* , *JHEP* **07** (2023) 112 [[2303.02174](#)].
- [22] R. Frezzotti, G. Gagliardi, V. Lubicz, G. Martinelli, C.T. Sachrajda, F. Sanfilippo et al., *The $B_s \rightarrow \mu^+\mu^-\gamma$ decay rate at large q^2 from lattice QCD*, *Phys. Rev. D* **109** (2024) 114506 [[2402.03262](#)].
- [23] CLEO collaboration, *Search for $B \rightarrow \mu\bar{\nu}_\mu\gamma$ and $B \rightarrow e\bar{\nu}_e\gamma$* , *Phys. Rev. D* **56** (1997) 11.
- [24] BABAR collaboration, *A Model-independent search for the decay $B^+ \rightarrow \ell^+\nu_\ell\gamma$* , *Phys. Rev. D* **80** (2009) 111105 [[0907.1681](#)].
- [25] BELLE collaboration, *Search for $B^+ \rightarrow \ell^+\nu_\ell\gamma$ decays with hadronic tagging using the full Belle data sample*, *Phys. Rev. D* **91** (2015) 112009 [[1504.05831](#)].
- [26] BELLE collaboration, *Search for the rare decay of $B^+ \rightarrow \ell^+\nu_\ell\gamma$ with improved hadronic tagging*, *Phys. Rev. D* **98** (2018) 112016 [[1810.12976](#)].
- [27] M. Beneke, V.M. Braun, Y. Ji and Y.-B. Wei, *Radiative leptonic decay $B \rightarrow \gamma\ell\nu_\ell$ with subleading power corrections*, *JHEP* **07** (2018) 154 [[1804.04962](#)].
- [28] S. Zhao and A.V. Radyushkin, *B-meson Ioffe-time distribution amplitude at short distances*, *Phys. Rev. D* **103** (2021) 054022 [[2006.05663](#)].
- [29] J. Xu, X.-R. Zhang and S. Zhao, *Inverse moment of the B-meson quasidistribution amplitude*, *Phys. Rev. D* **106** (2022) L011503 [[2202.13648](#)].

- [30] [ETM 13B] N. Carrasco et al., *B-physics from $N_f = 2$ tmQCD: the Standard Model and beyond*, *JHEP* **1403** (2014) 016 [[1308.1851](#)].
- [31] [ETM 16B] A. Bussone et al., *Mass of the b quark and B -meson decay constants from $N_f=2+1+1$ twisted-mass lattice QCD*, *Phys. Rev.* **D93** (2016) 114505 [[1603.04306](#)].
- [32] [HPQCD 12] H. Na, C.J. Monahan, C.T. Davies, R. Horgan, G.P. Lepage et al., *The B and B_s meson decay constants from lattice QCD*, *Phys.Rev.* **D86** (2012) 034506 [[1202.4914](#)].
- [33] R. Balasubramanian and B. Blossier, *Decay constant of B_s and B_s^* mesons from $N_f = 2$ lattice QCD*, *Eur. Phys. J. C* **80** (2020) 412 [[1912.09937](#)].
- [34] [FNAL/MILC 17] A. Bazavov et al., *B - and D -meson leptonic decay constants from four-flavor lattice QCD*, *Phys. Rev.* **D98** (2018) 074512 [[1712.09262](#)].
- [35] [FNAL/MILC 11] A. Bazavov et al., *B - and D -meson decay constants from three-flavor lattice QCD*, *Phys.Rev.* **D85** (2012) 114506 [[1112.3051](#)].
- [36] [HPQCD 13] R. J. Dowdall, C. Davies, R. Horgan, C. Monahan and J. Shigemitsu, *B -meson decay constants from improved lattice NRQCD and physical u , d , s and c sea quarks*, *Phys.Rev.Lett.* **110** (2013) 222003 [[1302.2644](#)].
- [37] [RBC/UKQCD 14] N. H. Christ, J.M. Flynn, T. Izubuchi, T. Kawanai, C. Lehner et al., *B -meson decay constants from $2+1$ -flavor lattice QCD with domain-wall light quarks and relativistic heavy quarks*, *Phys.Rev.* **D91** (2015) 054502 [[1404.4670](#)].
- [38] N. Carrasco, V. Lubicz, G. Martinelli, C.T. Sachrajda, N. Tantalo, C. Tarantino et al., *QED Corrections to Hadronic Processes in Lattice QCD*, *Phys. Rev.* **D91** (2015) 074506 [[1502.00257](#)].
- [39] [FLAG 21] Y. Aoki et al., *FLAG Review 2021*, *Eur. Phys. J. C* **82** (2022) 869 [[2111.09849](#)].
- [40] [HPQCD 17A] C. Hughes, C.T.H. Davies and C.J. Monahan, *New methods for B meson decay constants and form factors from lattice NRQCD*, *Phys. Rev.* **D97** (2018) 054509 [[1711.09981](#)].
- [41] [ETM 13E] N. Carrasco, P. Dimopoulos, R. Frezzotti, V. Giménez, P. Lami et al., *A $N_f = 2 + 1 + 1$ 'twisted' determination of the b -quark mass, f_B and f_{B_s}* , *PoS LATTICE2013* (2014) 313 [[1311.2837](#)].
- [42] [RBC/UKQCD 14A] Y. Aoki, T. Ishikawa, T. Izubuchi, C. Lehner and A. Soni, *Neutral B meson mixings and B meson decay constants with static heavy and domain-wall light quarks*, *Phys. Rev.* **D91** (2015) 114505 [[1406.6192](#)].
- [43] [RBC/UKQCD 13A] O. Witzel, *B -meson decay constants with domain-wall light quarks and nonperturbatively tuned relativistic b -quarks*, *PoS LATTICE2013* (2014) 377 [[1311.0276](#)].
- [44] [HPQCD 11A] C. McNeile, C.T.H. Davies, E. Follana, K. Hornbostel and G.P. Lepage, *High-precision f_{B_s} and HQET from relativistic lattice QCD*, *Phys.Rev.* **D85** (2012) 031503 [[1110.4510](#)].

- [45] [HPQCD 09] E. Gamiz, C.T. Davies, G.P. Lepage, J. Shigemitsu and M. Wingate, *Neutral B meson mixing in unquenched lattice QCD*, *Phys.Rev.* **D80** (2009) 014503 [[0902.1815](#)].
- [46] [ALPHA 14] F. Bernardoni et al., *Decay constants of B-mesons from non-perturbative HQET with two light dynamical quarks*, *Phys.Lett.* **B735** (2014) 349 [[1404.3590](#)].
- [47] [ALPHA 13] F. Bernardoni, B. Blossier, J. Bulava, M. Della Morte, P. Fritzsch et al., *B-physics with $N_f = 2$ Wilson fermions*, *PoS LATTICE2013* (2014) 381 [[1309.1074](#)].
- [48] [ETM 13C] N. Carrasco et al., *B-physics computations from $N_f=2$ tmQCD*, *PoS LATTICE2013* (2014) 382 [[1310.1851](#)].
- [49] [ALPHA 12A] F. Bernardoni, B. Blossier, J. Bulava, M. Della Morte, P. Fritzsch et al., *B-physics from HQET in two-flavour lattice QCD*, *PoS LAT2012* (2012) 273 [[1210.7932](#)].
- [50] [ETM 12B] N. Carrasco, P. Dimopoulos, R. Frezzotti, V. Gimenez, G. Herdoiza et al., *B-physics from the ratio method with Wilson twisted mass fermions*, *PoS LAT2012* (2012) 104 [[1211.0568](#)].
- [51] [ALPHA 11] B. Blossier, J. Bulava, M. Della Morte, M. Donnellan, P. Fritzsch et al., *M_b and f_B from non-perturbatively renormalized HQET with $N_f = 2$ light quarks*, *PoS LAT2011* (2011) 280 [[1112.6175](#)].
- [52] [ETM 11A] P. Dimopoulos et al., *Lattice QCD determination of m_b , f_B and f_{B_s} with twisted mass Wilson fermions*, *JHEP* **1201** (2012) 046 [[1107.1441](#)].
- [53] [ETM 09D] B. Blossier et al., *A proposal for B-physics on current lattices*, *JHEP* **1004** (2010) 049 [[0909.3187](#)].
- [54] [HPQCD 05B] A. Gray et al., *The upsilon spectrum and m_b from full lattice QCD*, *Phys.Rev.* **D72** (2005) 094507 [[hep-lat/0507013](#)].
- [55] [QCDSF/UKQCD/CSSM 22] S. Hollitt et al., *Measurements of $SU(3)_f$ symmetry breaking in B meson decay constants*, *PoS LATTICE2021* (2022) 549 [[2201.10779](#)].
- [56] [RBC/UKQCD 18A] P. A. Boyle, L. Del Debbio, N. Garron, A. Juttner, A. Soni, J.T. Tsang et al., *$SU(3)$ -breaking ratios for $D_{(s)}$ and $B_{(s)}$ mesons*, [1812.08791](#).
- [57] [RBC/UKQCD 10C] C. Albertus et al., *Neutral B-meson mixing from unquenched lattice QCD with domain-wall light quarks and static b-quarks*, *Phys.Rev.* **D82** (2010) 014505 [[1001.2023](#)].
- [58] [RBC/UKQCD 22] M. Black and O. Witzel, *B Meson Decay Constants Using Relativistic Heavy Quarks*, *PoS LATTICE2022* (2023) 405 [[2212.10125](#)].
- [59] [QCDSF/UKQCD 10] W. Bietenholz et al., *Tuning the strange quark mass in lattice simulations*, *Phys. Lett.* **B690** (2010) 436 [[1003.1114](#)].
- [60] [RBC/UKQCD 12A] Y. Aoki et al., *Nonperturbative tuning of an improved relativistic heavy-quark action with application to bottom spectroscopy*, *Phys.Rev.* **D86** (2012) 116003 [[1206.2554](#)].

- [61] [RBC/UKQCD 14B] T. Blum et al., *Domain wall QCD with physical quark masses*, *Phys. Rev.* **D93** (2016) 074505 [[1411.7017](#)].
- [62] H. Akaike, *A new look at the statistical model identification*, *IEEE Trans. Automatic Control* **19** (1974) 716.
- [63] G. Buchalla, A.J. Buras and M.E. Lautenbacher, *Weak decays beyond leading logarithms*, *Rev. Mod. Phys.* **68** (1996) 1125 [[hep-ph/9512380](#)].
- [64] PARTICLE DATA GROUP collaboration, *Review of Particle Physics*, *PTEP* **2020** (2020) 083C01.
- [65] F. Gabbiani, E. Gabrielli, A. Masiero and L. Silvestrini, *A Complete analysis of FCNC and CP constraints in general SUSY extensions of the standard model*, *Nucl. Phys.* **B477** (1996) 321 [[hep-ph/9604387](#)].
- [66] A. Lenz and U. Nierste, *Theoretical update of $B_s - \bar{B}_s$ mixing*, *JHEP* **0706** (2007) 072 [[hep-ph/0612167](#)].
- [67] M. Beneke, G. Buchalla and I. Dunietz, *Width difference in the $B_s - \bar{B}_s$ system*, *Phys.Rev.* **D54** (1996) 4419 [[hep-ph/9605259](#)].
- [68] [FLAG 13] S. Aoki, Y. Aoki, C. Bernard, T. Blum, G. Colangelo et al., *Review of lattice results concerning low-energy particle physics*, *Eur.Phys.J.* **C74** (2014) 2890 [[1310.8555](#)].
- [69] [FNAL/MILC 11A] C. M. Bouchard, E. Freeland, C. Bernard, A. El-Khadra, E. Gamiz et al., *Neutral B mixing from 2 + 1 flavor lattice-QCD: the Standard Model and beyond*, *PoS LAT2011* (2011) 274 [[1112.5642](#)].
- [70] [FNAL/MILC 16] A. Bazavov et al., *$B_{(s)}^0$ -mixing matrix elements from lattice QCD for the Standard Model and beyond*, *Phys. Rev.* **D93** (2016) 113016 [[1602.03560](#)].
- [71] [HPQCD 19A] R. J. Dowdall, C.T.H. Davies, R.R. Horgan, G.P. Lepage, C.J. Monahan, J. Shigemitsu et al., *Neutral B-meson mixing from full lattice QCD at the physical point*, *Phys. Rev.* **D100** (2019) 094508 [[1907.01025](#)].
- [72] J.T. Tsang and M. Della Morte, *B-physics from lattice gauge theory*, *Eur. Phys. J. ST* **233** (2024) 253 [[2310.02705](#)].
- [73] [HPQCD 06A] E. Dalgic, A. Gray, E. Gamiz, C.T. Davies, G.P. Lepage et al., *$B_s^0 - \bar{B}_s^0$ mixing parameters from unquenched lattice QCD*, *Phys.Rev.* **D76** (2007) 011501 [[hep-lat/0610104](#)].
- [74] [ETM 12A] N. Carrasco et al., *Neutral meson oscillations in the Standard Model and beyond from $N_f = 2$ twisted mass lattice QCD*, *PoS LAT2012* (2012) 105 [[1211.0565](#)].
- [75] J.L. Rosner, S. Stone and R.S. Van de Water, *Leptonic Decays of Charged Pseudoscalar Mesons*, in *Review of Particle Physics [232] 2015 update*, [1509.02220](#).
- [76] [FNAL/MILC 12] A. Bazavov, C. Bernard, C. Bouchard, C. DeTar, M. Di Pierro et al., *Neutral B-meson mixing from three-flavor lattice QCD: determination of the $SU(3)$ -breaking ratio ξ* , *Phys.Rev.* **D86** (2012) 034503 [[1205.7013](#)].

- [77] [FLAG 16] S. Aoki et al., *Review of lattice results concerning low-energy particle physics*, *Eur. Phys. J.* **C77** (2017) 112 [[1607.00299](#)].
- [78] P. Boyle, F. Erben, A. Jüttner, T. Kaneko, M. Marshall, A. Portelli et al., *BSM $B - \bar{B}$ mixing on JLQCD and RBC/UKQCD $N_f = 2 + 1$ DWF ensembles*, *PoS LATTICE2021* (2022) 224 [[2111.11287](#)].
- [79] M. Della Morte, B. Jäger, T. Rae and H. Wittig, *Improved interpolating fields for hadrons at non-zero momentum*, *Eur.Phys.J.* **A48** (2012) 139 [[1208.0189](#)].
- [80] [HPQCD 06] E. Dalgic et al., *B meson semileptonic form-factors from unquenched lattice QCD*, *Phys.Rev.* **D73** (2006) 074502 [[hep-lat/0601021](#)].
- [81] [FNAL/MILC 08A] J. A. Bailey et al., *The $B \rightarrow \pi \ell \nu$ semileptonic form factor from three-flavor lattice QCD: a model-independent determination of $|V_{ub}|$* , *Phys.Rev.* **D79** (2009) 054507 [[0811.3640](#)].
- [82] [FNAL/MILC 15] J. A. Bailey et al., *$|V_{ub}|$ from $B \rightarrow \pi \ell \nu$ decays and $(2+1)$ -flavor lattice QCD*, *Phys. Rev.* **D92** (2015) 014024 [[1503.07839](#)].
- [83] [RBC/UKQCD 15] J. M. Flynn, T. Izubuchi, T. Kawanai, C. Lehner, A. Soni, R.S. Van de Water et al., *$B \rightarrow \pi \ell \nu$ and $B_s \rightarrow K \ell \nu$ form factors and $|V_{ub}|$ from $2+1$ -flavor lattice QCD with domain-wall light quarks and relativistic heavy quarks*, *Phys. Rev.* **D91** (2015) 074510 [[1501.05373](#)].
- [84] [JLQCD 22] B. Colquhoun, S. Hashimoto, T. Kaneko and J. Koponen, *Form factors of $B \rightarrow \pi \ell \nu$ and a determination of $|V_{ub}|$ with Möbius domain-wall fermions*, *Phys. Rev. D* **106** (2022) 054502 [[2203.04938](#)].
- [85] Z. Gelzer et al., *Semileptonic B-meson decays to light pseudoscalar mesons on the HISQ ensembles*, *EPJ Web Conf.* **175** (2018) 13024 [[1710.09442](#)].
- [86] [FNAL/MILC 19A] Z. Gelzer et al., *B-meson semileptonic form factors on $(2+1+1)$ -flavor HISQ ensembles*, *PoS LATTICE2019* (2019) 236 [[1912.13358](#)].
- [87] J. Flynn, R. Hill, A. Jüttner, A. Soni, J.T. Tsang and O. Witzel, *Semileptonic $B \rightarrow \pi \ell \nu$, $B \rightarrow D \ell \nu$, $B_s \rightarrow K \ell \nu$, and $B_s \rightarrow D_s \ell \nu$ decays*, *PoS LATTICE2019* (2019) 184 [[1912.09946](#)].
- [88] [HPQCD 15A] B. Colquhoun, R.J. Dowdall, J. Koponen, C.T.H. Davies and G.P. Lepage, *$B \rightarrow \pi \ell \nu$ at zero recoil from lattice QCD with physical u/d quarks*, *Phys. Rev.* **D93** (2016) 034502 [[1510.07446](#)].
- [89] [HPQCD 12C] C. M. Bouchard, G.P. Lepage, C.J. Monahan, H. Na and J. Shigemitsu, *Form factors for B and B_s semileptonic decays with NRQCD/HISQ quarks*, *PoS LAT2012* (2012) 118 [[1210.6992](#)].
- [90] [HPQCD 13F] C. M. Bouchard, G.P. Lepage, J.C. Monahan, H. Na and J. Shigemitsu, *B and B_s semileptonic decay form factors with NRQCD/HISQ quarks*, *PoS LATTICE2013* (2014) 387 [[1310.3207](#)].

- [91] J. Flynn, R. Hill, A. Juettner, A. Soni, J.T. Tsang and O. Witzel, *Form factors for semileptonic $B \rightarrow \pi$, $B_s \rightarrow K$ and $B_s \rightarrow D_s$ decays*, *PoS LATTICE2021* (2022) 306 [[2112.10580](#)].
- [92] [BMW 12A] S. Borsanyi, S. Dür, Z. Fodor, C. Hoelbling, S.D. Katz et al., *High-precision scale setting in lattice QCD*, *JHEP* **1209** (2012) 010 [[1203.4469](#)].
- [93] J. Bijnens and I. Jemos, *Hard Pion Chiral Perturbation Theory for $B \rightarrow \pi$ and $D \rightarrow \pi$ Formfactors*, *Nucl. Phys.* **B840** (2010) 54 [[1006.1197](#)], [Erratum: Nucl. Phys.B844,182(2011)].
- [94] G. Colangelo, M. Procura, L. Rothen, R. Stucki and J. Tarrus Castella, *On the factorization of chiral logarithms in the pion form factors*, *JHEP* **09** (2012) 081 [[1208.0498](#)].
- [95] P. Ball and R. Zwicky, *$|V_{ub}|$ and constraints on the leading-twist pion distribution amplitude from $B \rightarrow \pi \ell \nu$* , *Phys. Lett. B* **625** (2005) 225 [[hep-ph/0507076](#)].
- [96] D. Bećirević and A.B. Kaidalov, *Comment on the heavy \rightarrow light form-factors*, *Phys.Lett.* **B478** (2000) 417 [[hep-ph/9904490](#)].
- [97] R.J. Hill, *Heavy-to-light meson form-factors at large recoil*, *Phys.Rev.* **D73** (2006) 014012 [[hep-ph/0505129](#)].
- [98] C.G. Boyd, B. Grinstein and R.F. Lebed, *Constraints on form-factors for exclusive semileptonic heavy to light meson decays*, *Phys.Rev.Lett.* **74** (1995) 4603 [[hep-ph/9412324](#)].
- [99] BABAR collaboration, *Study of $B \rightarrow \pi \ell \nu$ and $B \rightarrow \rho \ell \nu$ Decays and Determination of $|V_{ub}|$* , *Phys.Rev.* **D83** (2011) 032007 [[1005.3288](#)], 47 pages, 26 postscript figures, accepted by Phys. Rev. D.
- [100] BELLE collaboration, *Study of Exclusive $B \rightarrow X_u \ell \nu$ Decays and Extraction of $\|V_{ub}\|$ using Full Reconstruction Tagging at the Belle Experiment*, *Phys. Rev.* **D88** (2013) 032005 [[1306.2781](#)].
- [101] BELLE-II collaboration, *Reconstruction of $B \rightarrow \rho \ell \nu_\ell$ decays identified using hadronic decays of the recoil B meson in 2019 – 2021 Belle II data*, [2211.15270](#).
- [102] [UKQCD 04] K. C. Bowler, J.F. Gill, C.M. Maynard and J.M. Flynn, *$B \rightarrow \rho \ell \nu$ form-factors in lattice QCD*, *JHEP* **05** (2004) 035 [[hep-lat/0402023](#)].
- [103] J.M. Flynn, Y. Nakagawa, J. Nieves and H. Toki, *$|V_{ub}|$ from Exclusive Semileptonic $B \rightarrow \rho$ Decays*, *Phys. Lett. B* **675** (2009) 326 [[0812.2795](#)].
- [104] M. Lüscher, *Volume Dependence of the Energy Spectrum in Massive Quantum Field Theories. 2. Scattering States*, *Commun. Math. Phys.* **105** (1986) 153.
- [105] M. Lüscher, *Two particle states on a torus and their relation to the scattering matrix*, *Nucl. Phys.* **B354** (1991) 531.
- [106] M. Lüscher, *Signatures of unstable particles in finite volume*, *Nucl. Phys.* **B364** (1991) 237.

- [107] M. Lage, U.-G. Meissner and A. Rusetsky, *A Method to measure the antikaon-nucleon scattering length in lattice QCD*, *Phys. Lett.* **B681** (2009) 439 [[0905.0069](#)].
- [108] V. Bernard, M. Lage, U.G. Meissner and A. Rusetsky, *Scalar mesons in a finite volume*, *JHEP* **01** (2011) 019 [[1010.6018](#)].
- [109] M. Doring, U.-G. Meissner, E. Oset and A. Rusetsky, *Unitarized Chiral Perturbation Theory in a finite volume: Scalar meson sector*, *Eur. Phys. J.* **A47** (2011) 139 [[1107.3988](#)].
- [110] M.T. Hansen and S.R. Sharpe, *Multiple-channel generalization of Lellouch-Luscher formula*, *Phys. Rev.* **D86** (2012) 016007 [[1204.0826](#)].
- [111] R.A. Briceño and Z. Davoudi, *Moving multichannel systems in a finite volume with application to proton-proton fusion*, *Phys. Rev.* **D88** (2013) 094507 [[1204.1110](#)].
- [112] [HS 14] J. J. Dudek, R.G. Edwards, C.E. Thomas and D.J. Wilson, *Resonances in coupled $\pi K - \eta K$ scattering from quantum chromodynamics*, *Phys. Rev. Lett.* **113** (2014) 182001 [[1406.4158](#)].
- [113] R.A. Briceño, M.T. Hansen and A. Walker-Loud, *Multichannel $1 \rightarrow 2$ transition amplitudes in a finite volume*, *Phys. Rev. D* **91** (2015) 034501 [[1406.5965](#)].
- [114] R.A. Briceño and M.T. Hansen, *Multichannel $0 \rightarrow 2$ and $1 \rightarrow 2$ transition amplitudes for arbitrary spin particles in a finite volume*, *Phys. Rev. D* **92** (2015) 074509 [[1502.04314](#)].
- [115] L. Leskovec, S. Meinel, M. Petschlies, J. Negele, S. Paul, A. Pochinsky et al., *A lattice QCD study of the $B \rightarrow \pi\pi\ell\bar{\nu}$ transition*, *PoS LATTICE2022* (2023) 416 [[2212.08833](#)].
- [116] L. Leskovec, S. Meinel, M. Petschlies, J. Negele, S. Paul, A. Pochinsky et al., *Lattice outlook on $B \rightarrow \rho\ell\bar{\nu}$ and $B \rightarrow K^*\ell\bar{\ell}$* , in *12th International Workshop on the CKM Unitarity Triangle*, 3, 2024 [[2403.19543](#)].
- [117] [HPQCD 14] C. M. Bouchard, G.P. Lepage, C. Monahan, H. Na and J. Shigemitsu, *$B_s \rightarrow K\ell\nu$ form factors from lattice QCD*, *Phys. Rev.* **D90** (2014) 054506 [[1406.2279](#)].
- [118] [RBC/UKQCD 23] J. M. Flynn, R.C. Hill, A. Jüttner, A. Soni, J.T. Tsang and O. Witzel, *Exclusive semileptonic $B_s \rightarrow K\ell\nu$ decays on the lattice*, *Phys. Rev. D* **107** (2023) 114512 [[2303.11280](#)].
- [119] [FNAL/MILC 19] A. Bazavov et al., *$B_s \rightarrow K\ell\nu$ decay from lattice QCD*, *Phys. Rev. D* **100** (2019) 034501 [[1901.02561](#)].
- [120] J.M. Flynn, A. Jüttner and J.T. Tsang, *Bayesian inference for form-factor fits regulated by unitarity and analyticity*, *JHEP* **12** (2023) 175 [[2303.11285](#)].
- [121] T. Blake, S. Meinel, M. Rahimi and D. van Dyk, *Dispersive bounds for local form factors in $\Lambda_b \rightarrow \Lambda$ transitions*, *Phys. Rev. D* **108** (2023) 094509 [[2205.06041](#)].
- [122] [JLQCD 24] P. Mohanta, T. Kaneko and S. Hashimoto, *$B_s \rightarrow K\ell\nu$ form factors from lattice QCD with domain-wall heavy quarks*, *PoS LATTICE2023* (2024) 267 [[2401.01570](#)].

- [123] H. Jeong, C. DeTar, A.X. El-Khadra, E. Gámiz, Z. Gelzer, S. Gottlieb et al., *Form factors for semileptonic B-decays with HISQ light quarks and clover b-quarks in Fermilab interpretation*, *PoS LATTICE2023* (2024) 253 [[2402.14924](#)].
- [124] A. Lytle, C. DeTar, E. Gámiz, S. Gottlieb, W. Jay, A.X. El-Khadra et al., *B-meson semileptonic decays from highly improved staggered quarks*, *PoS LATTICE2023* (2024) 240 [[2403.03959](#)].
- [125] F. Bahr, D. Banerjee, F. Bernardoni, M. Koren, H. Simma and R. Sommer, *Extraction of bare form factors for $B_s \rightarrow K\ell\nu$ decays in nonperturbative HQET*, *Int. J. Mod. Phys. A* **34** (2019) 1950166 [[1903.05870](#)].
- [126] [ALPHA 14B] F. Bahr, F. Bernardoni, J. Bulava, A. Joseph, A. Ramos, H. Simma et al., *Form factors for $B_s \rightarrow K\ell\nu$ decays in Lattice QCD*, in *8th International Workshop on the CKM Unitarity Triangle (CKM2014) Vienna, Austria, September 8-12, 2014*, 2014, <https://inspirehep.net/record/1328088/files/arXiv:1411.3916.pdf> [[1411.3916](#)].
- [127] M. Antonelli et al., *Flavor physics in the quark sector*, *Phys.Rept.* **494** (2010) 197 [[0907.5386](#)].
- [128] B. Grinstein and D. Pirjol, *Exclusive rare $B \rightarrow K^*\ell^+\ell^-$ decays at low recoil: Controlling the long-distance effects*, *Phys. Rev. D* **70** (2004) 114005 [[hep-ph/0404250](#)].
- [129] M. Beylich, G. Buchalla and T. Feldmann, *Theory of $B \rightarrow K^{(*)}\ell^+\ell^-$ decays at high q^2 : OPE and quark-hadron duality*, *Eur. Phys. J. C* **71** (2011) 1635 [[1101.5118](#)].
- [130] M. Beneke, T. Feldmann and D. Seidel, *Systematic approach to exclusive $B \rightarrow V\ell^+\ell^-$, $V\gamma$ decays*, *Nucl. Phys. B* **612** (2001) 25 [[hep-ph/0106067](#)].
- [131] Z. Liu et al., *Form factors for rare B decays: strategy, methodology, and numerical study*, *PoS LAT2009* (2009) 242 [[0911.2370](#)].
- [132] [HPQCD 22] W. G. Parrott, C. Bouchard and C.T.H. Davies, *$B \rightarrow K$ and $D \rightarrow K$ form factors from fully relativistic lattice QCD*, *Phys. Rev. D* **107** (2023) 014510 [[2207.12468](#)].
- [133] [FNAL/MILC 15D] J. A. Bailey et al., *$B \rightarrow K\ell^+\ell^-$ decay form factors from three-flavor lattice QCD*, *Phys. Rev. D* **93** (2016) 025026 [[1509.06235](#)].
- [134] [HPQCD 13E] C. Bouchard, G.P. Lepage, C. Monahan, H. Na and J. Shigemitsu, *Rare decay $B \rightarrow K\ell^+\ell^-$ form factors from lattice QCD*, *Phys. Rev. D* **88** (2013) 054509 [[1306.2384](#)], [Erratum: *Phys. Rev. D* **88** (2013) no. 7 079901].
- [135] [FNAL/MILC 15E] J. A. Bailey et al., *$B \rightarrow \pi\ell\ell$ form factors for new-physics searches from lattice QCD*, *Phys. Rev. Lett.* **115** (2015) 152002 [[1507.01618](#)].
- [136] [HPQCD 13D] C. Bouchard, G.P. Lepage, C. Monahan, H. Na and J. Shigemitsu, *Standard Model predictions for $B \rightarrow K\ell\ell$ with form factors from lattice QCD*, *Phys. Rev. Lett.* **111** (2013) 162002 [[1306.0434](#)], [Erratum: *Phys. Rev. Lett.* **112** (2014) 149902].

- [137] [FNAL/MILC 15F] D. Du, A.X. El-Khadra, S. Gottlieb, A.S. Kronfeld, J. Laiho, E. Lunghi et al., *Phenomenology of semileptonic B-meson decays with form factors from lattice QCD*, *Phys. Rev. D* **D93** (2016) 034005 [[1510.02349](#)].
- [138] LHCb collaboration, *First measurement of the differential branching fraction and CP asymmetry of the $B^\pm \rightarrow \pi^\pm \mu^+ \mu^-$ decay*, *JHEP* **10** (2015) 034 [[1509.00414](#)].
- [139] C.B. Lang, D. Mohler, S. Prelovsek and R.M. Woloshyn, *Predicting positive parity B_s mesons from lattice QCD*, *Phys. Lett. B* **B750** (2015) 17 [[1501.01646](#)].
- [140] [HPQCD 20D] D. Hatton, C.T.H. Davies, G.P. Lepage and A.T. Lytle, *Renormalization of the tensor current in lattice QCD and the J/ψ tensor decay constant*, *Phys. Rev. D* **102** (2020) 094509 [[2008.02024](#)].
- [141] [HPQCD 22A] W. G. Parrott, C. Bouchard and C.T.H. Davies, *Standard Model predictions for $B \rightarrow K \ell^+ \ell^-$, $B \rightarrow K \ell_1^- \ell_2^+$ and $B \rightarrow K \nu \bar{\nu}$ using form factors from $N_f=2+1+1$ lattice QCD*, *Phys. Rev. D* **107** (2023) 014511 [[2207.13371](#)], [Erratum: Phys.Rev.D 107, 119903 (2023)].
- [142] R.R. Horgan, Z. Liu, S. Meinel and M. Wingate, *Lattice QCD calculation of form factors describing the rare decays $B \rightarrow K^* \ell^+ \ell^-$ and $B_s \rightarrow \phi \ell^+ \ell^-$* , *Phys. Rev. D* **D89** (2014) 094501 [[1310.3722](#)].
- [143] R.R. Horgan, Z. Liu, S. Meinel and M. Wingate, *Calculation of $B^0 \rightarrow K^{*0} \mu^+ \mu^-$ and $B_s^0 \rightarrow \phi \mu^+ \mu^-$ observables using form factors from lattice QCD*, *Phys. Rev. Lett.* **112** (2014) 212003 [[1310.3887](#)].
- [144] R.R. Horgan, Z. Liu, S. Meinel and M. Wingate, *Rare B decays using lattice QCD form factors*, *PoS LATTICE2014* (2015) 372 [[1501.00367](#)].
- [145] [RBC/UKQCD 15B] J. Flynn, A. Jüttner, T. Kawanai, E. Lizarazo and O. Witzel, *Hadronic form factors for rare semileptonic B decays*, in *Proceedings, 33rd International Symposium on Lattice Field Theory (Lattice 2015)*, vol. LATTICE2015, p. 345, 2016, <http://inspirehep.net/record/1405735/files/arXiv:1511.06622.pdf> [[1511.06622](#)].
- [146] J. Flynn, T. Izubuchi, A. Jüttner, T. Kawanai, C. Lehner, E. Lizarazo et al., *Form factors for semi-leptonic B decays*, *PoS LATTICE2016* (2016) 296 [[1612.05112](#)].
- [147] E. Lizarazo and O. Witzel, *Non-perturbative determinations of B-meson decay constants and semi-leptonic form factors*, *PoS ICHEP2016* (2016) 558 [[1612.06113](#)].
- [148] A. Sirlin, *Large m_W , m_Z behavior of the $O(\alpha)$ corrections to semileptonic processes mediated by W*, *Nucl.Phys. B* **B196** (1982) 83.
- [149] M.E. Luke, *Effects of subleading operators in the heavy quark effective theory*, *Phys. Lett. B* **B252** (1990) 447.
- [150] N. Isgur and M.B. Wise, *Weak transition form-factors between heavy mesons*, *Phys.Lett. B* **B237** (1990) 527.
- [151] N. Isgur and M.B. Wise, *Weak decays of heavy mesons in the static quark approximation*, *Phys.Lett. B* **B232** (1989) 113.

- [152] M. Neubert, *Heavy quark symmetry*, *Phys. Rept.* **245** (1994) 259 [[hep-ph/9306320](#)].
- [153] A.F. Falk and M. Neubert, *Second order power corrections in the heavy quark effective theory. 1. Formalism and meson form-factors*, *Phys. Rev. D* **47** (1993) 2965 [[hep-ph/9209268](#)].
- [154] M. Neubert, *Short distance expansion of heavy quark currents*, *Phys. Rev. D* **46** (1992) 2212.
- [155] M. Neubert, *Higher order perturbative corrections to $b \rightarrow c$ transitions at zero recoil*, *Phys. Lett. B* **341** (1995) 367 [[hep-ph/9409453](#)].
- [156] A.S. Kronfeld, *Application of heavy quark effective theory to lattice QCD. 1. Power corrections*, *Phys.Rev.* **D62** (2000) 014505 [[hep-lat/0002008](#)].
- [157] J. Harada, S. Hashimoto, A.S. Kronfeld and T. Onogi, *Application of heavy-quark effective theory to lattice QCD. 3. Radiative corrections to heavy-heavy currents*, *Phys.Rev.* **D65** (2002) 094514 [[hep-lat/0112045](#)].
- [158] S. Hashimoto et al., *Lattice QCD calculation of $\bar{B} \rightarrow D\ell\bar{\nu}$ decay form factors at zero recoil*, *Phys. Rev.* **D61** (1999) 014502 [[hep-ph/9906376](#)].
- [159] [HPQCD 15] H. Na, C.M. Bouchard, G.P. Lepage, C. Monahan and J. Shigemitsu, *$B \rightarrow D\ell\nu$ form factors at nonzero recoil and extraction of $|V_{cb}|$* , *Phys. Rev.* **D92** (2015) 054510 [[1505.03925](#)].
- [160] [HPQCD 17] C. J. Monahan, H. Na, C.M. Bouchard, G.P. Lepage and J. Shigemitsu, *$B_s \rightarrow D_s\ell\nu$ Form Factors and the Fragmentation Fraction Ratio f_s/f_d* , *Phys. Rev.* **D95** (2017) 114506 [[1703.09728](#)].
- [161] [FNAL/MILC 15C] J. A. Bailey et al., *$B \rightarrow D\ell\nu$ form factors at nonzero recoil and $-V_{cb}$ from 2+1-flavor lattice QCD*, *Phys. Rev.* **D92** (2015) 034506 [[1503.07237](#)].
- [162] [HPQCD 19] E. McLean, C.T.H. Davies, J. Koponen and A.T. Lytle, *$B_s \rightarrow D_s\ell\nu$ Form Factors for the full q^2 range from Lattice QCD with non-perturbatively normalized currents*, *Phys. Rev. D* **101** (2020) 074513 [[1906.00701](#)].
- [163] [FNAL/MILC 21] A. Bazavov et al., *Semileptonic form factors for $B \rightarrow D^*\ell\nu$ at nonzero recoil from 2 + 1-flavor lattice QCD: Fermilab Lattice and MILC Collaborations*, *Eur. Phys. J. C* **82** (2022) 1141 [[2105.14019](#)], [Erratum: *Eur.Phys.J.C* 83, 21 (2023)].
- [164] [JLQCD 23] Y. Aoki, B. Colquhoun, H. Fukaya, S. Hashimoto, T. Kaneko, R. Kellermann et al., *$B \rightarrow D^*\ell\nu_\ell$ semileptonic form factors from lattice QCD with Möbius domain-wall quarks*, *Phys. Rev. D* **109** (2024) 074503 [[2306.05657](#)].
- [165] [HPQCD 23] J. Harrison and C.T.H. Davies, *$B \rightarrow D^*$ and $B_s \rightarrow D_s^*$ vector, axial-vector and tensor form factors for the full q^2 range from lattice QCD*, *Phys. Rev. D* **109** (2024) 094515 [[2304.03137](#)].
- [166] [HPQCD 20B] J. Harrison, C.T.H. Davies and A. Lytle, *$B_c \rightarrow J/\psi$ form factors for the full q^2 range from lattice QCD*, *Phys. Rev. D* **102** (2020) 094518 [[2007.06957](#)].

- [167] [FNAL/MILC 04A] M. Okamoto et al., *Semileptonic $D \rightarrow \pi/K$ and $B \rightarrow \pi/D$ decays in 2+1 flavor lattice QCD*, *Nucl.Phys.Proc.Suppl.* **140** (2005) 461 [[hep-lat/0409116](#)].
- [168] [FNAL/MILC 13B] S.-W. Qiu, C. DeTar, A.X. El-Khadra, A.S. Kronfeld, J. Laiho et al., *Semileptonic decays $B \rightarrow D^{(*)}\ell\nu$ at nonzero recoil*, *PoS LATTICE2013* (2014) 385 [[1312.0155](#)].
- [169] M. Atoui, V. Morenas, D. Becirevic and F. Sanfilippo, *$b_s \rightarrow d_s \ell \nu_\ell$ near zero recoil in and beyond the standard model*, *Eur. Phys. J.* **C74** (2014) 2861 [[1310.5238](#)].
- [170] C.J. Monahan, H. Na, C.M. Bouchard, G.P. Lepage and J. Shigemitsu, *$B_{(s)} \rightarrow D_{(s)}$ semileptonic decays with NRQCD-HISQ valence quarks*, *PoS LATTICE2016* (2016) 298 [[1611.09667](#)].
- [171] LHCb collaboration, *Measurement of $|V_{cb}|$ with $B_s^0 \rightarrow D_s^{(*)-} \mu^+ \nu_\mu$ decays*, *Phys. Rev. D* **101** (2020) 072004 [[2001.03225](#)].
- [172] LHCb collaboration, *Precise measurement of the f_s/f_d ratio of fragmentation fractions and of B_s^0 decay branching fractions*, *Phys. Rev. D* **104** (2021) 032005 [[2103.06810](#)].
- [173] C. Bernard and D. Toussaint, *Effects of nonequilibrated topological charge distributions on pseudoscalar meson masses and decay constants*, *Phys. Rev.* **D97** (2018) 074502 [[1707.05430](#)].
- [174] T. Kaneko, Y. Aoki, B. Colquhoun, M. Faur, H. Fukaya, S. Hashimoto et al., *$B \rightarrow D^{(*)}\ell\nu$ semileptonic decays in lattice QCD with domain-wall heavy quarks*, *PoS LATTICE2021* (2022) 561 [[2112.13775](#)].
- [175] J.G. Korner and G.A. Schuler, *Exclusive Semileptonic Heavy Meson Decays Including Lepton Mass Effects*, *Z. Phys. C* **46** (1990) 93.
- [176] D. Bigi, P. Gambino and S. Schacht, *A fresh look at the determination of $|V_{cb}|$ from $B \rightarrow D^* \ell \nu$* , *Phys. Lett.* **B769** (2017) 441 [[1703.06124](#)].
- [177] BELLE collaboration, *Measurement of the CKM matrix element $|V_{cb}|$ from $B^0 \rightarrow D^{*-} \ell^+ \nu_\ell$ at Belle*, *Phys. Rev. D* **100** (2019) 052007 [[1809.03290](#)], [Erratum: *Phys.Rev.D* 103, 079901 (2021)].
- [178] [FNAL/MILC 08] C. Bernard et al., *The $\bar{B} \rightarrow D^* \ell \bar{\nu}$ form factor at zero recoil from three-flavor lattice QCD: a model independent determination of $|V_{cb}|$* , *Phys.Rev.* **D79** (2009) 014506 [[0808.2519](#)].
- [179] [FNAL/MILC 14] J. A. Bailey et al., *Update of $|V_{cb}|$ from the $\bar{B} \rightarrow D^* \ell \bar{\nu}$ form factor at zero recoil with three-flavor lattice QCD*, *Phys. Rev.* **D89** (2014) 114504 [[1403.0635](#)].
- [180] J. Harrison, C. Davies and M. Wingate, *$|V_{cb}|$ from the $\bar{B}^0 \rightarrow D^{*+} \ell^- \bar{\nu}$ zero-recoil form factor using $2 + 1 + 1$ flavour HISQ and NRQCD*, *PoS LATTICE2016* (2017) 287 [[1612.06716](#)].
- [181] [HPQCD 17B] J. Harrison, C. Davies and M. Wingate, *Lattice QCD calculation of the $B_{(s)} \rightarrow D_{(s)}^* \ell \nu$ form factors at zero recoil and implications for $|V_{cb}|$* , *Phys. Rev.* **D97** (2018) 054502 [[1711.11013](#)].

- [182] M. Neubert, *Theoretical update on the model independent determination of $|V(cb)|$ using heavy quark symmetry*, *Phys. Lett. B* **338** (1994) 84 [[hep-ph/9408290](#)].
- [183] S. Hashimoto, A.S. Kronfeld, P.B. Mackenzie, S.M. Ryan and J.N. Simone, *Lattice calculation of the zero recoil form-factor of $\bar{B} \rightarrow D^* \ell \bar{\nu}$: toward a model independent determination of $|V_{cb}|$* , *Phys.Rev.* **D66** (2002) 014503 [[hep-ph/0110253](#)].
- [184] L. Randall and M.B. Wise, *Chiral perturbation theory for $B \rightarrow D^*$ and $B \rightarrow D$ semileptonic transition matrix elements at zero recoil*, *Phys.Lett.* **B303** (1993) 135 [[hep-ph/9212315](#)].
- [185] M.J. Savage, *Heavy meson observables at one loop in partially quenched chiral perturbation theory*, *Phys.Rev.* **D65** (2002) 034014 [[hep-ph/0109190](#)].
- [186] [FNAL/MILC 22] A. Bazavov et al., *D-meson semileptonic decays to pseudoscalars from four-flavor lattice QCD*, *Phys. Rev. D* **107** (2023) 094516 [[2212.12648](#)].
- [187] [HPQCD 19B] E. McLean, C.T.H. Davies, A.T. Lytle and J. Koponen, *Lattice QCD form factor for $B_s \rightarrow D_s^* \ell \nu$ at zero recoil with non-perturbative current renormalisation*, *Phys. Rev. D* **99** (2019) 114512 [[1904.02046](#)].
- [188] [HPQCD 21B] J. Harrison and C.T.H. Davies, *$B_s \rightarrow D_s^*$ Form Factors for the full q^2 range from Lattice QCD*, *Phys. Rev. D* **105** (2022) 094506 [[2105.11433](#)].
- [189] T. Bhattacharya et al., *Current progress on the semileptonic form factors for $\bar{B} \rightarrow D^* \ell \bar{\nu}$ decay using the Oktay-Kronfeld action*, *PoS LATTICE2023* (2023) 245 [[2401.01561](#)].
- [190] HFLAV collaboration, *Averages of b-hadron, c-hadron, and τ -lepton properties as of 2021*, *Phys. Rev. D* **107** (2023) 052008 [[2206.07501](#)].
- [191] R. Fleischer, N. Serra and N. Tuning, *A New Strategy for B_s Branching Ratio Measurements and the Search for New Physics in $B_s^0 \rightarrow \mu^+ \mu^-$* , *Phys. Rev. D* **82** (2010) 034038 [[1004.3982](#)].
- [192] LHCb collaboration, *Determination of f_s/f_d for 7 TeV pp collisions and a measurement of the branching fraction of the decay $B_d \rightarrow D^- K^+$* , *Phys. Rev. Lett.* **107** (2011) 211801 [[1106.4435](#)].
- [193] [FNAL/MILC 12C] J. A. Bailey et al., *$B_s \rightarrow D_s/B \rightarrow D$ semileptonic form-factor ratios and their application to $BR(B_s^0 \rightarrow \mu^+ \mu^-)$* , *Phys.Rev.* **D85** (2012) 114502 [[1202.6346](#)].
- [194] A. Lytle, B. Colquhoun, C. Davies, J. Koponen and C. McNeile, *Semileptonic B_c decays from full lattice QCD*, *PoS BEAUTY2016* (2016) 069 [[1605.05645](#)].
- [195] [HPQCD 16] B. Colquhoun, C. Davies, J. Koponen, A. Lytle and C. McNeile, *B_c decays from highly improved staggered quarks and NRQCD*, *PoS LATTICE2016* (2016) 281 [[1611.01987](#)].
- [196] [HPQCD 20C] J. Harrison, C.T.H. Davies and A. Lytle, *$R(J/\psi)$ and $B_c^- \rightarrow J/\psi \ell^- \bar{\nu}_\ell$ Lepton Flavor Universality Violating Observables from Lattice QCD*, *Phys. Rev. Lett.* **125** (2020) 222003 [[2007.06956](#)].

- [197] LHCb RICH GROUP collaboration, *Performance of the LHCb RICH detector at the LHC*, *Eur. Phys. J. C* **73** (2013) 2431 [[1211.6759](#)].
- [198] LHCb collaboration, *Determination of the quark coupling strength $|V_{ub}|$ using baryonic decays*, *Nature Phys.* **11** (2015) 743 [[1504.01568](#)].
- [199] T. Feldmann and M.W.Y. Yip, *Form Factors for $\Lambda_{cb} \rightarrow \Lambda$ Transitions in SCET*, *Phys. Rev.* **D85** (2012) 014035 [[1111.1844](#)], [Erratum: *Phys. Rev.* **D86**,079901(2012)].
- [200] W. Detmold, C. Lehner and S. Meinel, *$\Lambda_b \rightarrow p \ell^- \bar{\nu}_\ell$ and $\Lambda_b \rightarrow \Lambda_c \ell^- \bar{\nu}_\ell$ form factors from lattice QCD with relativistic heavy quarks*, *Phys. Rev.* **D92** (2015) 034503 [[1503.01421](#)].
- [201] A. Datta, S. Kamali, S. Meinel and A. Rashed, *Phenomenology of $\Lambda_b \rightarrow \Lambda_c \tau \bar{\nu}_\tau$ using lattice QCD calculations*, *JHEP* **08** (2017) 131 [[1702.02243](#)].
- [202] S. Meinel, *Status of next-generation $\Lambda_b \rightarrow p, \Lambda, \Lambda_c$ form-factor calculations*, *PoS LATTICE2023* (2024) 275 [[2309.01821](#)].
- [203] S. Meinel and G. Rendon, *$\Lambda_b \rightarrow \Lambda_c^*(2595, 2625) \ell^- \bar{\nu}$ form factors from lattice QCD*, *Phys. Rev. D* **103** (2021) 094516 [[2103.08775](#)].
- [204] S. Meinel and G. Rendon, *$\Lambda_c \rightarrow \Lambda^*(1520)$ form factors from lattice QCD and improved analysis of the $\Lambda_b \rightarrow \Lambda^*(1520)$ and $\Lambda_b \rightarrow \Lambda_c^*(2595, 2625)$ form factors*, *Phys. Rev. D* **105** (2022) 054511 [[2107.13140](#)].
- [205] T.D. Cohen, H. Lamm and R.F. Lebed, *Precision Model-Independent Bounds from Global Analysis of $b \rightarrow c \ell \nu$ Form Factors*, *Phys. Rev. D* **100** (2019) 094503 [[1909.10691](#)].
- [206] M. Papucci and D.J. Robinson, *Form factor counting and HQET matching for new physics in $\Lambda_b \rightarrow \Lambda_c^* \ell \nu$* , *Phys. Rev. D* **105** (2022) 016027 [[2105.09330](#)].
- [207] V. Di Risi, D. Iacobacci and F. Sannino, *$\Lambda_b \rightarrow \Lambda_c^*$ at $1/m_c^2$ heavy quark mass order*, *Phys. Rev. D* **109** (2024) 036021 [[2309.03553](#)].
- [208] T. Blake and M. Kreps, *Angular distribution of polarised Λ_b baryons decaying to $\Lambda \ell^+ \ell^-$* , *JHEP* **11** (2017) 138 [[1710.00746](#)].
- [209] LHCb collaboration, *Angular moments of the decay $\Lambda_b^0 \rightarrow \Lambda \mu^+ \mu^-$ at low hadronic recoil*, *JHEP* **09** (2018) 146 [[1808.00264](#)].
- [210] W. Detmold, C.J.D. Lin, S. Meinel and M. Wingate, *$\Lambda_b \rightarrow \Lambda \ell^+ \ell^-$ form factors and differential branching fraction from lattice QCD*, *Phys. Rev.* **D87** (2013) 074502 [[1212.4827](#)].
- [211] W. Detmold and S. Meinel, *$\Lambda_b \rightarrow \Lambda \ell^+ \ell^-$ form factors, differential branching fraction, and angular observables from lattice QCD with relativistic b quarks*, *Phys. Rev.* **D93** (2016) 074501 [[1602.01399](#)].
- [212] T. Blake, S. Meinel and D. van Dyk, *Bayesian Analysis of $b \rightarrow s \mu^+ \mu^-$ Wilson Coefficients using the Full Angular Distribution of $\Lambda_b \rightarrow \Lambda (\rightarrow p \pi^-) \mu^+ \mu^-$ Decays*, *Phys. Rev. D* **101** (2020) 035023 [[1912.05811](#)].

- [213] LHCb collaboration, *Differential branching fraction and angular analysis of $\Lambda_b^0 \rightarrow \Lambda \mu^+ \mu^-$ decays*, *JHEP* **06** (2015) 115 [[1503.07138](#)], [Erratum: JHEP 09, 145 (2018)].
- [214] M. Algueró, B. Capdevila, A. Crivellin, S. Descotes-Genon, P. Masjuan, J. Matias et al., *Emerging patterns of New Physics with and without Lepton Flavour Universal contributions*, *Eur. Phys. J. C* **79** (2019) 714 [[1903.09578](#)], [Addendum: Eur.Phys.J.C 80, 511 (2020)].
- [215] S. Meinel and G. Rendon, $\Lambda_b \rightarrow \Lambda^*(1520) \ell^+ \ell^-$ form factors from lattice QCD, *Phys. Rev. D* **103** (2021) 074505 [[2009.09313](#)].
- [216] W. Detmold, C.J.D. Lin, S. Meinel and M. Wingate, $\Lambda_b \rightarrow p \ell^- \bar{\nu}_\ell$ form factors from lattice QCD with static b quarks, *Phys. Rev. D* **88** (2013) 014512 [[1306.0446](#)].
- [217] BELLE collaboration, *Measurement of $B^- \rightarrow \tau^- \bar{\nu}_\tau$ with a hadronic tagging method using the full data sample of Belle*, *Phys. Rev. Lett.* **110** (2013) 131801 [[1208.4678](#)].
- [218] BABAR collaboration, *A search for $B^+ \rightarrow \ell^+ \nu_\ell$ recoiling against $B^- \rightarrow D^0 \ell^- \bar{\nu} X$* , *Phys. Rev. D* **81** (2010) 051101 [[0912.2453](#)].
- [219] BABAR collaboration, *Branching fraction and form-factor shape measurements of exclusive charmless semileptonic B decays, and determination of $|V_{ub}|$* , *Phys. Rev. D* **86** (2012) 092004 [[1208.1253](#)].
- [220] BELLE collaboration, *Measurement of the decay $B^0 \rightarrow \pi^- \ell^+ \nu$ and determination of $|V_{ub}|$* , *Phys. Rev. D* **83** (2011) 071101 [[1012.0090](#)].
- [221] BELLE collaboration, *Measurement of the decay $B \rightarrow D \ell \nu_\ell$ in fully reconstructed events and determination of the Cabibbo-Kobayashi-Maskawa matrix element $|V_{cb}|$* , *Phys. Rev. D* **93** (2016) 032006 [[1510.03657](#)].
- [222] BABAR collaboration, *Measurement of $|V(cb)|$ and the Form-Factor Slope in $\bar{B} \rightarrow D \ell^- \bar{\nu}_\ell$ Decays in Events Tagged by a Fully Reconstructed B Meson*, *Phys. Rev. Lett.* **104** (2010) 011802 [[0904.4063](#)].
- [223] D. Bigi and P. Gambino, *Revisiting $B \rightarrow D \ell \nu$* , *Phys. Rev. D* **94** (2016) 094008 [[1606.08030](#)].
- [224] BELLE collaboration, *Measurement of differential distributions of $B \rightarrow D^* \ell \bar{\nu}_\ell$ and implications on $|V_{cb}|$* , *Phys. Rev. D* **108** (2023) 012002 [[2301.07529](#)].
- [225] BELLE-II collaboration, *Determination of $|V_{cb}|$ using $\bar{B}^0 \rightarrow D^{*,+} \ell^- \bar{\nu}_\ell$ decays with Belle II*, *Phys. Rev. D* **108** (2023) 092013 [[2310.01170](#)].
- [226] BELLE-II collaboration, *Measurement of the semileptonic $\bar{B}^0 \rightarrow D^{*,+} \ell^- \nu_\ell$ branching fraction with fully reconstructed B meson decays and 34.6 fb^{-1} of Belle II data*, [2008.10299](#).
- [227] PARTICLE DATA GROUP collaboration, *Review of Particle Physics*, *Phys. Rev. D* **98** (2018) 030001.
- [228] M. Bordone, B. Capdevila and P. Gambino, *Three loop calculations and inclusive V_{cb}* , *Phys. Lett. B* **822** (2021) 136679 [[2107.00604](#)].

- [229] [HFLAV 18] Y. Amhis et al., *Averages of b -hadron, c -hadron, and τ -lepton properties as of 2018*, *Eur. Phys. J. C* **81** (2021) 226 [[1909.12524](#)].
- [230] LHCb collaboration, *First observation of the decay $B_s^0 \rightarrow K^- \mu^+ \nu_\mu$ and Measurement of $|V_{ub}|/|V_{cb}|$* , *Phys. Rev. Lett.* **126** (2021) 081804 [[2012.05143](#)].
- [231] P. Gambino, K.J. Healey and S. Turczyk, *Taming the higher power corrections in semileptonic B decays*, *Phys. Lett.* **B763** (2016) 60 [[1606.06174](#)].
- [232] PARTICLE DATA GROUP collaboration, *Review of Particle Physics*, *Chin. Phys.* **C38** (2014) 090001 and 2015 update.